Three dimensional quantitative textural analysis of nickel sulphide ore using X-ray computed tomography and grey level co-occurrence matrices on drill core

by

Mitchel Jardine

A thesis submitted at the University of Cape Town of the requirements for the degree of

Master of Science

Department of Chemical Engineering

University of Cape Town

February 2016

Ipsa scientia potestas est.

Declaration

I declare that this thesis, submitted for the degree of Master of Science in Engineering at the University of Cape Town is my own work, and has not been submitted prior to this for any degree at this University or any other institution. I know the meaning of plagiarism and declare that all work in this document, save for that which is properly acknowledged is my own.

Mitchel Jardine

Signed by candidate

Synopsis

Alongside the global trend to mine and process lower grade and more mineralogically complex ores, there has been an increased awareness of the prevalence of ore heterogeneity. Ore texture - the interrelationship of minerals comprising a rock, has been identified as one of the primary geometallurgical indicators of ore variability. It is well known that a relationship exists between ore texture and the resultant metallurgical performance (ore hardness, throughput, liberation, grade, recovery). Consequently, there exists a need to rapidly, routinely, cost effectively, and reliably quantify ore texture and its variability prior to mining. This information can thereafter be incorporated into the geometallurgical block model and used for decision making informing mine planning, plant operation and optimisation, forecasting, and mine closure.

The ability to rapidly, routinely, cost effectively and reliably quantify ore texture remains an ongoing challenge. In this study, the use of 3D X-ray computed tomography (XCT) is proposed as an innovative solution to non-destructively image the internal structure of drill core. Thereafter, an established, discipline independent two dimensional (2D) image analysis technique known as grey level co-occurrence matrices (GLCM) is specially adapted into three dimensions (3D) to quantify ore texture using XCT grey level volumes of drill core.

The first phase of the study focused on the development of a methodology for the mineralogical and textural analysis of geomaterials using XCT coupled with 3D GLCM. This entailed the adaptation and customisation of the GLCM software script into 3D for the image analysis of XCT volumes. XCT image sections perpendicular to the length of the drill core and spaced 20µm apart were used in multi-dimensional arrays within MATLAB in order to analyse the 13 unique pixel pair relationships in 3D. The resultant GLCM were thereafter interrogated using both the conventional GLCM statistics, and as ‘heat maps’ which are less commonly used. The resultant GLCM produced from quantitative 3D image analysis of the XCT volumes indicated sensitivity to ore variability. A simple mineralogy was captured by the position and intensity of the peaks within the GLCM heat maps: peaks located in the bottom right quadrant representing dense minerals, and peaks located in the top left quadrant representing light minerals. A simple grain size distribution was captured using the width of the GLCM distribution, since the width perpendicular to the diagonal and originating from the peaks of the distribution indicated the frequency with which the grey level populations interact with one another. A narrow distribution indicated a coarse mineral grain size population, whereas a broad distribution indicated a fine grain size population.

The second phase of the study focused on assessing the application of XCT coupled with 3D GLCM for the quantitative textural analysis of drill core using a case study from the Nkomati Nickel MMZ sulfide ore. Drill core samples were manually extracted from various rock types and textures representing the deposit. The remaining sample material was thereafter comminuted in a laboratory scale rod mill and subdivided into four groups on the basis of the particle size distribution. Complimentary QEMSCAN mineralogical analyses were used to facilitate the interpretation of the

GLCM for the Nkomati case study. Overall, the GLCM results in the D1 unique direction captured variations in the simple mineralogy (sulfide/oxides, silicate minerals SG>3, silicate minerals SG<3) and grain size distribution (coarse vs fine) in the drill core samples. Three of the four textural groupings showed relatively unique GLCM.

This MSc study has successfully developed a methodology for the quantitative textural analysis of drill core in 3D using XCT and GLCM and illustrated its application for the Nkomati MMZ nickel sulfide ore. The methodology is sensitive to variations in simple mineralogy and texture and with suitable further development has the potential to be used as an automated, rapid, repeatable and consistent measure of ore variability in geometallurgy. When this information is coupled with metallurgical performance, it could allow for rapid decision making to improve breakage, throughput and recovery, and decrease losses and energy consumption for improved sustainability.

Acknowledgements

This thesis is the product of collaboration between the student and the two supervisors. Drs Becker and Miller provided guidance with the development of aims and objectives and helped to shape the methodology. Both supervisors assisted with developing the organisation of the thesis and read and provided feedback on chapters. Mr Jardine was responsible for implementation and execution of the methodology including selection of the appropriate methodological framework (subsequently approved by Dr Becker). Mr Jardine developed the code on his own and conducted all experiments himself. He was responsible for creating all the outputs and diagrams for the thesis

My two year journey to complete my master thesis has been great to say the least. I have grown beyond my expectations. The support and advice I have received has been invaluable.

To my supervisors – Dr. Megan Becker from the University of Cape Town, and Dr. Jodie Miller from the University of Stellenbosch. To start I would like to acknowledge Dr. Megan Becker my supervisor. After working with Megan for two years it is not hard to believe that people like her are few and far between. Thank you for being an exceptional teacher. Your attention to detail and unique take of beneficiation from a mineralogy point of view has been a fundamental stepping stone in the development of this study. I would also like to acknowledge Dr. Jodie Miller my co-supervisor. Thank you for the years of input into my life, teaching me about geology, mineral identification, optical microscopy, and for being my honours project supervisor (my introduction to X-ray Computed Tomographic imaging). Thank you for the consultation and guidance you have given me during this project. Your dedication to you students does not go unnoticed. To both my supervisors, without whom this would not have been possible, thank you.

To the staff in the department of Chemical Engineering at UCT - Prof. Dee Bradshaw, Martin Harris, Jeremy Mann, Gaynor Yorath, Lorraine Nkemba, Monde Bekaphi and Graham Inggs. To Prof. Dee Bradshaw for the encouragement and valuable input into the project scope and deliverables, and also for a little helping hand to ensure I had the equipment I needed to complete the thesis. To Martin Harris for guidance and perspective on the projects deliverable to industry. To Jeremy for the providing the perspective of technology readiness and technology deliverables. To Gaynor for her dedication to ensure the best QEMSCAN analysis of my samples, and for always offering a helping hand. To Lorraine for preparing tens of samples for QEMSCAN analysis. To Monde for helping me carry over 200kg of rock around campus and for helping with sample crushing and teaching me correct bench scale comminution test work procedures. To Graham for his patience and invaluable help in setting up server connections and MATLAB for remote analysis for the proposed methodology. Thank you, you all have been instrumental to the success of this project.

To the staff at the Stellenbosch Central Analytical Facility and Department of Process Engineering - Dr. Lydia Auret, Dr. Anton du Plessis and Stephan le Roux. To Dr. Lydia Auret for consultation of the

proposed methodology and for allowing that I use the MATLAB GUI at Stellenbosch for the primary development of the MATLAB image analysis scripts written for this project. To Dr. Anton du Plessis for introducing me to XCT analysis techniques and providing advice and recommendation to achieve the best possible XCT image results. To Stephan le Roux for performing all the XCT scans with excellence. Thank You.

To Nkomati staff - Grant Cockburn, Bryn Edwards. To Grant for the hospitality during the mine visit and mentorship throughout the project To Bryn for helping with sample collection and selection. Thank You.

To project sponsors - SAMMRI and NRF. To SAMMRI for the scholarship, project funding and financial support. To NRF for the financial support. Thank You.

To friends and family - Byron Coetsee, Michael Hartnady and Ashleigh Hillary. To Byron for his programming tutoring lessons and his aid during programming challenges. To Michael for reading though my thesis and for his advice and support. To Ash Hillary, for her motivation and support. Thank You.

Last but not least, To Mom and Dad. Thank you for the years of motivation and guidance throughout my life which has lead me to this point and will surely push me far further. Thank you.

Presentations and Publications

Jardine, M. A., Becker, M., Miller, J., and Harris M., 2014. Towards the use of x-ray computed tomography to quantify ore textures in a mineral processing framework. *SAIMM Mineral Processing Conference*, 7 - 8 August, Cape Town.

Jardine, M. A., Becker, M., Miller, J., and Harris M., 2014. Towards the use of x-ray computed tomography to quantify ore textures in a mineral processing framework. *The 21st General Meeting of the International Mineralogical Association*, 1 – 5 September, Sandton Convention Centre, South Africa.

Jardine, M. A., Becker, M., Miller, J., and Harris M., 2014. Towards the use of x-ray computed tomography to quantify ore textures in a mineral processing framework. *Minerals Engineering, 3rd Process Mineralogy Conference,* 17-19 November, Cape Town, South Africa.

Jardine, M. A., Becker, M., Miller, J., and Harris M., 2015. X-ray Computed Tomography: A mine-site tool for 3D textural analysis of ore? *SAIMM Mineral Processing Conference*, 7 - 8 August, Cape Town.

Jardine, M. A., Becker, M., Miller, J., and Harris M., *2015.* Using XCT and GLCM for the 3D textural analysis of Nkomati MMZ drill core. *Imaging and Radiation Conference,* 10-11 September*, Stellenbosch University, South Africa.*

Becker, M., Jardine, M. A., Miller, J., and Harris M., submitted for presentation 2016. X-ray Computed Tomography: A geometallurgical tool for 3D textural analysis of drill core?, *The 3rd AusIMM International Geometallurgy Conference*, 15 - 17 June, Perth, Australia.

Table of Contents

List of Figures

List of Tables

Acronyms

2D	Two-Dimensional
3D	Three-Dimensional
BMS	Base Metal Sulphide
BSE	Back Scattered Electrons
CAT	Computer Axial Tomography
CPX	Clinopyroxene
GLCM	Grey Level Co-occurrence Matrix
GUI	Graphics User Interface
OPX	Orthopyroxene
PSD	Particle Size Distribution
ROM	Run of Mine
QEMSCAN	Quantitative Evaluation of Minerals by Scanning Electron Microscope
SEM	Scanning Electron Microscope
XCT	X-Ray Computed Tomography
XRD	X-Ray Diffraction
XRF	X-Ray Fluorescence

Glossary

Auto-SEM:	An automated scanning electron microscope that takes incremental spatial X-ray and back scattered electron readings to build a detailed image of the scanned surface.
Autonomicity:	The ability of a system to perform tasks and achieve goals without operator input.
Aphanitic:	An igneous rock with a mineral grain size smaller than the eye can see.
Array:	In computation an array is a container that holds a predetermined number of values.
Concatenate:	The addition of data to a string array in computer programming using a loop.
Chadacryst:	An igneous texture term describing smaller mineral grains enclosed in a larger oikocryst.
Disseminated texture:	A distinct lack in connectivity between individual BMS minerals within ore.
Dolostone:	A rock is almost entirely made up of dolomite.
Electron Microscope:	A microscope that uses an electron beam rather than light to image objects of interest.
Bleb texture:	Sulphides that form disseminated clusters while within the clusters the sulphides demonstrate a net texture.
Fabric:	Refers to the structures within rocks.
Foliation	A rock fabric that is planar in structure.
GLCM Contrast:	Measure of the local variation in the grey-level co-occurrence matrix.
GLCM Correlation:	Measures the joint probability occurrence of specific pixel pairs.
GLCM Energy:	Provides the sum of squared elements in the GLCM.
GLCM Homogeneity:	Measures the closeness of the distribution of elements in the GLCM to the GLCM diagonal.
Geometallurgy:	A discipline that couples geology and metallurgy to create a predictive geological model for minerals processing.
Gabbro:	A coarse grained igneous rock consisting of pyroxene and plagioclase minerals with 0-5% olivine.

Grade:	The measure of a valuable metal content in ore.
Grain:	A single mineral grain is a mineral phase.
Harzburgite:	A rock dominated by olivine and orthopyroxene with 1-5% clinopyroxene.
Oikocrystic:	An igneous rock texture term given to large mineral that encloses other smaller mineral grains (chadacryst).
Particle:	An aggregate composed of many mineral grains.
Pixel:	A single square, positioned spatially in relation to many other pixels, which is assigned a grey or colour value which displays that particular grey level or colour. When in conjunction with the other pixels displaying their grey levels or colours make up an image.
Porphyroblast:	A single mineral grain that is much larger than the surrounding mineral grains that make up a rock.
Poikiloblastic:	A textural term used to describe mineral grains that contain inclusions of the previous unaltered mineral.
Process Mineralogy:	A discipline that encompasses geology, mineralogy and metallurgy that is aimed at addressing problems associated with minerals processing.
Pyroxenite:	A rock composed of 95% or more pyroxene minerals.
Saussuritization:	The metamorphic or hydrothermal alteration process which occurs when plagioclase is altered to form zoisite, chlorite, amphibole and carbonates.
Stereology:	Error associated with extending 2D information to represent 3D data.
Texture:	The spatial arrangement of minerals that comprise a rock.
Uralitization:	The metamorphic or hydrothermal alteration process that causes the development of amphibole from pyroxene.
Vein:	A crack like structure in rock that is filled with mineralogy that is different to its surrounding material.
Voxel:	A volumetric pixel. A cube positioned spatially in relation to many other voxels in 3D, which is assigned a grey or colour value which displays that particular grey level or colour. When in conjunction with the other voxels displaying their grey levels or colours make up a 3D image.
Xenolith:	A rock fragment, such as country rock, that is enveloped into magma during intrusion and crystallisation of igneous rocks.

Chapter 1 : Introduction

1.1 Introduction

The move to the processing of more mineralogically complex low grade ores has become a global trend: strengthening world economies have accelerated metal production, increased energy consumption, water consumption and greenhouse gas emission in mining activities, while there has been a steady move away from the processing of high grade ores as they are gradually depleted. (Northey et al. 2014; West 2011; Prior et al. 2012). Resource grade depletion is a worldwide problem. It is particularly well illustrated by looking at changes in Nickel ore grades in Australia which have dropped from 10% in 1920 to 5% in 1970 and are currently around the 2% level (Figure 1-1)(Prior et al. 2012). There is therefore a common goal to sustainably produce a metal product. This is achievable though better use of inherent mineralogical and textural information associated with these complex ores.

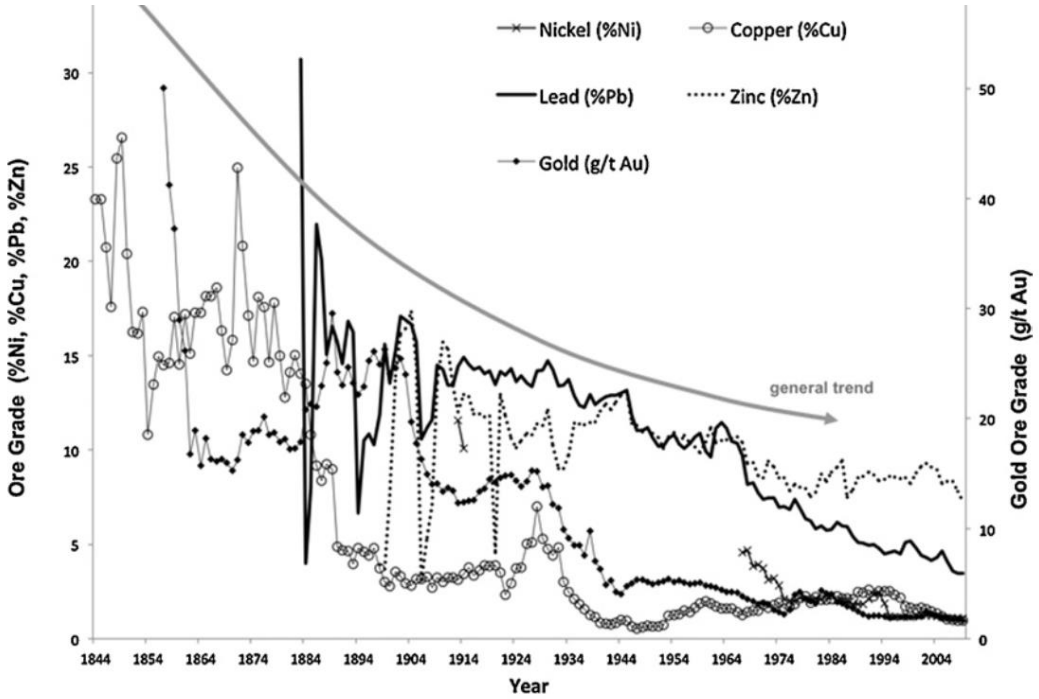

Figure 1-1: Declining base and precious metals in Australia (Prior et al. 2012).

A complex ore may be defined as an ore that is difficult to recover through conventional beneficiation methods or a texturally heterogeneous ore body (Deveci et al. 2004). The key to unlocking the value in these low grade complex ores is through better usage of the mineralogical properties (and

knowledge thereof) to develop innovative technologies that exploit these characteristics for the efficient, cost effective and sustainable beneficiation (West 2011).

The two most important of these mineralogical properties are: 1) the bulk mineralogy, which provides information on the quantities and composition of valuable and gangue minerals, and 2) texture, which provides information on mineral association as well as mineral grain size and shape. This mineralogical information is used extensively in the disciplines of process mineralogy and geometallurgy. Process mineralogy focuses on 'addressing problems associated with the processing of ores' (Bradshaw, et al. 2014; Wightman, et al. 2008; Lotter et al. 2011) whereas geometallurgy (of which process mineralogy is part of), focuses on ore body block modelling and mine planning.

Geometallurgy consists of four major components for mine planning. These are 1) the geological and mineralogical information of appropriately selected ore samples, 2) minerals processing test work to establish the metallurgical response in various unit operations which must be cost effective, quantitative and easy to apply throughout variable ore bodies, 3) a geostatistical measure of the metallurgical responses throughout an ore body (geometallurgical units) and 4) the development of a spatial model for minerals processing and mineral resource management for the prediction of plant behaviour and the overall economic impact (Farrell et al. 2011; Stradling. 2011; Bulled. 2007 & 2005; Dunham and Vann. 2007). Geometallurgy is therefore a crucial tool used in mine planning to optimise ore resources. It does this by integrating geology, mineralogy, metallurgy and mine planning to better realise the economic viability of an ore reserve while minimising operation cost.

Historically, ore processing plants were designed for the 'average' ore. As a consequence, blending of good quality ore with poor quality ore has been common practice to produce a more uniform plant feed and so minimize and prevent fluctuations which the plant design cannot cope with. Ultimately this is detrimental to grade, recovery and throughput (Williams and Holtzhausen 2001). However, the flaws of such an approach are increasingly being documented and ore variability is fast becoming a factor that cannot be ignored in process design (Lotter et al. 2011; Powell, 2013). One of the first indications of variability in ore properties is the change in ore texture. Texture is usually defined qualitatively, through the use of macro and micro optical studies, as a change in the visual appearance of the arrangement or grain size of minerals in an ore. The texture of an ore refers to the primary grain size, shape and mineralogical association (Schwartz 1951). It has a controlling influence on the following: 1) comminution response, specifically, product particle size distributions and target grind size, 2) mineral liberation (the release of a target mineral from gangue) and association, 3) grindability of the ore, the available surface area of a target mineral for reagent attachment during flotation, 4) the quantity of fines produced during comminution and 5) the presence of coarse composite particles (MinAssist, 2005). All of these factors ultimately affect the grade-recovery performance in flotation, as well as leaching applications (Gottlieb et al. 2000; Gaspar and Pinto. 1991). Consequently, having an understanding of the variation in texture of an ore body is crucial to process design and optimisation. Accounting for ore variability is one of the core aspects of geometallurgy and therefore, having appropriate and applicable measures of this variability is critical to define the geometallurgical domains within an ore body. This will ultimately allow the development

of a more accurate geometallurgical model (Knight et al. 2011; Bulled, 2005), allowing the prediction of its mineral processing behaviour such as energy consumption, throughput, grade and recovery, and even its potential for acid rock drainage (Parbhakar-Fox and Bradshaw 2013; Oyarzún and Arévalo 2011).

Lotter et al. (2011) in his paper on “Modern Process Mineralogy” provides a useful illustration of the relationship between plant design and ore texture in a nickel sulphide ore from the Nickel Rim South located in the Sudbury region in Canada (Figure 1-2). The first stage of this circuit is a coarse grind, for the liberation of the coarse grained (massive) sulphide texture, with a flash flotation. The second stage has a smaller target grind, for the liberation of the medium grained net-textured sulphide ore, with a rougher flotation. The final stage has the smallest target grind, for the liberation of the fine grained disseminated sulphide ore, with a cleaner flotation circuit. The auto-SEM false colour images of ore presented by Lotter et al. (2011) in this figure 1-2 illustrate three geometallurgical domains of the numerous variations and mixtures of ore textures that exist within the ore body. Understanding the ore texture variability is thus critical for process mineralogy and requires detailed analysis through techniques such as auto-SEM (QEMSCAN or MLA).

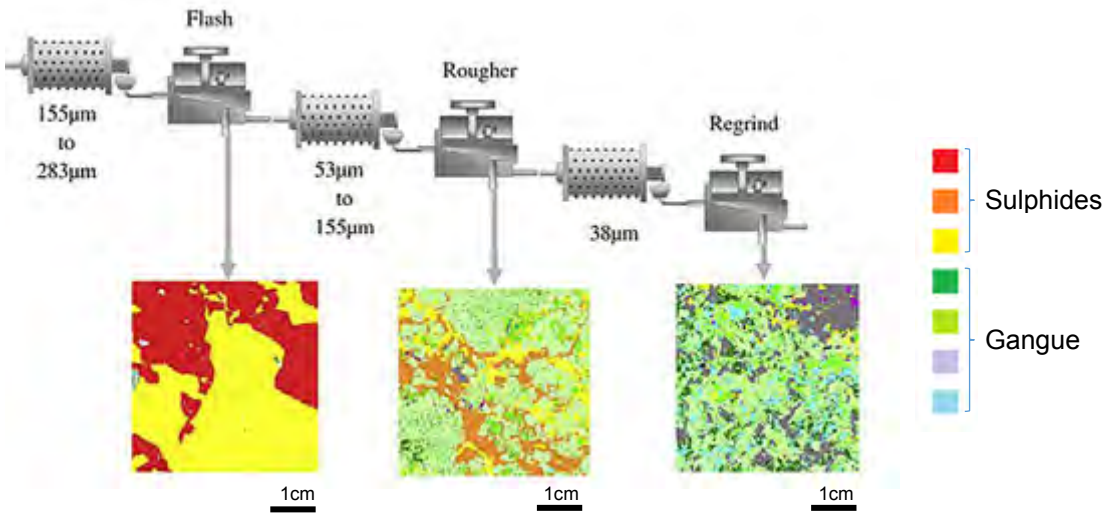

Figure 1-2: Concentrator flow sheet: staged grind approach proposed by Lotter et al (2011).

Auto-SEM technology, providing quantitative mineralogical information for ore characterisation, has become the work horse in process mineralogy (Figure 1-2). The information obtained through this technology is quantitative information on bulk mineralogy, mineral specific liberation, mineralogical association and mineral shapes and sizes. It has the potential to aid in process design and minerals processing (Andersen et al. 2009; Baum 2014; Gottlieb et al. 2000; Gu and Rd 2003; Lotter et al. 2011; Pascoe et al. 2007; Rollinson et al. 2011). However, there are several drawbacks with the use of this technique which may limit its application in geometallurgy. These include: slow turnaround time (extensive sample preparation associated with metallurgical test work, auto-SEM sample preparation and lengthy analysis time), error associated with 2D image data caused by the lack of data in the third dimension (stereological error), high cost and the need for skilled personnel. X-ray computed

tomography (XCT) has been identified as an emerging technology capable of providing rapid quantitative 3D information of ore.

Charikinya et al. (2015) demonstrates the ability to view internal structure within ore. In this study, XCT was used to generate 3D images of microwave treated ore to examine the distribution, orientation and size of cracks generated (Figure 1-3).

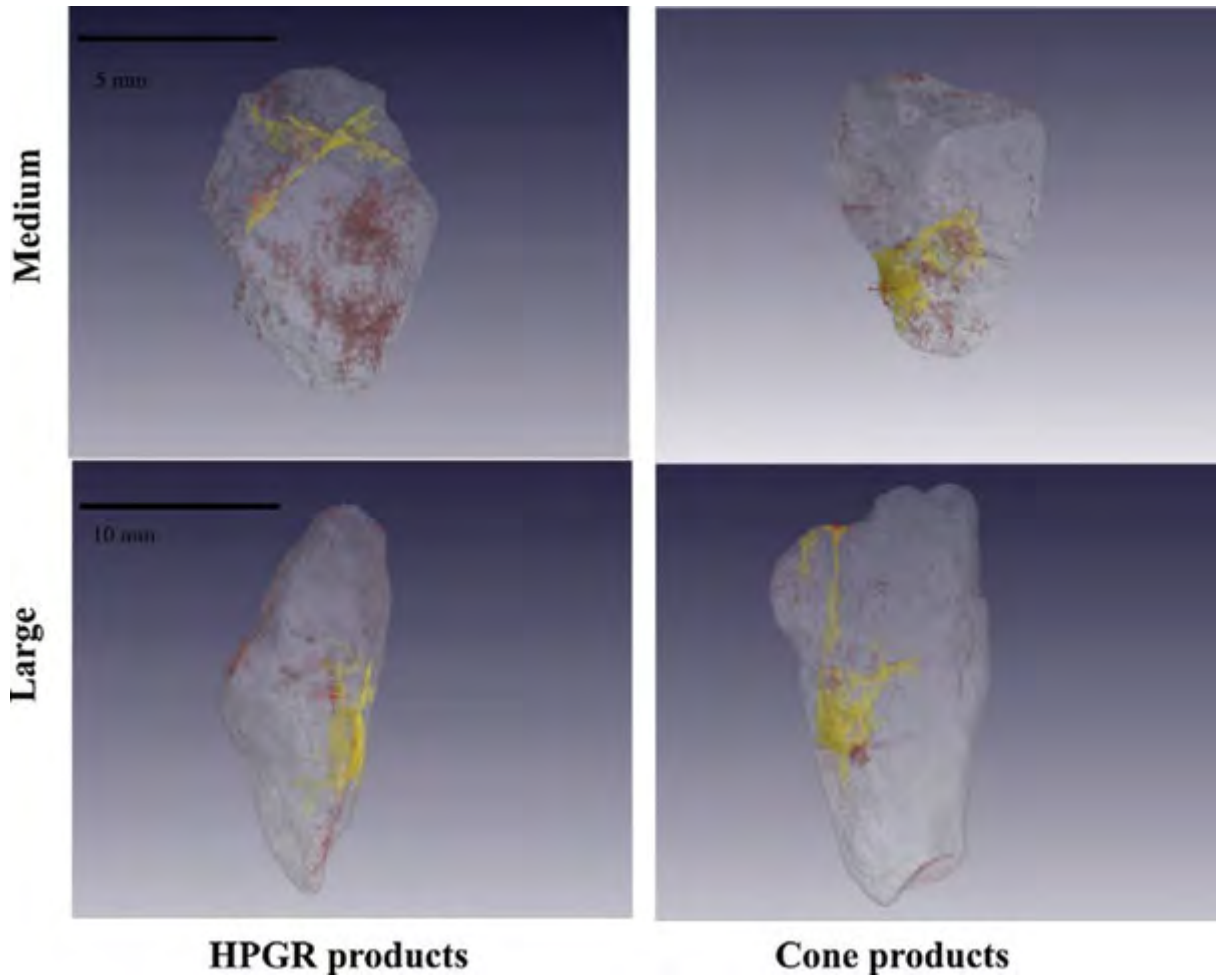

Figure 1-3: 3D crack structure reveal using XCT imaging. The yellow represent large crack voids and the red represent micro cracks (Charikinya et al. 2015).

Numerous examples exist in the literature illustrating how XCT has been used to further understand various minerals-related applications (Baker et al. 2012; Charikinya et al. 2015; Denison et al. 1997; Dhawan et al. 2012; Dominy et al. 2011; Ghorbani et al. 2011; Godel 2006; Godel et al. 2010; Howard et al. 2011; Lin and Miller 1996; Videla et al. 2007). However, the focus of XCT in these studies has been as a research tool, rather than an operational tool. With the advent of technology allowing the continuous, XCT scanning on an industrial scale in the forestry industry for the scanning of tree logs (Figure 1-4) (Gazo and Benes 2013, MicroTec™), opportunity exists to determine the benefits of continuous XCT scanning of drill core.

Conceptually, the application of XCT scanning in geometallurgy has the following merits: 1) the technique is non-destructive meaning drill cores will remain intact for future use, 2) the analysis is fast

in comparison to assay and metallurgical test work, 3) the quantitative 3D data reveals more information of the ore texture than surface studies such as core logging and optical microscopy, 4) there is no sample preparation needed since drill core can be XCT scanned as it is collected, 5) the 3D data of the scanned drill core has the potential to be directly implemented into a geometallurgical model for visual inspection of ore within the ore body block model. However, the following drawbacks are acknowledged for analysis by XCT: 1) the technique is data intensive and requires a high level of computing power, 2) the grey level information, as opposed to mineralogical data, requires tailored processing to extract the relevant mineralogical information (Roux et al. 2015), and 3) there is also no accepted method to analyse texture in XCT images and since XCT provides 3D information showcasing mineral associations and grain size, shape and boundary interaction (texture), there is a need for the development of quantitative textural measures.

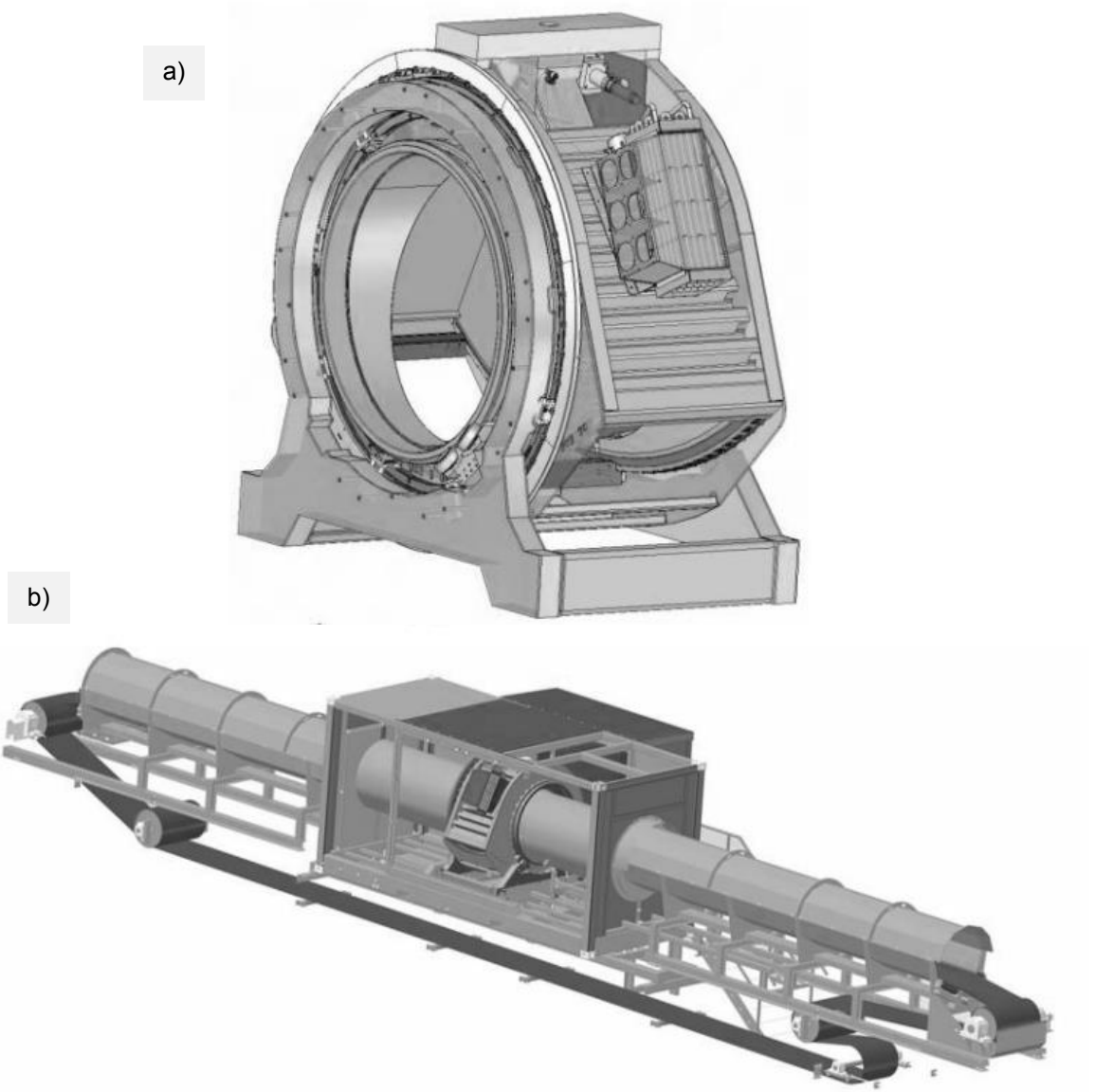

Figure 1-4: The use of computed tomography in industry is already in use, Microtec™ developed a computed tomography scanner (CT.Log™) for logs (a) with the use of an enclosed conveyer (b). This CT scanner is a Computed Axial Tomography (CAT) scanner (Image taken from ISCHP 2013; Gazo & Benes. 2013).

The objective of this project is to examine the application of 3D texture analysis using XCT images to classify ore texture in drill core. From amongst the established discipline independent 2D image analysis techniques (Denison et al. 1997; Pérez-Barnuevo et al. 2013; Haralick et al. 1973): linear intercept method, wavelet analysis, steerable pyramids, local binary patterns (LBP) and grey level co-occurrence matrices (GLCM), the GLCM have been identified as an appropriate starting point to quantify ore texture in geometallurgy. The Nkomati Nickel Main Mineralized Zone (MMZ) ore from South Africa will be used as a case study.

1.2 Problem Statement

Due to declining metal grades and increasing ore complexity, quantitative characterisation of the mineralogy and texture of ores, as well as the associated metallurgical responses and variability thereof is critically important in geometallurgy. Texture is one of the primary indicators of ore variability and conventional analytical equipment (e.g. auto-SEM) does not provide a 'fit for purpose' ability to capture this variation in 3D in geometallurgical applications. 3D XCT has been identified as a potential 'fit for purpose' tool to rapidly image 3D texture of drill core, but as yet no standard methodology exists to quantify this texture in 3D.

1.3 Objectives and Key Questions

The objectives and key questions of this study are therefore:

Objective 1: To develop a methodology for the mineralogical and textural analysis of geomaterials using XCT coupled with 3D GLCM.

i. What development is needed of the conventional 2D GLCM texture MATLAB code to analyse 3D XCT images?

ii. What mineralogical and textural information can be drawn from the matrices and respective statistics?

iii. What are the potential opportunities in the geosciences where the XCT and 3D GLCM information could provide value?

Objective 2: To assess the application of XCT coupled with 3D GLCM for the quantitative textural analysis of drill core: Case study of the Nkomati nickel sulphide ore.

iv. Is the 3D GLCM sensitive to changes in mineralogy and texture of Nkomati ore and is this comparable to the particle size distribution (PSD) information?

v. What are the potential opportunities in the mining industry where the XCT and 3D GLCM information could provide value?

This will involve the identification and development as needed in objective 1 an image processing methodology for 3D textural analysis of XCT grey level volumes of Nkomati MMZ drill core, and to compare the quantitative textural measure of this methodology with conventional metallurgical characterisation test results, to evaluate the applicability of this technique in fulfilment of objective 2.

1.4 Scope of Research

Aspects of geometallurgy, process mineralogy, advanced image analysis techniques, economic geology and comminution will be considered in this study. The development of this 3D texture analysis technique will quantitatively characterise ore textures, independent of subjective geological description but rather using a metallurgical discrimination of ore textures based on a rod mill product particle size distribution. The case study is based on a single ore only: the Nkomati MMZ nickel sulphide ore. The scope and limitation of this study are illustrated in Figure 1-5. Conceptually the drill core extracted from an ore sample represents the specific tools which are used in this study, whereas the remainder of the sample cube represents other areas within these disciplines which fall beyond the scope of the study (i.e. standard comminution test such JKRBT and Axb). The study is also limited to one sample set as a case study. Although thresh holding is a popular topic in the context of post XCT image processing, it is not part of this studies focus since thresh holding requires manual manipulation by an operator.

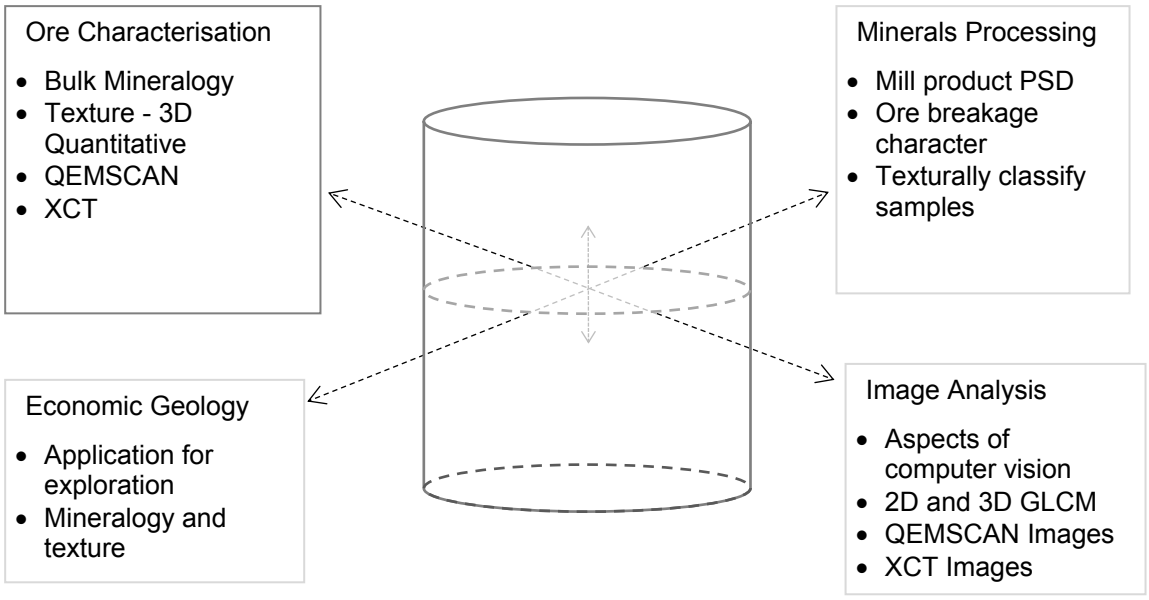

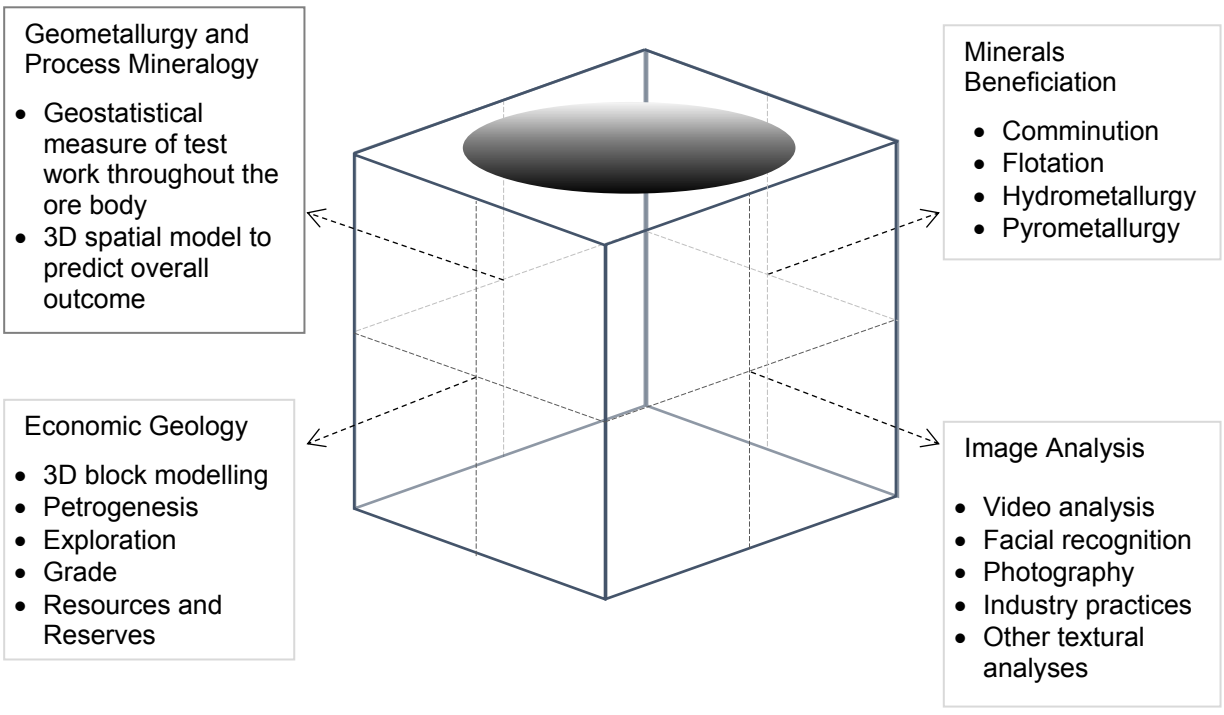

Figure 1-5: Conceptual illustration of the scope of this study. The drill core sample represents all the tools extracted from the relevant disciplines that will be used in this study while the remaining sample represents all the tools that fall outside of the scope.

1.5 Organisation of the Dissertation

The thesis is divided into six chapters: The introduction has formed the first chapter, where the background, scope, objectives and key questions are presented. Chapter 2 follows with an in-depth critical review of the literature, focussing on minerals processing, ore texture and common image analysis techniques that may be adapted for 3D images, analytical tools and techniques used in process mineralogy, as well as some background on the Nkomati ore as a case study. The sampling and experimental methods as well as detailed QEMSCAN and XCT parameter and data validation methods are documented in Chapter 3. The formal results are divided into two separate chapters, each with its own integrated results and discussion. Chapter 4 describes the development of the image analysis methods. This involves the extension of the well-established 2D GLCM image texture analysis technique to work on 3D images produced by XCT of drill core samples. The 3D texture analysis demonstrated in Chapter 4 will be applied to XCT images of Nkomati drill core extracted from the collected hand samples and will presented and discussed in Chapter 5. Chapter 6 is the conclusion of the findings before presenting recommendations for future research. The full set of raw data results and MATLAB code is given in the Appendices.

Chapter 2 : Literature Review

2.1 Rock and Ore Texture

Texture, in the geosciences, may be defined as the interrelationship of minerals comprising the rock (Craig 2001; Tarbuck & Lutgens 2008). The concept of texture in geoscience is a fundamental tool used to define the physical and mineralogical character of rocks. There are many distinct textures that are instantly differentiable to the human eye. Figure 2-1 is a composite figure that demonstrates various concepts used to describe rock texture. Figure 2-1a demonstrates three end member grain boundary types which are interlocking, matrix supported and glass or no visible boundary. Interlocking grain boundaries show clear contact between individual minerals comprising the rock whereas matrix supported show individual grain within either a larger mineral or in a glass matrix. Figure 2-1b demonstrates the visible difference between the grain size definitions fine, medium and coarse grained. Figure 2-1c demonstrates that a sample may contain more than one grain size, in this case there is equigranular where all the minerals are roughly the same size and bimodal grain size where there are two mineral populations present with distinctly different grain sizes. Finally, figure 2-1d demonstrates the presence of a preferred spatial arrangement of minerals in a rock where the mineral may be randomly oriented or parallel. The above mentioned textural descriptions are the simplest and most intuitive. Illustrations of more complex textures are given in figure 2-2. Variations in texture are caused by geological events such as igneous intrusions, sedimentation or metamorphism of pre-existing rocks. In igneous rocks, such is the character of Nkomati Ore, the texture is effected by the cooling rate of the magma, chemical interaction with surrounding country rock, nucleation and alteration to name a few.

Figure 2-1 is a graphical illustration of a few end-member textures of ore. It is a key variable which influences liberation and association (Gottlieb et al. 2000; Gaspar and Pinto 1991). There is a common goal to establish a sustainable balance between maximizing liberation, minimizing energy requirements and reducing environmental implications in comminution. Since texture is an influencing factor on this goal of sustainability, then defining it for an ore deposit is critically important.

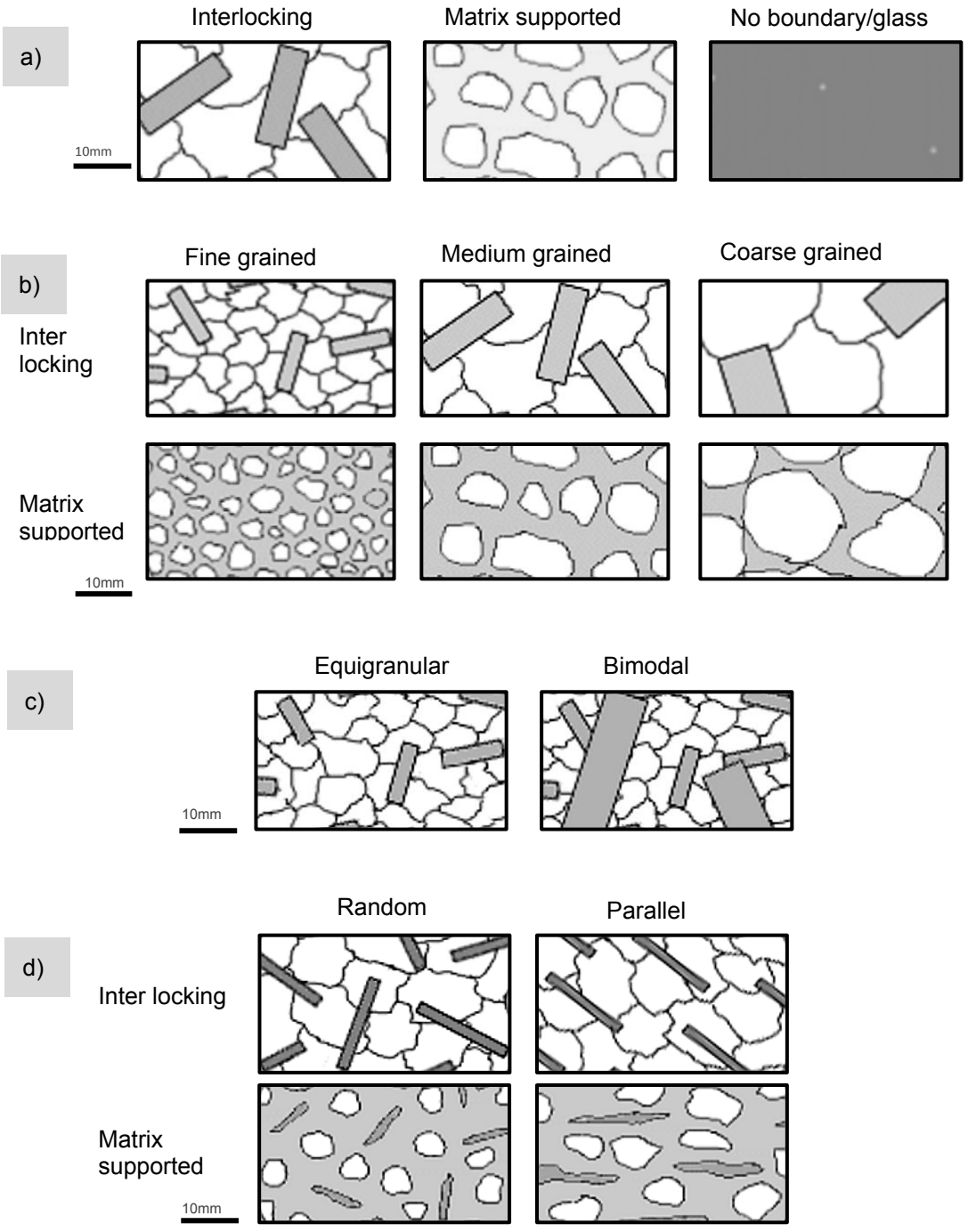

Figure 2-1: a) Endmember grain boundary types. b) Grain size definition of visual grain size. c) Grain size comparison of associated minerals. d) Mineral orientation.
(adapted from http://academic.brooklyn.cuny.edu).

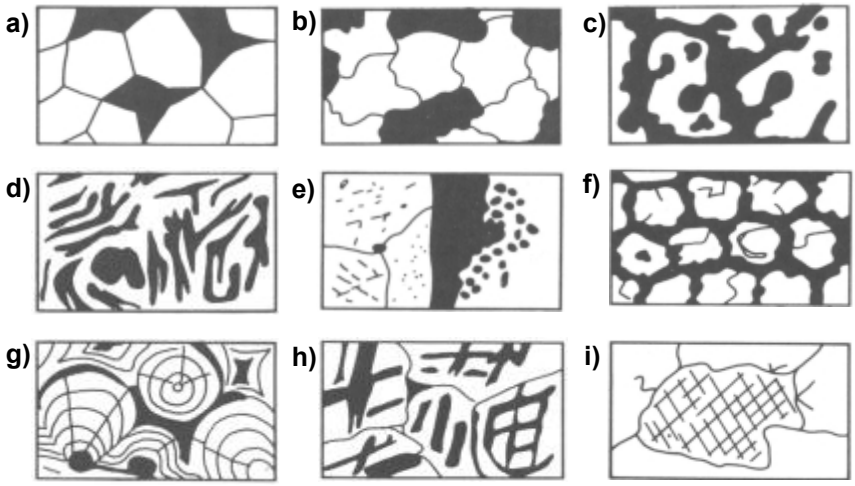

Figure 2-2: Graphical illustration of various ore textures taken from Craig and Vaughan. (1981). (a) equigranular with straight grain boundaries, (b) equigranular with curved grain boundaries, (c) Mottled or net with partial penetration, (d) micro penetration, (e) disseminated, (f) intergranular or rimmed, (g) concentric, (h) planar, (i) intergrowth textures.

2.2 Texture and Comminution

This section will explore various apparatus, tools, analytical techniques and methodology used in minerals processing as well as some advanced process mineralogy techniques and innovations. This section focuses on comminution, since comminution is the first step in minerals processing and also the most energy intensive. Therefore the better use of textural information to understand breakage is a major opportunity.

It is well known that ore texture is a controlling factor of the minerals processing behaviour of valuable minerals (Pillay et al. 2011; Oyarzún and Arévalo 2011; Ghorbani et al. 2013), and that minerals processing must be optimised to deal with ore variability (Lotter et al. 2011). An example of this is the development of IsaMill technology for fine grinding of ultrafine grained sphalerite at Mt Isa in Australia (Pease et al. 2004). Pease (2004) explained that the sulphides from McArthur River ore deposit display high mineralogical complexities and smaller grain sizes than the massive sulphide ore from Broken hill. The major difference in the mineralogy is the grain size distribution (Figure 2-3). Consequently the development of the stirred milling technology which is a more efficient technology to achieve size reduction for ultra-fine grinding (Jankovic, 2003).

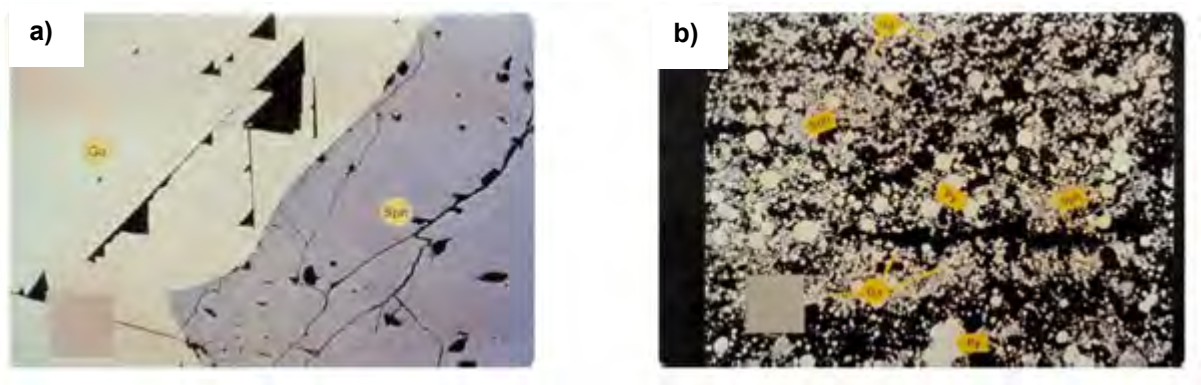

Figure 2-3: Two texturally different sulphide ores types. a) Image of Broken hill ore showing massive texture of galena and sphalerite. b) Image of McArthur River ore showing fine grained sulphide ore (Pease et al. 2004). Both images given at same magnification, no scale bar given.

Vizcarra et al. (2010) investigated the effects of two breakage mechanisms on the liberation of two ore types (a massive sulphide ore and a complex fine grained sulphide ore). The ore types were milled using a particle bed breakage mechanism and an impact breakage mechanism. Figure 2-4a shows the grain size distribution of quartz vs the degree of liberation of quartz in ore type 1. the overall trend indicates that the quartz was initially coarse grained with a constant grain size reduction. Figure 2-4b shows the grain size distribution of quartz vs the degree of liberation of quartz in ore type 2, the overall trend indicates that the insitu quartz may be bimodal in size and larger grained than that in ore type 1. The coarser fractions show less liberation and the finer fractions show greater liberation. The results illustrate the dependence of liberation on ore texture (coarse vs. fine grained).

Another useful concept for describing liberation is the theoretical grade recovery curve (Figrie 2-5a) and the actual grade recovery curve (Figure 2-5b)(MinAssist, 2005). If the actual grade recovery curve is below the theoretical curve, as in B this indicates that there is room to improve grade and recovery. Similarly, for the actual curve to match the theoretical curve the texture of the ore must be favourable to the breakage mechanism since the liberation of a target mineral is a function of the overall ore texture and the mechanism used to break the ore. This means that defining and understanding the metallurgical performance of each ore texture type then planning the minerals processing of which presents the opportunity for improving grade and recovery at the current liberation.

There are also numerous instances where texture has been used to indicate ore behaviour. Textural indexing for the prediction of acid rock drainage (ARD) (Parbhakar-Fox et al. 2011) was developed to predict the risk of ARD formation based on intact rock textures. Mineralogy, texture and association are key components for formation of ARD. Oyarzún and Arévalo (2011) introduced the grindability index (BWi measured as kWh/st) for rock textures in a geometallurgical application. The study was carried out on igneous rock with a variety of textures. Their findings indicate that the linkage (grains boundaries condition) between minerals is a controlling function of a rock's grindability (a resistance to crushing). Simple mineral interfaces require less energy to break, and vise versa.

a)

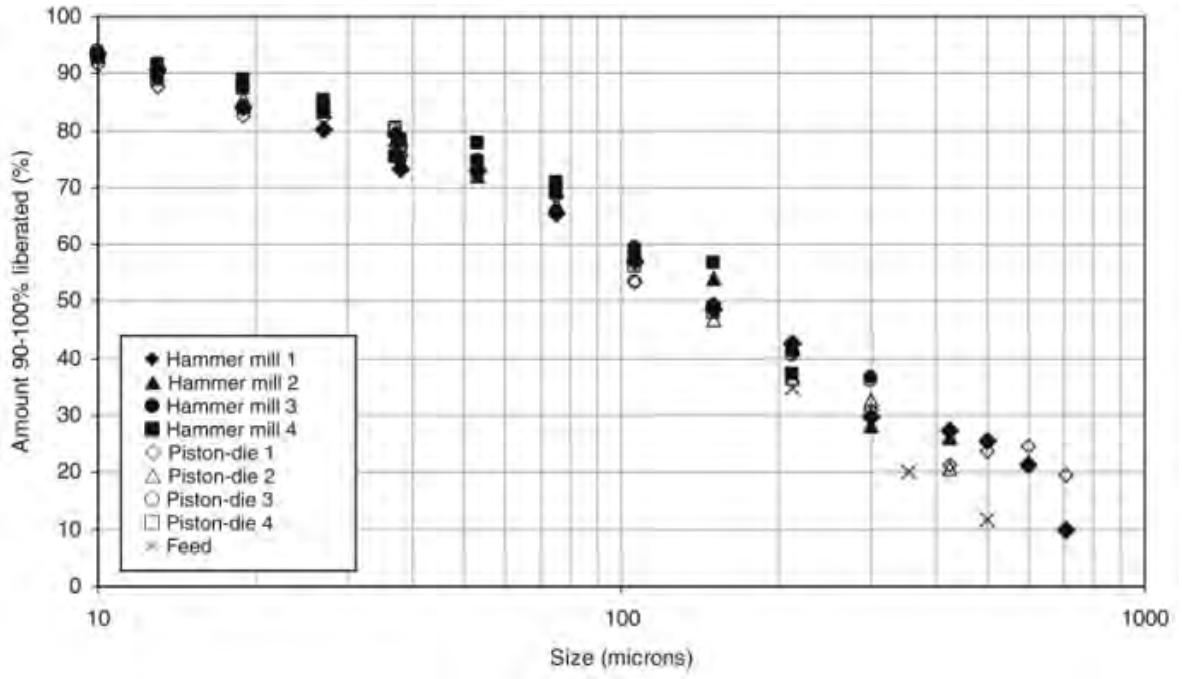

b)

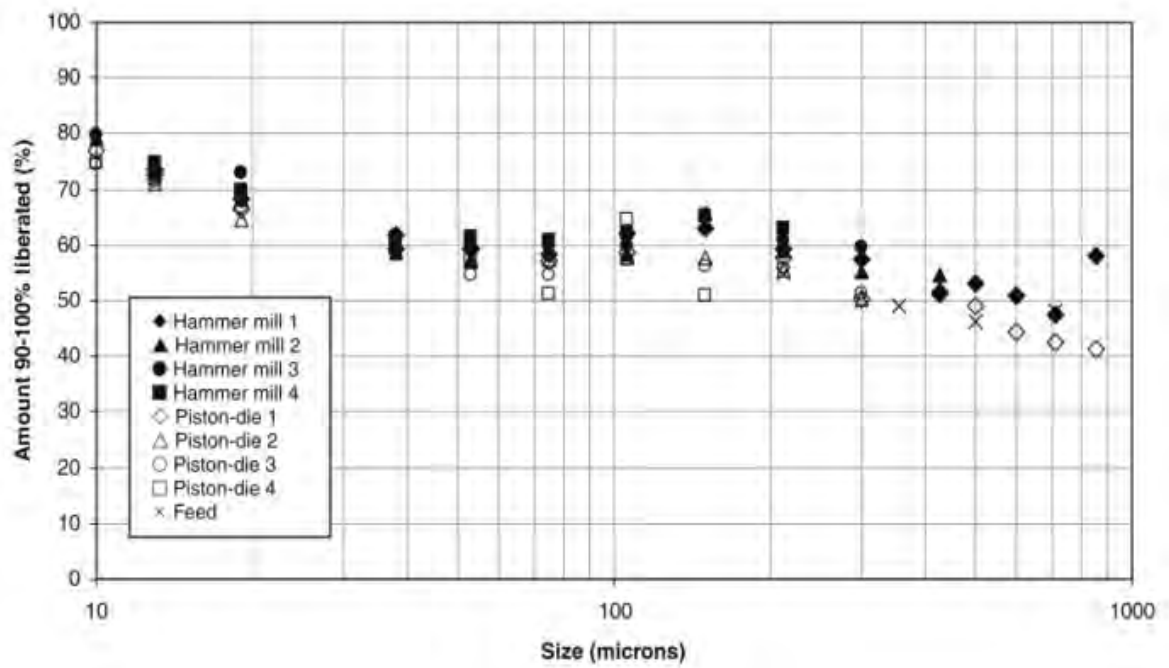

Figure 2-4: The grain size distribution of quartz in the two different ore type tested by. a) Ore type 1 is dominated with feldspar magnetite and mica with 8 wt% quartz. b) Ore type 2 is dominated by quartz (40 wt%), sphalerite and carbonates (Vizcarra et al. 2010).

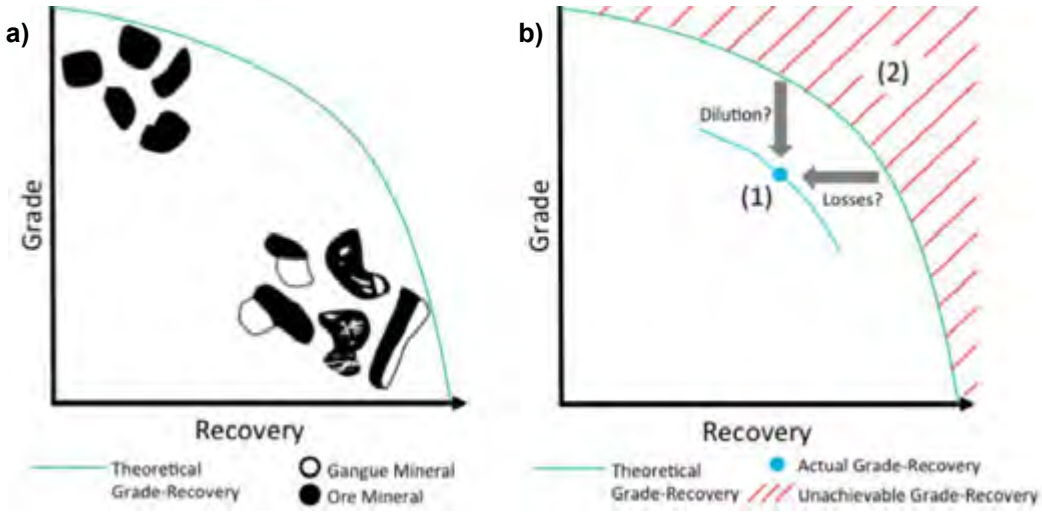

Figure 2-5: Illustration taken from MinAssist, (2005). a) Theoretical grade recovery curve. b) Actual grade recovery curve.

Work done by Wightman and Evans (2013) on the development of the liberation spectrum demonstrates how variations in the size by size liberation pattern reflect on the character of ore mineralogy, this liberation spectrum is presented in figure 2-6. This spectrum presents three important measurements for the interpretation of ore texture and association based on liberation. These are the head grade (Figure 2-6 A), the grain size at which liberation begins (Figure 2-6 B) and the particle size population (Figure 2-6 C). All of these measurements are a direct function of ore texture and association. The concept of a liberation spectrum has value in identifying whether an ore has a single compositional grain size population or multiple grain size populations. For example, in the case of identifying a target mineral with a single grain size distribution trend, the assumption can be made that the ore will logically require a single milling stage or parameter. However, if the ore has multiple target mineral grain populations it may need a carefully designed milling flowsheet and milling parameters such as that presented by Lotter et al. (2011) in figure 1-2.

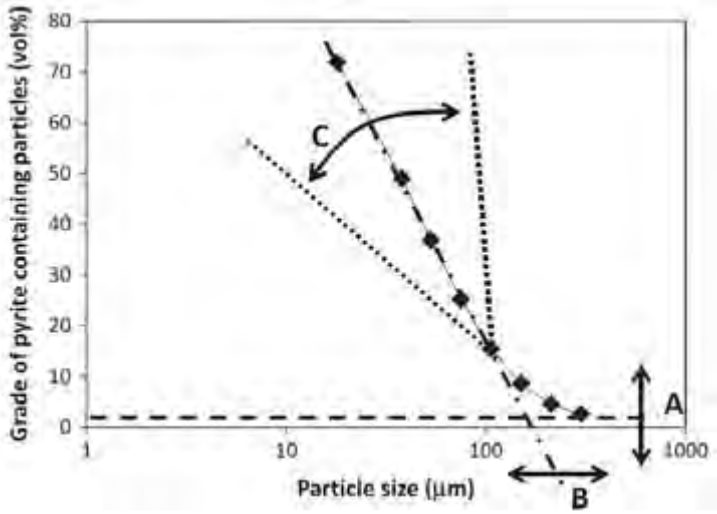

Figure 2-6: Graphical representation of the liberation spectrum form MLA data as seen in Wightman and Evans(2013). (A) Represents the head grade of the ore. (B) Represents the grain size at which liberation begins. (C) is the slope of the curve which represents the distribution of grain sizes.

2.3 Tools Used in the Acquisition of Mineralogical and Textural Data

The study of mineralogy has evolved from the use of optical techniques, which generally produce small data sets, to established analytical techniques such as auto-SEM technology (e.g. QEMSCAN, MLA, TIMA) which are generally accepted analytical methods for ore characterisation (Hartner et al. 2011; Chetty et al. 2009; Liebezeit et al. 2011). These instruments provide detailed quantitative information on bulk mineralogy, grain shape, size, liberation and association in two dimensions.

2.3.1 AutoSEM Technology

The method to analyse mineralogy by quantitative evaluation of minerals by scanning electron microscope or QEMSCAN (one of a few autoSEM instruments on the market) has given the mineralogist the ability to acquire and organise large amounts of mineralogical data of the analysed specimen. This, along with adequate software, allows for endless data analysis, such as: bulk mineralogy, mineral associations, ore texture, mineral and particle grain size distributions, mineral grain and particle shape characteristics, liberation, elemental deportment, and the capturing of field images to name a few. The data acquisition is automated following a predefined raster scan pattern (Gottlieb et al. 2000; Fandrich et al. 2007; Pascoe et al. 2007). The apparatus is complete with a scanning electron microscope, a large specimen chamber, Energy-dispersive X-ray spectroscopy (EDS) detectors, and iDiscover software (Andersen et al. 2009; Rollinson et al. 2011). Although autoSEM technology has been implemented on site in the mining industry there are significant limitations. The extensive sample preparation and long scanning times act as a bottle neck if there are a large number of samples that need to be analysed.

2.3.2 X-ray Computed Tomography (XCT)

The use of 3D XCT for mineral and textural characterisation based on the X-ray attenuation coefficients of mineral phases presents an alternative rapid method for non-destructive ore characterisation and textural classification, especially when the results are coupled with auto-SEM technology. The area in which XCT has the most potential to deliver value in minerals processing however, has yet to be clearly ascertained (e.g. evaluation of drill core, crusher product, mill product, flotation products etc.).

The XCT scanner is purely an X-ray emitting analytical machine. A mineralogical specimen exposed to the incident X-ray will attenuate the X-rays. The attenuation of X-rays is proportional to the mineral density and atomic number (Z) through which X-rays pass (Ketcham and Carlson 2001). The use of

linear attenuation coefficients of minerals as a function of X-ray energy aids in the discrimination of minerals in XCT data (Kyle et al. 2008; Cnudde and Boone 2013). The X-ray beam, which is conical is shape, is generated from the choice of two X-ray tubes; one tube which emits a strong X-ray beam while the other emits softer X-rays. The same concept can be applied to a CT scanner configuration as displayed in figure 2-7 (Cnudde and Boone 2013). The closer the object is placed in front of the X-ray source, the larger the X-ray shadow will be on the detectors and thus increasing the final image resolution.

The ability to image structures and the spatial relationships of minerals in 3D is a significant advantage that XCT has over other advanced 2D imaging techniques since the data is not subject to stereological error. Figure 2-8 illustrates the effect of stereological error in the 2D image analysis of a sphere (Van Dalen and Koster 2012). In mineral processing it is common practice to analyse this-sections through a rock to identify minerals and characterise ore. As illustrated in figure 2-8, if a mineral is represented as a sphere in a section, there is a relatively high frequency that the mineral will be intersected with a radius of r at a distance away from its centre point (where the true radius is R). Imaging by XCT presents the opportunity to remove this streological error.

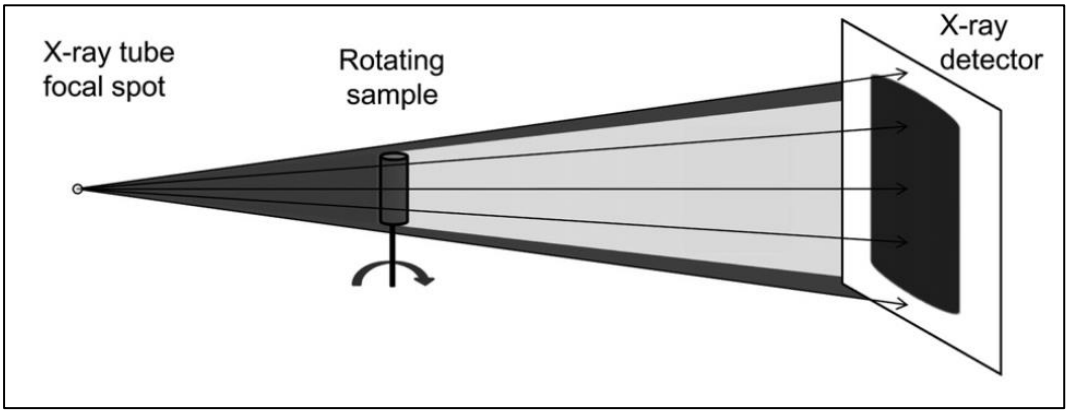

Figure 2-7: Conical shape of X-ray beam from X-ray tube to detector with the sample rotating in the centre (Cnudde and Boone 2013).

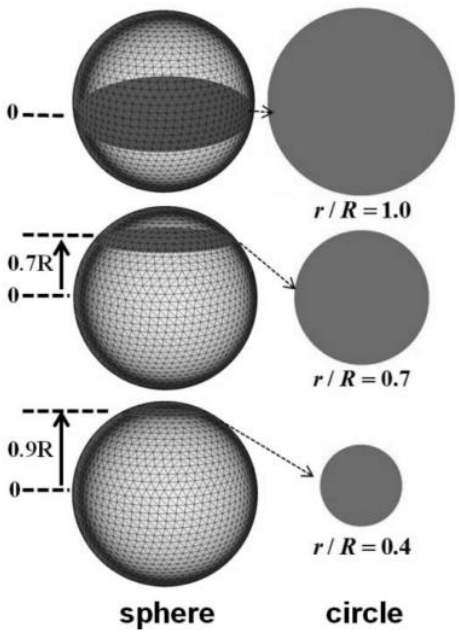

Figure 2-8:Stereological error associated with 2D image analysis of a section through various heights of a sphere (Van Dalen and Koster 2012)**.**

Some of the XCT applications in the geosciences are presented in table 2-1. Although XCT imaging may open the door to 3D quantitative sample analysis, there are a few limitations that need to be overcome. In the field of geoscience the most prominent limitation is its ability to accurately identify detailed mineralogy. This is largely due to the fact that X-ray differentiates material by density, and since some compositionally different minerals have similar densities they appear to have the same pixel brightness in XCT images. Artefacts are unavoidable in CT scanning but can be minimized or limited by proper choice of parameter set up. The most prominent artefact is a beam hardening which is due to the polychromatic nature of an X-ray beam (Cnudde and Boone 2013).

The CT scanner produces a series of two dimensional projection images through the sample analysed. X-ray images are produced at predetermined incremental rotations of the sample and are compiled and reconstructed with volume rendering software to produce a three dimensional version of the object scanned. This digital volume maps out the density variations throughout the entire object. The resultant volume comprises a number of voxels (volumetric pixels) each with an assigned grey value.

Table 2-1: Application of XCT in the Geosciences.

XCT applications	
Description	**Source**
Characterisation of oil reservoir sediments.	Ketcham and Carlson 2001; Cnudde and Boone 2013
Association of PGM's between grain boundaries of sulphide and chromite minerals.	Godel et al. 2010; Godel 2006
Gold characterisation	Dominy et al. 2011
Monitoring leaching applications of valuable minerals.	Dhawan et al. 2012; Ghorbani et al. 2013; Kodali et al. 2011
A comparison between high pressure roll grinding (HPGR) and conventional tumble milling. HPGR caused higher fracturing and better leaching performance.	Dhawan et al. 2012
Compositional population distributions as volumetric measurements.	Lin and Miller 1996
Variation in X-ray energy for the discrimination of minerals phase.	Kyle et al. 2008
Mineral deposit origin, evaluation, and processing	Kyle and Ketcham 2015

2.4 Computer vision: Modern texture analysis and classification techniques

There are numerous computer vision techniques that aim to acquire, process, analyse and understand images in order to produce symbolic or numerical information. The main idea behind computer vision is to replicate the human ability to perceive and understand an image so that the information can be used to make accurate decisions. This is done by unfolding the image data using geometric, physical and statistical methods. Figure 2-11 is taken from Brosnan and Sun (2002) and illustrates the computer vision system. The overall objective of this system is to provide the appropriate information for a control, recognition, decision or other similar systems.

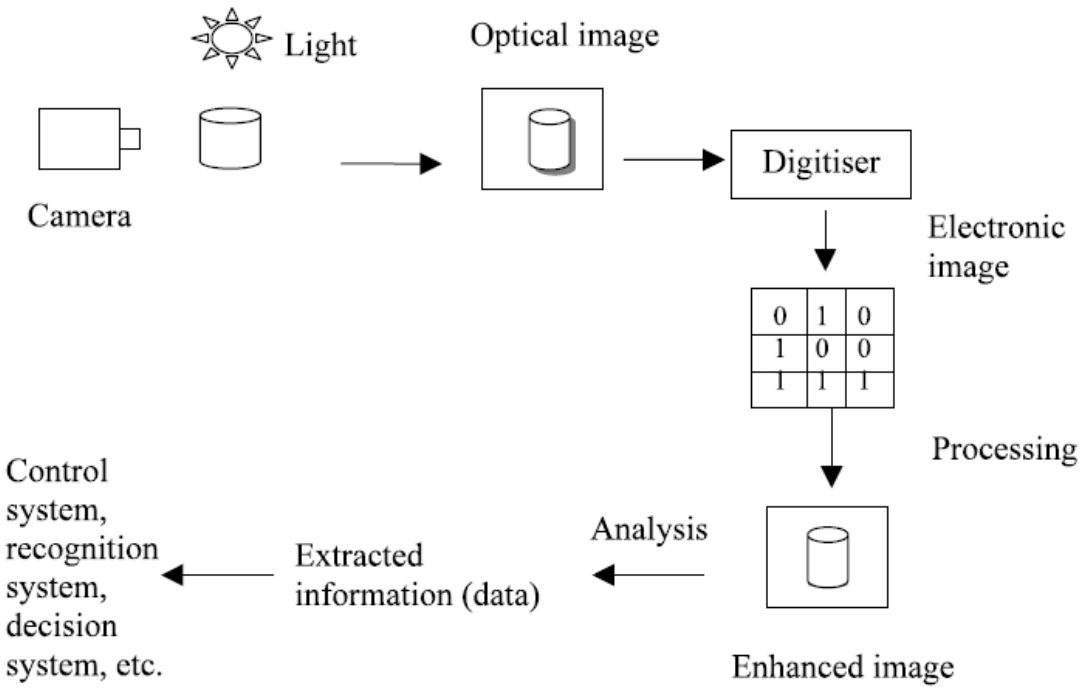

Figure 2-9: Conceptualisation of a computer vision system (Brosnan and Sun 2002).

XCT produces excellent 3D imagery of the internal structures within the cores scanned in this project. The objective in this section is to review the relevant image processing techniques that may be appropriate to analyse XCT imagery. The technique must act to classify ore according to its internal structures and texture. This section reviews relevant image processing techniques for minerals processing, to provide a holistic view of the importance of the contribution of computer vision. The following methods are considered for QEMSCAN and XCT imagery, because these are the two techniques employed in this study.

2.4.1 Linear Intercept Method

Pérez-Barnuevo et al. (2013) used linear intercepts to perform textural analysis of 2D images (for any 2D imaging technique) of ore particles in mill feed for texture analysis. This is a 2D method where information is extrapolated to define 3D character but the method is limited by stereological error. The method is applied by superimposing lines on an image of a particle. The lines are set regular distances apart where each line that intercepts a grain boundary is counted. The method detects whether the intercepts of the grain boundaries are phase-phase or phase-background transitions. The distances between interceptions on a line is also measured, this is the distance the line occurs within one phase. Once all the distances and intersections have been totalled, a new line direction is considered. There are 18 line directions for this method. In the work done by Pérez-Barnuevo et al. (2013) there are three important parameters derived from this data, which are: phase area, phase perimeter and surface area. Figure 2-10 illustrates synthetic textures that may exist in a particle for a

complex copper ore. These synthetic texture descriptors are proposed as texture identifiers. The study concluded that there is a 95% accuracy in classifying mineral phases according to texture type.

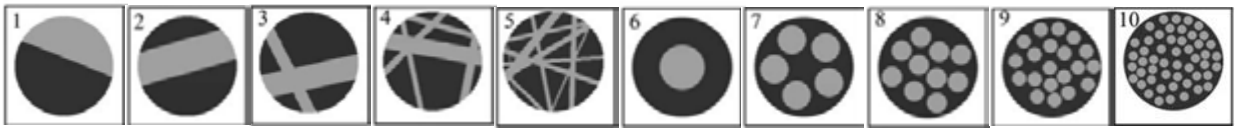

Figure 2-10, 10 synthetic textural descriptors used to validate the linear intercept method results (Pérez-Barnuevo et al. 2013).

2.4.2 Nucleation Digitiser

Deison et al, (1997) created an image analysis technique to determine crystal size distribution. The data was compared to conventionally accepted numerical simulations. The image analysis was applied to XCT images as can be seen in Figure 2-11. The image analysis software generates an idealised digital replica with well-defined circles that indicate the position and size of the porphyroblasts. This method is limited to the analysis of porphyroblastic nucleation (special location at which the large mineral, in a bimodal mineral size rock, begins crystalizing), although it does shed light on the possibility of defining texture to an extent. The analysis is specific to spherical crystallisation and therefore limited to the analysis of spherical particles and grains.

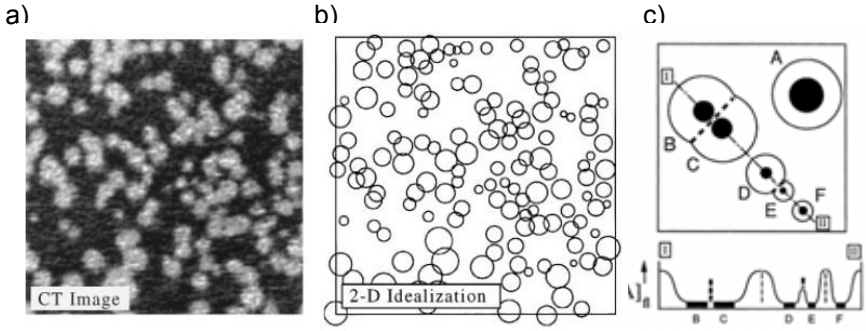

Figure 2-11: a) XCT image of a porphyroblastic igneous texture. b) Processed imaged to clarify prophyroblast grain boundaries. c) Porphroblastic descriptors (Deison et al. 1997).

2.4.3 Local Binary Patterns

Local binary patterns or LBP are used in computer vision for image classification. LBPs were first proposed as part of the texture spectrum established in 1990 (Wang and He 1990) and further described in detail by Ojala et al. (1996). LBPs determine the local variation in neighbouring pixels from a selected pixel of interest (POI). Figure 2-12 illustrate the concept of textural analysis by the LBP calculation. This method works by selecting a POI and comparing this pixel to its neighbouring pixels. It first considers the top left most neighbour and calculates if the neighbouring pixel value is higher or lower. If the value is higher then the local binary pattern is credited with a 1 and if the neighbour is lower then the first value in the LBP is credited with a 0. This calculation is repeated for

each of the neighbouring pixels in a clockwise manner, where each 0 or 1 is concatenated to the LBP. Once the LBP for the POI is completed the next pixel is selected as the POI until all the pixels in the image have been considered. The biggest advantage with this method is that it is directionally invariant, meaning that image orientation is not a controlling factor of the binary output. The combined LPB information for that image acts as a finger print. This computer vision technology has been used in face regognition software (Face recognition with OpenCV, 2015). Local binary patterns have also been used in the analysis of 3D CT images in the medical field for the identificaiton of problematic brain tissue (Gao et al. 2011).

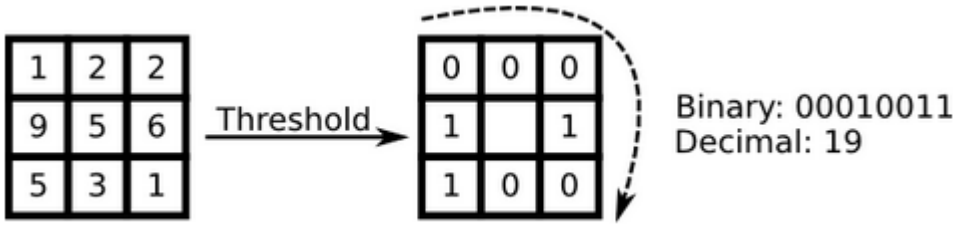

Figure 2-12: Diagram illustrating the fundamental analysis of a local binary pattern (LBP).

2.4.4 Grey Level Co-occurrence Matrices (GLCM)

Since the introduction by Haralick et al. in 1973, grey level co-occurrence matrices (GLCM)(also referred to as grey tone special dependence matrices), have become well established in the digital examination of image textures. A GLCM is a summary of the spatial relationship between grey values in an image. Once GLCMs have been defined, statistical information can be extracted relating to the textures present in the image.

Haralick (1973) mathematically described two-dimensional images as a function of two variables (x, y), stored digitally as a two-dimensional array in computation. If $\mathrm{Lx} = \{1, 2, , Nx\}$ and $\mathrm{Ly} = \{1, 2, , Ny\}$ are the spatial domains for X and Y, then $\mathrm{Lx} \times \mathrm{Ly}$ represents the image pixel resolution. The image I is then a functions which assigns some grey value $\mathrm{g} \in \{1, 2, , Ng\}$ to each of the resolutions cells;

$$I: Lx \times Ly \rightarrow g \qquad (1)$$

Grey values intensities in an image I may range from 8-bit to 32-bit, this is 2^8 = 256 and 2^{32} = 4294967296 grey level values (G) respectively. GLCM may be direction specific or a combination of all the possible four pixel pair directionalities in 2D (Figure 2-13a), which is expressed as a function of displacement $d = (dx, dy)$. This differs from the conventional Cartesian orientations, dx measures vertical displacement increasing downwards and dy measures horizontal displacement increasing to the right. The remaining 4 pixel pair directions can be defined by the transposition of their corresponding directional GLCM. This is because the addition of a directional matrix with its opposing directional matrix will result in a symmetric matrix.

For example, the greyscale image in figure 2-13b presented as a 4 x 5 table of pixel values is subject to a GLCM analysis which considers a pixel pair direction of 0° (0, 1) (a reference cell and its right-hand neighbour) to populate a GLCM with dimensions 8x8 as presented in figure 2-13c. The result is a unique matrix for each of the texture types analysed in 2D. This presents the ability to accurately and autonomously group images displaying similar texture. GLCM have been used extensively in 2D applications such as texture retrieval, texture segmentation and in the monitoring of textural changes in video feed (Kistner et al, 2013; Tuceryan. 1998; Vacchetti et al. 2004). In a geological context, texture retrieval by GLCM is one application that has been used successfully in the image analysis of photomicrographs of thinsections or macrographs of polished rock sections (Partio et al. 2002). This texture analysis is a 2D distribution that represents the spatial relationship between all the pixel pair combinations in an image. The application of GLCMs has been extended to 3D seismic data (See figure 2-14 adapted from Eichkitz et al. 2013), as well as its development in the medical field (Dhara et al. 2012).

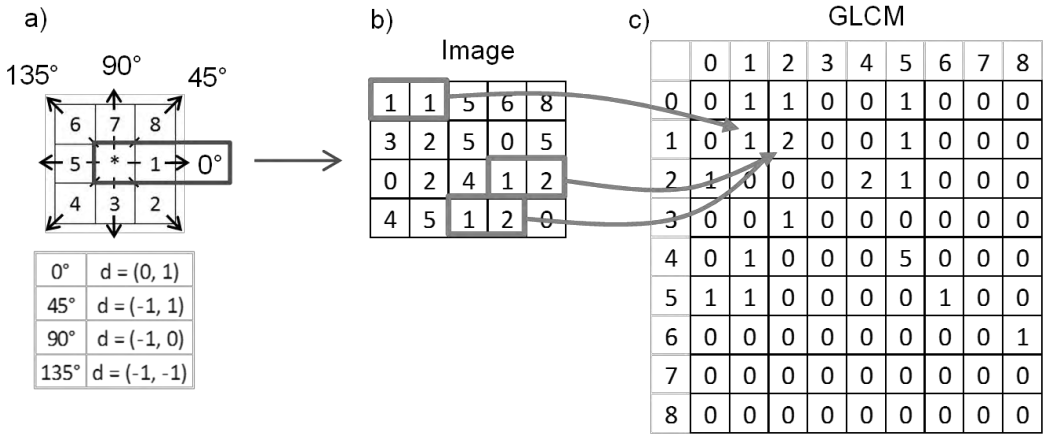

0°	d = (0, 1)
45°	d = (-1, 1)
90°	d = (-1, 0)
135°	d = (-1, -1)

Figure 2-13: a) the four main pixel pair directions for calculating GLCM. b) a grey level value grid of n image. c) the corresponding GLCM calculated form the image in (b) of the 0° (0,1) pixel pair direction.

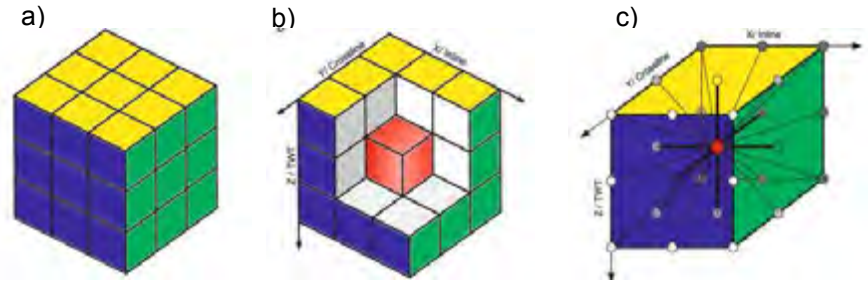

Figure 2-14: Three dimensional illustration of the application of GLCM on a three dimensional image. Rubik's cube best illustrates three dimensional adjacency of voxels in a, b and c. The flow plan that links the two dimensional analyses together is illustrated in d. (Eichkitz et al. 2013).

2.5 Nkomati Nickel Mine: Case Study

Ore from Nkomati Nickel mine in South Africa will be used as a case study. The mine is jointly owned by Norisk Nickel and African Rainbow Minerals. There is a measured and indicated resource of 281 Mt at 0.34% Ni and 0.86 $g.t^{-1}$ PGMs as well as 0.23 Mt at 33.95% Cr_2O_3. It has proved and probable reserves of 128.61 Mt at 0.32% Ni and 0.93 $g.t^{-1}$ PGE as well as 0.23 Mt at 27.92% Cr_2O_3. Since 2009 until 2014 nickel production has been ramping up from 4 400 tonnes to 22 800 tonnes, copper from 2 200 to 10 100 tonnes, PGM from 26 700 to 185 100 ounces. As expected milling tonnage has also increased over this period from 1 200 000 tonnes to 7 900 000 tonnes with an overall decrease in the head grade of nickel from 0.54% to 0.39% (AMR Annual Report 2014).

2.5.1 Geology

The Uitkomst complex is located in the Eastern Transvaal (Figure 2-15)(Li et al. 2002) and is comparable to Bushveld Complex ore since it is composed of the same source material, has a similar age and is located in the Transvaal Supergroup (a sedimentary succession that is host to the Bushveld Complex)(De Waal et al. 2001).

The physical emplacement mechanism is different to that of the Bushveld Complex. It has been identified as a feeder pipe that once fed a magma chamber. The conduit body is 800m wide, 800m thick and is roughly 8km long, with a gently dipping northwest plunge. Conduits generally reactivate multiple times when injecting magma into a chamber (De Waal et al. 2001). This reactivation is partly responsible for the high degree of mineralogical variations and metamorphism that is so prevalent in the Uitkomst Complex.

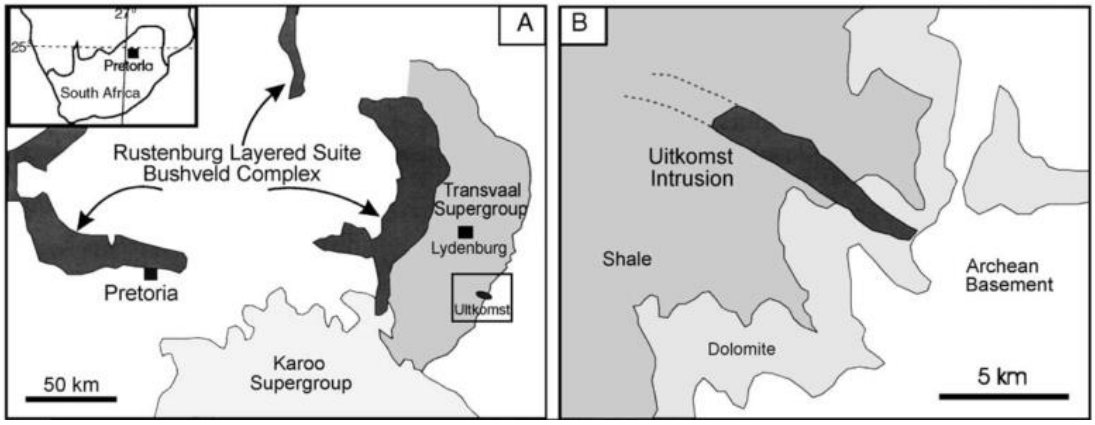

Figure 2-15: Geological map of the Uitkomst Complex (Li et al. 2002).

Similar to the Bushveld Complex, the Uitkomst Complex has a layered character (Table 2-2). The base units comprise basal gabbro which range from 0-12m in thickness and contains a chill zone characterised by the presence of aphanitic gabbro roughly a 1m thick in contact with the quatzite Oaktree Formation. The gabbro consists of orthopyroxene, clinopyroxene and plagioclase with low

occurrence of olivine. Accessory minerals that are present are quartz, magnetite and sulphides. The basal gabbro transitions into a lower harzburgite unit which consists of ultramafic harzburgite, wherlite, peridotitie, websterite and xenoliths of dolostone. The mineralogy of this unit is typically olivine, ortho- and clino-pyroxene, plagioclase, and chrome spinel. The chromite content in this unit increases with decreasing depth resulting in a cumulate chromian spinel of the chromitiferous harzburgite unit. The mineralogy of this unit is predominantly poikiloblastic olivine and chrome spinel with orthopyroxene as an interstitial phase. The top of this unit consists of massive chromite. The main harzburgite unit overlies this massive chromite and consists of oikocrystic orthopyroxene with chadacrysts of olivine and chromite. The overlying pyroxenite unit is defined by the sudden increase of modal orthopyroxene (Gauert. 2001; Gauert et al. 1995; De Waal et al. 2001).

Pentlandite is the primary nickel sulphide ore mineral and is strongly associated with pyrrhotite, which is the most abundant sulphide mineral within the ore body. Sulphide mineralisation occurs in the Basal Mineralised zone (BMZ), the Main Mineralised Zone (MMZ), the Chromititic Peridotite Mineralised Zone (PCMZ) and the Massive Sulphide ore body (MSB)(De Waal et al. 2001; Gauert. 2001; Gauert et al. 1995).

Table 2-2: Summary of the lithological units of the Uitkomst Complex and their spatial relation to the proved ore reserves (Adapted from Li et al. (2002)).

Ore zones	Lithologic Unit	Types of contacts	Petrography	Sulphide mineralisation	Alteration
None	**Upper Gabbro**	Chilled contact with hanging wall sediments.	Sub horizontal modal layering.	Mostly sulphide barren.	Weak uralitization and saussuritization.
	Gabbronorite	Sharp with upper gabbro.	Massive to intergranular.	Mostly sulphide barren.	Weak uralitization and saussuritization.
	Pyroxenite	Gradational with gabbronorite.	Intergranular with cumulus augite.	Sulphide-barren to weakly disseminated sulphide.	Weak saussuritization.
	Main Harzburgite	Transitional with pyroxenite.	Olivine + minor chromite cumulate.	Weakly disseminated sulphide in places.	Moderate serpentinization.
Peridotitic Chromititic Mineralized Zone	**Chromitiferous Harzburgite**	Grading into Main harzburgite.	Olivine + chromite orthocumulate	Weakly disseminated	Extensive serpentinization, talc-carbonate alteration.
Main Mineralized Zone	**Lower Harzburgite**	Grading into chromitiferous harzburgite with increasing olivine and chromite.	Between feldspathic harzburgite to olivine websterite with cumulus olivine and chromite.	Disseminated to Net-textured.	Moderate serpentinization, talc-carbonate alteration.
Massive Sulphide Body & Basal Mineralized Zone	**Basal Gabbro**	Transitional with Lower harzburgite, discontinuity along strike.	Phaneritic with plagioclase, augite and rare olivine.	Blotchy sulphide to massive vein.	Moderate uralitization and saussuritization.

2.5.2 Mineral Processing Flowsheet

Cockburn (2013) highlighted the challenges and successes faced on the processing plant at Nkomati (problematic peddle sizes that cause reduced throughput and increase crusher down time, and factors that increase energy consumption). The site currently operates two plants processing MMZ and PCMZ ore respectively. The two ore types have similar mineralogy only differing in chromite content. The PCMZ is chromite containing whereas the MMZ has very low amount of chromite. The boundary between the ore types is not well defined and thus is difficult to delineate and separate the two ores efficiently.

Figure 2-16 illustrates the flow sheet design for the MMZ ore consisting of crushing, grinding, classification and flotation.

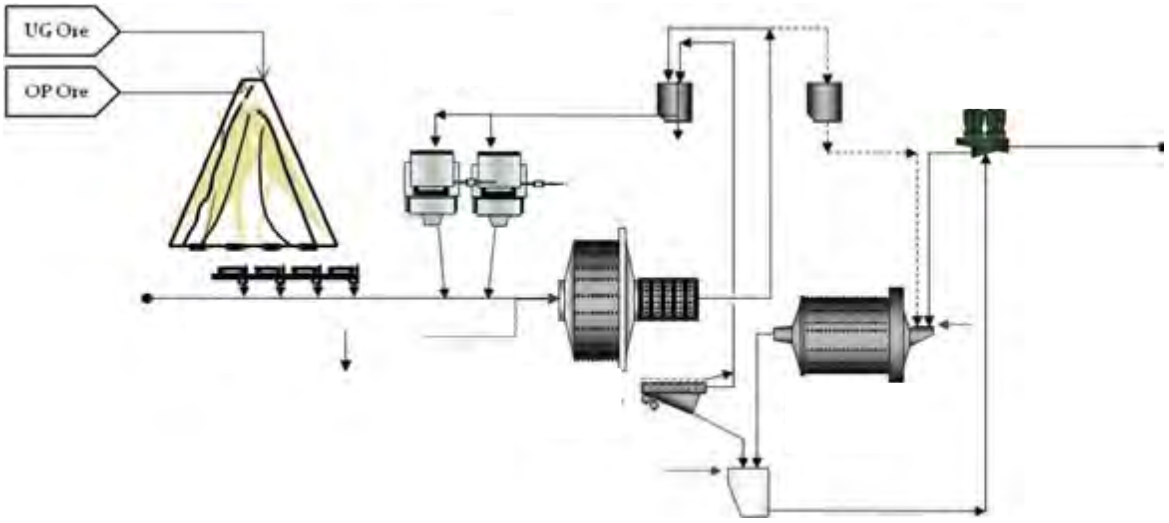

Figure 2-16: MMZ milling circuit flow sheet (Cockburn 2013).

2.5.3 Process Mineralogy Studies

Mishra et al, (2013) conducted a study of the influence of mineralogy and ore texture on the flotation performance of pentlandite for the Nkomati nickel mine in South Africa. The study show cased six dominant textures: coarse-net, fine-net, bleb, coarse-disseminated, fine-disseminated, and massive textures. The study concluded that fast flotation high grade concentrates are characteristic of the coarse sulphides which have a low abundance of silicate and alteration minerals. These are texturally described as massive, semi-massive, coarse-disseminated, coarse net-textured and coarse bleb-textured. The ore that have an intermediate flotation response has lower nickel concentrate grade which have a high abundance of silicate and associated minerals. This ore texture is fine-disseminated, bleb-textured, and fine-net textured. Ore that has a slow flotation response has a low nickel concentrate grade, which has a high abundance of altered amphibole and pyroxene. Pyrrhotite is also present with fine flame textured pentlandite. This ore is bleb-textured and fine net-textured. Figure 2-20 shows greyscale photographs of the texture types defined in this study (Mishra et al. 2013).

Pillay et al. (2011) conducted a density medium separation of MMZ ore for the pre-concentration of pentlandite (increased Ni grade from 0.4% to 0.7% in flotation feed) and the removal of unwanted gangue prior to flotation. Further mineralogical investigation showed the effective removal of the alteration minerals such as chlorite, quartz and carbonates while increasing the relative concentration of the BMS, pyroxene and olivine. Pillay noted that particle size has an effect on the efficiency of the separation mechanism and that ore texture is a contributing factor of mill product particle size distribution.

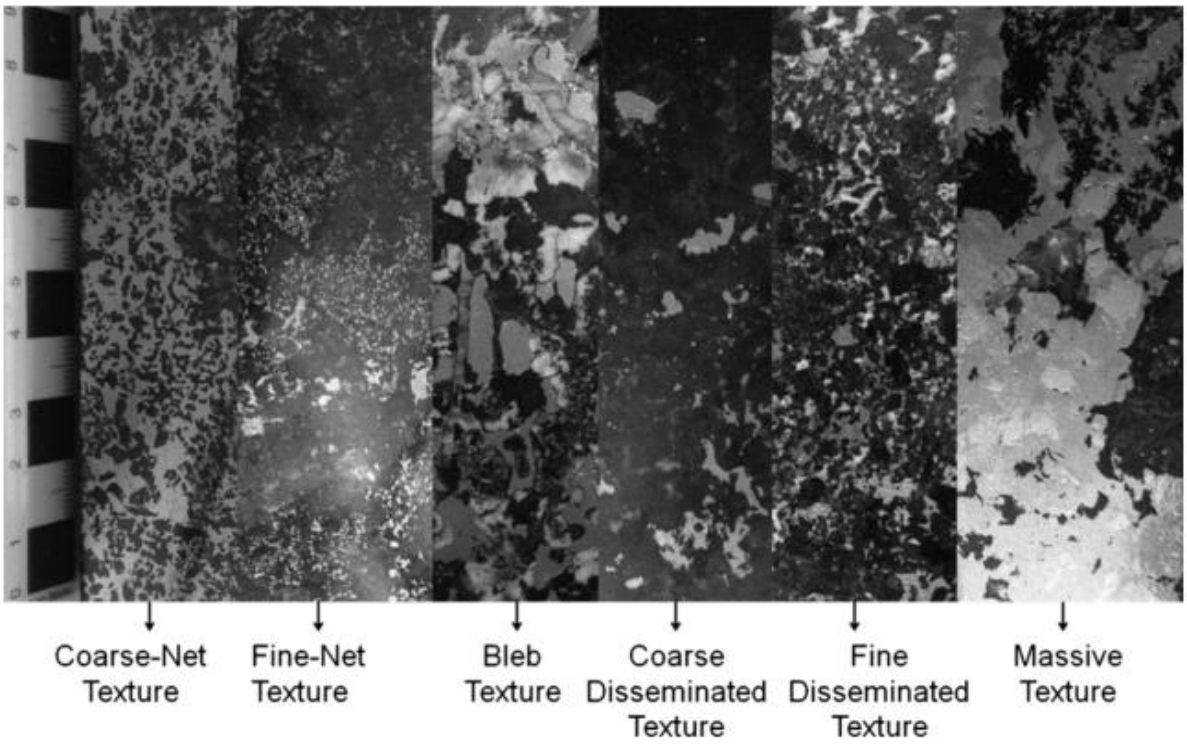

Figure 2-17: Photographs of typical sulphide textures found in the MMZ of Nkomati nickel mine in South Africa (Mishra et al. 2013).

2.6 Critical Review of the Literature

Texture, defined as the interrelationship of minerals comprising the rock, is a critical parameter controlling downstream minerals processing. The work of Vizcarra et al. 2010 has been used as a key example to illustrate the effect of ore texture on breakage and liberation. The prevalence of complex fine grained textures have even led to the development of new stirred milling technology for energy efficient liberation. Some practical concepts for illustrating liberation such as the theoretical grade recovery curve, and liberation spectrum have also been described in Section 2.2.

Mineralogy and texture can be described by a number of methods, varying from subjective, qualitative descriptions by the geologist to the quantitative auto-SEM technology (e.g. QEMSCAN, MLA, Mineralogic, TIMA). Although auto-SEM techniques are considered the work horses in process mineralogy, the method is not practical as a routine, online method for quantitative textural analysis of drill core. The XCT has the potential to rapidly, and non-destructively image the internal structure and texture in 3D. XCT data is not subject to stereological error. However, the lack of mineral phase delineation in XCT data, and the ability to quantify internal textures is an on-going challenge.

Several existing techniques for quantitative texture analysis were reviewed in section 2.3, namely; linear intercept method, nucleation digitiser, local binary patterns (LBP) and grey level co-occurrence matrices (GLCM).Of the four techniques described, only LBP and GLCM do not require calibration

with model-like images such as the descriptor presented for the linear intercept method. A key goal of the analysis technique is whether it has potential to be fully automated method, and since the nucleation digitiser required advanced post processing it was discounted. Both the LBP and GLCM consider the spatial arrangement of pixels, which is the preferred, more fundamental approach requiring only minor post XCT scan processing. The difference between the two is that the LBP stores neighbourhood pixel information as a single line array or code, whereas the GLCM stores this information as a matrix which accounts for every occurrence of any two adjacent grey values. GLCM provides more information than the concise LBP. The GLCM method is ideally suited for XCT input data, since the XCT images are grey scale images and the GLCM analyse grey scale images (consequently there is no need for further XCT image processing). The aspect of a significantly reduced analytical turnaround time and potential to incorporate into a computer vision system makes this application a viable avenue for further investigation.

Nkomati Nickel mine is an example of a complex ore body that exhibits a high degree of textural and mineralogical variation as a result of its complex geological history. This necessitates its own unique flowsheet for mineral processing. Dominant sulphide textures in the MMZ ore are massive, disseminated, net textured and bleb textured, the latter three are subject to varying grain size populations. The MMZ ore has the appropriate texturally different ore types and associations to facilitate the development of a method for 3D quantitative analysis of drill core.

2.7 Project Aims

The aim of this process mineralogy study is to investigate the application of XCT to quantify ore texture in a minerals processing framework. This approach will assess the usefulness of XCT as a tool for rapid ore texture classification of drill core samples for the intended use in geometallurgical assessment of an ore body. This will typically take place during exploration, during feasibility and during run of mine. The following aims have been put forward:

For Objective (1):

a. To develop as needed a 3D GLCM texture analysis for the analysis of XCT images of drill core using MATLAB.

b. To establish the type of mineralogical and textural information that can be drawn from the matrices and statistics in (a).

c. To identify and highlight the potential opportunities in the geosciences where the XCT and 3D GLCM information could provide value.

For Objective 2:

d. To determine how sensitive the 3D GLCM measure is to changes in mineralogy and texture of Nkomati ore and weather this is comparable to the particle size distribution (PSD) information.

e. To highlight the potential opportunities in the mining industry where the XCT and 3D GLCM information could provide value.

Chapter 3 : Experimental Materials and Methods

3.1 Introduction and Approach

The development of a texture analysis protocol called for a specific and well planned experimental approach as illustrated in figure 3-1 and summarised in Table 3-1. Following the sample collection, the experimental work is broadly divided into two: the first focusing on the characterisation of drill core extracted from the initial samples, and the second on the characterisation of the residual sample material once it has been crushed and milled. This chapter describes details of the sample collection and preparation, as well the standard XCT and QEMSCAN measurement conditions needed for the acquisition of high quality analytical data for ore characterisation. Unless otherwise noted, all sample preparation and analysis was done at the Centre for Minerals Research (CMR) in the Department of Chemical Engineering at the University of Cape Town (UCT).

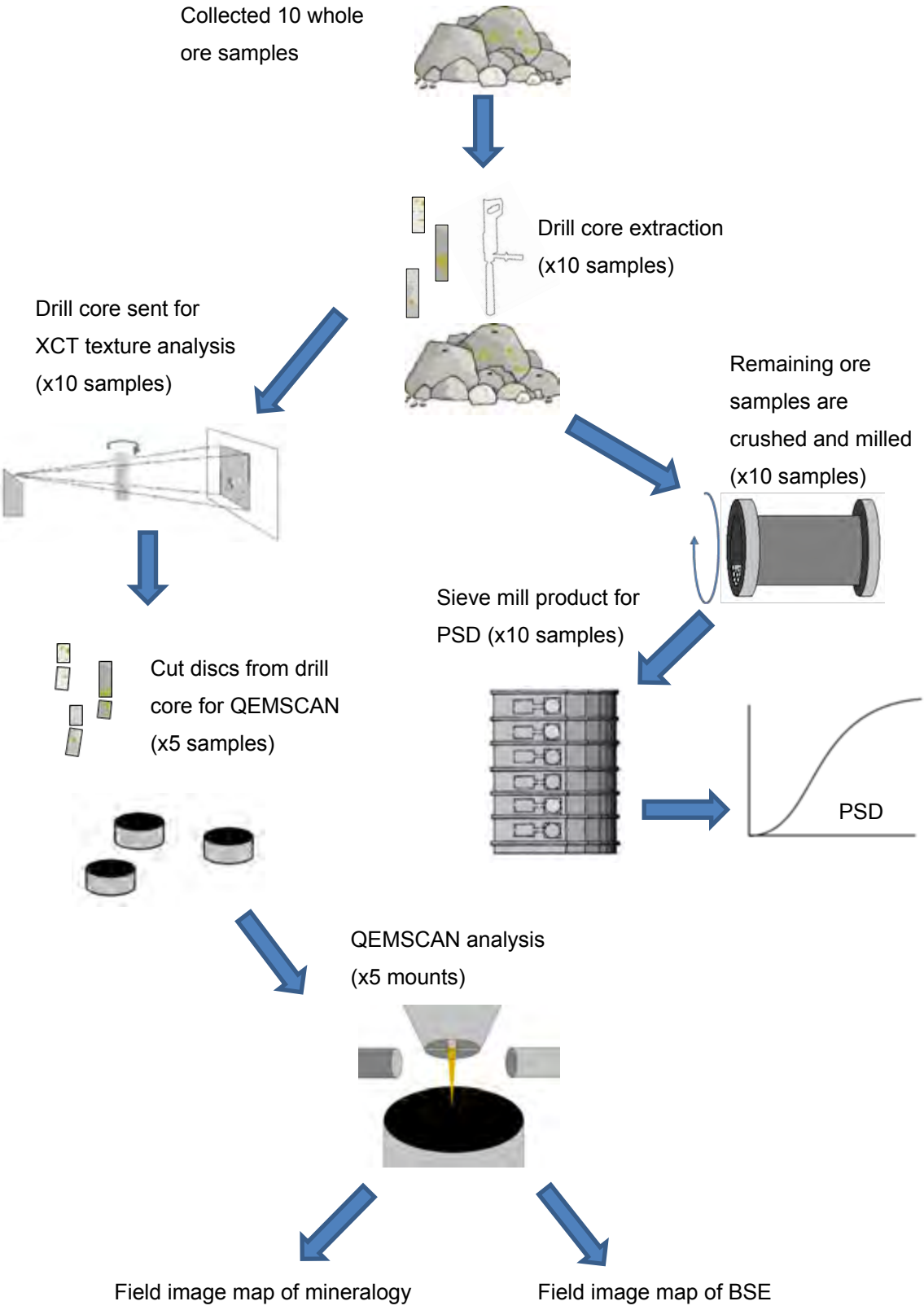

Figure 3-1 Diagram illustrating experimental methods applied to ten hand samples selected from Nkomati Nickel mine, South Africa.

Table 3-1: Tabulated summary of research methodology.

Step	Action	Notes
Sample selection and preparation	Select 10 texturally and mineralogically different nickel sulphide ore samples.	Texture: massive, coarse-net and coarse disseminated, fine-net and fine disseminated, and bleb textured. Samples from Nkomati nickel mine.
	Drill core from each sample.	25mm core samples will allow for a 20 micron resolution XCT scan.
Analytical Method	XCT scan cores.	Scan each drill core at 20 micron resolution and keeping scan parameters constant.
	Render digital volumes and create image stacks.	Done using volume rendering software: VG Studio.
	Develop 3D GLCM code.	Done using image analysis tool kits in MATLAB in writing semi-automated programming scripts.
	Run 3D GLCM on rendered volume.	Tabulate and present statistical data. Classify images according to GLCM texture results.
	Crush and grind each of the remaining sample material after drill core extraction.	Use bench scale rod mill with constant milling conditions.
	Sieve mill products for each sample to produce PSD trends.	PSD used to classify material into independent textural groupings.
	Cut section out of selected drill core samples for QEMSCAN analysis.	Will provide a compositional field image used to correlate mineralogical information with grey level XCT information (data validation).

3.2 Sample Preparation.

3.2.1 Sample collection and preliminary characterisation

Ten samples of varying weight that appear to be mineralogical and texturally different were chosen from the Nkomati MMZ open pits and stock pile with the help of the mine geologist. A preliminary characterisation of these samples using standard photography and simple geological descriptions of each is given in this section. Nine of the ten samples are from the MMZ, one of the ten is a gangue sample of a diabase intrusion. It must be noted that the samples were chosen on the basis that all the

texture types have been sampled and that these samples are not representative of the quantities that these textures are found at Nkomati.

Figure 3-2 show photographs of the ten selected samples used in this study. Table 3-2 presents a simple geological description of the different ore samples.

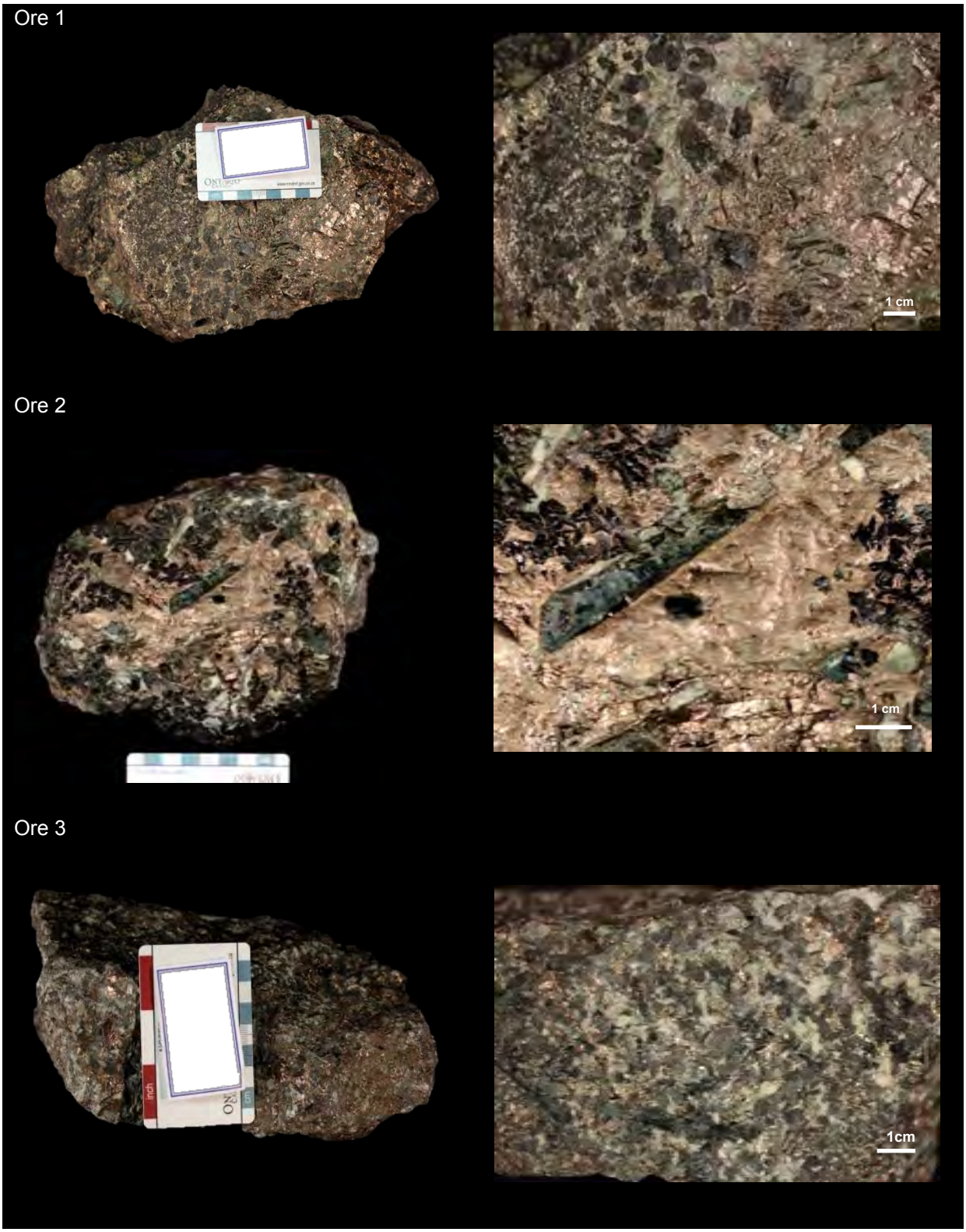

Ore 4

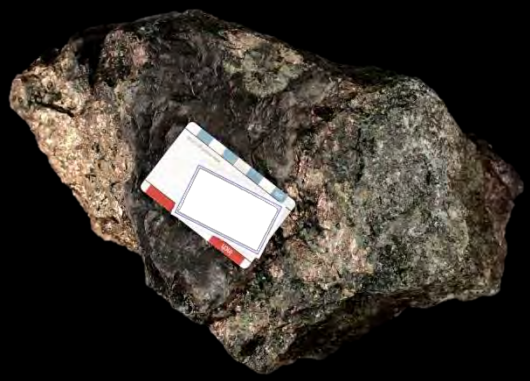

Ore 5

Ore 6

Ore 7

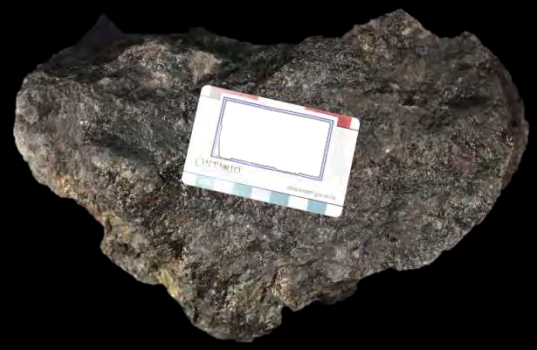

Ore 8

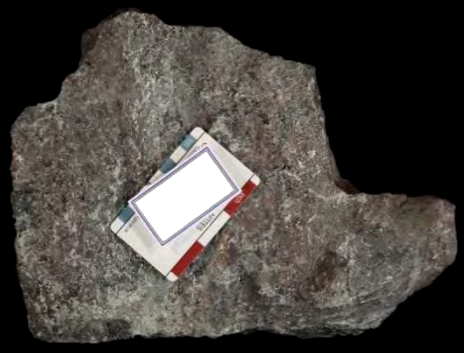

Ore 9

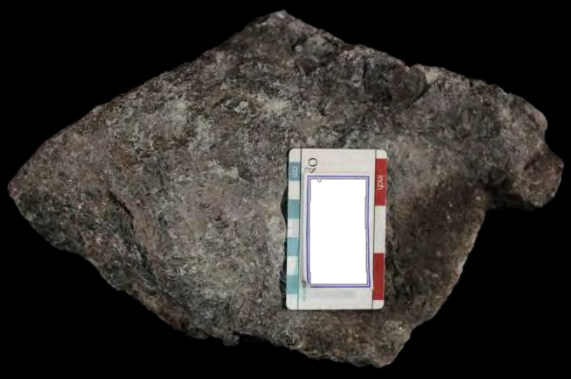

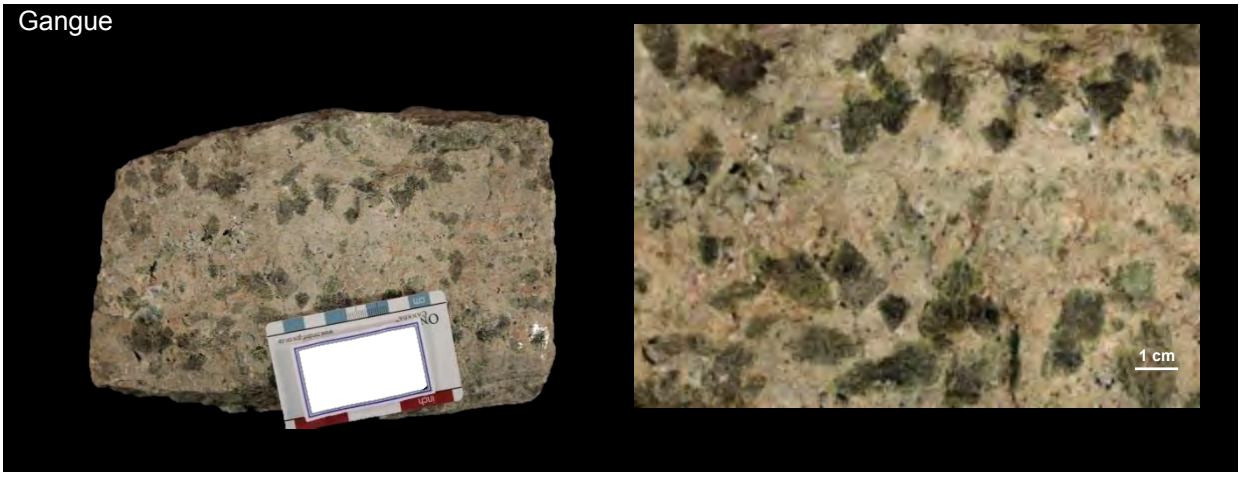

Figure 3-2: Photographs of the ten hand samples taken from the Nkomati MMZ ore in this study.

Table 3-2: Summary table with simple geological descriptions of the ten hand samples from the Nkomati MMZ ore.

Sample number	Geological description
Ore 1	Stock pile sample. Sample has a high sulphide content and has well defined foliations. There are three dominant layers that contribute to the foliation, these are: 1) Massive and coarse grained sulphides that contain sparse well-formed silicate crystals (1-2cm long), 2) Low sulphide content layer in a silicate host, 3) layer with high number of fractures with the same orientation overall foliation planes. The large silicate in layer (1) display regular crystallographic shape while smaller silicate grains display irregular shape.
Ore 2	Stock pile sample. The sample has a high sulphide content and a distinct foliation. The foliation three major layers that define it, these are; 1) coarse grained silicates and net-textured massive sulphides, 2) a layer composed of alternating silicate and sulphides, the layers have been pinch folded (fold 3cm long), 3) silicates and sulphides are medium grained, while sulphides display a net-texture.
Ore 3	In pit sample. Sample has a medium to high concentration of sulphide minerals and a high plagioclase content. The BMS and gangue mineralogy is medium to course grained in size. The sulphide phase is net-textured.
Ore 4	Stock pile sample. The sample has a well-defined foliation. There are two layers that define this foliation, these are: 1) Black and green coloured massive textured silicate minerals, 2) Coarse net-textured sulphides in a silicate host, there is also cluster of massive sulphides which are approximately 10cm large.
Ore 5	In pit sample. Sample has a medium to high concentration of sulphides. The grains are fine to medium in size (0.5-2mm) and are elongate in shape.

	Suphides are net textured.
Ore 6	In pit sample. The sample has a high sulphide content and has well defined foliations. There are three dominant layers that define the foliation, these are: 1) Massive sulphide layer, 2) Fine grained (less than 0.2cm) silicate layer, 3) medium grained layer (0.2-1cm). The sample contains a dark green silicate mineral exhibiting well defined crystal shape.
Ore 7	Stock pile sample. The sample contains a low relative quantity of coarse and fine grained disseminated sulphides, the surface of which appears to be tarnished which may be a result of weathering. The sulphides display a ring like clustering around a central silicate mineral cluster. The sample also contains clusters of a light green silicate mineral.
Ore 8	Stock pile sample. This sample has a low sulphide content in a silicate host. The sulphides are coarse and fine grained, demonstrate clustering, and are partially net-textured and partially disseminated.
Ore 9	Stock pile sample. The sample has a low sulphide content. The sulphides are medium grained disseminated clusters that sometimes display a net-texture. This may also be referred to as bleb textured.
Gangue	In pit sample. This a diabase gangue sample. It has large green well shaped minerals supported in a dull green matrix. The hand sample has a tabular geometry. There are no visible sulphide minerals.

3.2.2 Core Extraction

Core samples were extracted from each of the ten samples collected from the pit and the stock pile. Two cores, 25mm in diameter, were extracted from each of the samples using a portable field hand held core drill (Figure 3-3) at the Department of Earth Sciences at Stellenbosch University.

Figure 3-3: Hand held core drill.

3.2.3 Crushing and Splitting

The residual sample from the core extraction was then further reduced in size using a hydraulic splitter before it was jaw crushed to obtain particles with a maximum size of 3mm. The jaw crush product was then split using a ten-way rotatory splitter to acquire one kilogram samples which were accordingly bagged, labelled and stored.

3.2.4 Milling and Sieving Test Work Procedure

A bench scale stainless steel rod mill charged with a 1kg sample, 500ml of municipal tap water and 20 stainless steel rods of varying diameters was used for milling (Figure 3-4). The rod sets were made up as follows: 6 x 12 mm diameter, 8 x 16mm diameter and 6 x 21mm diameter. A run of mine (ROM) Nkomati MMZ sample from a previous study at the Centre for Minerals Research (Nyambayo 2014) was used to define a milling curve of 40% passing 106 µm. The milling curve was preferably created using this ROM sample since it more adequately captures the ore variability and it preserved the sample mass of the ten hand samples in this study. The curve illustrated in figure 3-5 indicates a milling time of 8min and 36sec to achieve a P40 of 106µm. This milling time was thereafter used for each of the ten samples in this study. The mill products of each of the samples was then wet sieved at 106 microns (figure 3-6) and filter pressed (figure 3-7) and placed in an oven set at 80°C overnight to dry the material.

Once the mill product samples had dried, each was split down to 300g samples in preparation for sieving (figure 3-6). Each of the 300g samples was wet sieved through 38µm screen into buckets until there was no more oversize material. The sub 38µm material in the bucket was filter pressed (figure 3-7) and the filter cake oven dried overnight. This process was repeated with a 75µm sieve for the remaining oversize material. Once the material in each of the size fractions had dried the mass of the material was recorded. The remaining material that was larger than 75 microns was oven dried and dry sieved using a sieve stack. The aperture sizes of the sieves used were: 106µm, 180µm, 250µm, 355µm, 425µm, 600µm, 850µm, 1000µm, 1180µm, 1400µm, 2000µm, 2800µm, 4000µm and 5600µm.

Once the sieving was completed for each sample the resultant particle size distribution (PSD) was calculated and graphed.

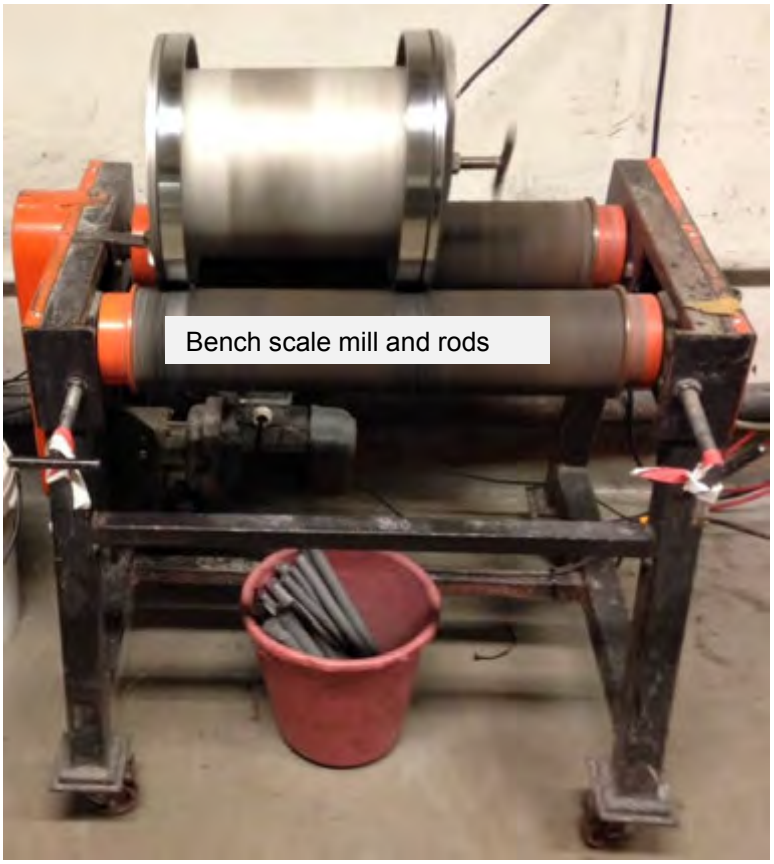

Figure 3-4: Bench scale laboratory rod mill used for the comminution of the ten selected ore samples. Parameters such as rotation frequency, water content, sample weight and milling time were kept constant

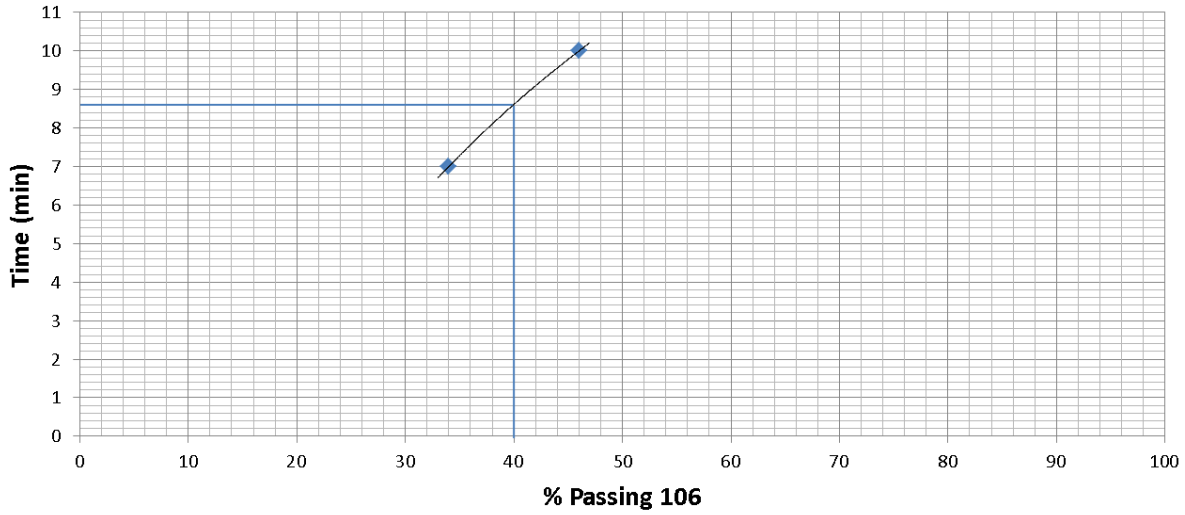

Figure 3-5: Milling curve used to determine a milling time to achieve a P40 of 106µm.

Figure 3-6: Wet sieving apparatus consisting of a vibrating screen holder, a screen, a collecting bucket and running water.

Figure 3-7: A filter press apparatus consisting of a lower drainage block, containing cylinder, a lid with attachments for the input and output of air, a sealing clamp, a pressurised air hose and a drainage pipe. Filter paper can be seen placed between the drainage block and the cylinder.

3.3 X-ray Computer Tomography

All XCT scans were done on a General Electric Phoenix VTomeX L240 X-ray micro computed tomography scanner (XCT) facility at Stellenbosch University, in the Department of Forestry. Ten drill cores taken from the hand samples were XCT scanned using a set parameter configuration (Table 3-4), to allow the volumes of the different core samples to be comparable in downstream data processing.

Table 3-3: Standard parameters used in XCT scanning.

Potential (kV)	180
Voxel size (µm)	20
Frames averaging	3
No. of images per rotation increment	1000
Filter	2mm thick copper plate
Measurement time (min)	20

All XCT volumes were reconstructed using VG Studio Max 2.2 software. The XCT images were normalised so that the sulphide mineral phase appeared within the same grey value interval for all the XCT images. A defined cubic volume of interest (870 x 870 x 1500 voxels) was extracted from the XCT images.

3.4 Quantitative evaluation of minerals by scanning electron microscopy (QEMSCAN)

Selected core samples from each of the textural groupings as determined using the PSD, was chosen for QEMSCAN analysis. The drill cores were sent to the thin section laboratory in the Department of Geology at UCT for sectioning. Regions of interest were selected for sectioning, perpendicular to the length of the drill cores, based on information provided by the XCT images of the drill cores.

All QEMSCAN analyses were done on an FEI 650F FEG QEMSCAN. The focus of this study was on the detailed mineralogical characterisation of the various drill core sections. However, prior to this, it was important to ensure that the mineralogy data produced by the QEMSCAN was accurate and reliable. A combination of mineralogical analyses from previous Nkomati MMZ studies in the CMR

(Nyambayo, 2014; Pillay 2015) and chemical assays from an analytical WDXRF were used to tailor the QEMSCAN species identification list (SIP) and primary mineral lists to accurately assign the various minerals in the Nkomati MMZ ore. Ultimately a comparison of the actual chemical assays of the material with QEMSCAN calculated chemical assays (derived using mineral compositional data from Pillay, 2015) was performed to demonstrate that the analysis were trustworthy (Figure 3-8).

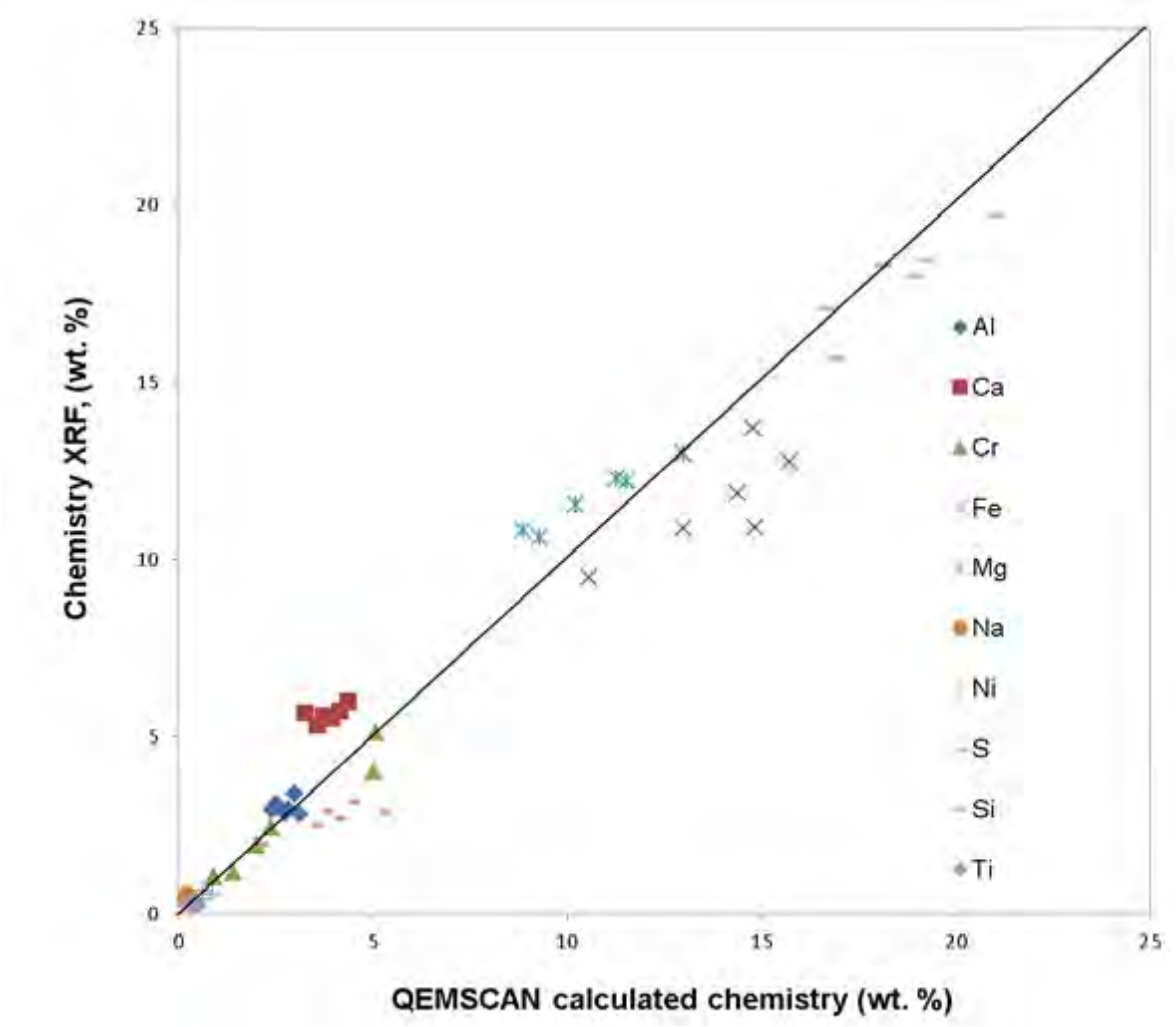

Figure 3-8: Major elements correlation using XRF chemical assay against QEMSCAN calculated assay. The y=x line is also given to illustrate parity between the measurements.

The QEMSCAN field images of drill core samples were analysed at a 15µm pixel resolution at a beam current of 25 kV. The analysis produced 357 frames at 140 times magnification. The data was processed in iDiscover where the frames were stitched together to create the false colour drill core section image. Further data processing was done to classify isolated pixels constituting various boundary phases. Two secondary mineral lists were created that grouped the primary minerals identified into a simple mineral list (for bulk mineralogy) and a BSE mineral list (For comparison with XCT data). The field images were exported as .png images.

Table 3-4: Table summarising bulk ROM mineralogy sample from Nyambayo 2014, that which was processed in this study.

Mineral	Density ($g.cm^{-3}$)	Mass Percentage (%)
Pentlandite	5.01	1.1
Chalcopyrite	4.10	0.5
Pyrrhotite	4.61	4.6
Pyrite	5.01	0.6
Olivine	3.27	2.6
OPX(Enstatite)	3.55	14
CPX(Augite)	3.40	29
Actinolite	3.04	6.6
Serpentine	2.53	8.0
Talc	2.75	1.5
Chlorite	2.65	8.4
Mica	3.09	3.2
Plagioclase	2.62	5.3
Quartz	2.62	2.1
Calcite	2.71	1.9
Chromite	4.79	5.4
Fe-oxides	4.80	3.8
Other	NA	1.5

Table 3-5: Standard parameters used in QEMSCAN analysis of drill core section field images.

Potential (kV)	25
Pixel size (μm)	15
Frames / Fields	357
Magnification	140
Measurement time (hrs)	+- 4 hrs

Chapter 4 : Development of a Methodology for the 3D Mineralogical & Textural Analysis of Rocks

4.1 Introduction

In the last decade or so, the application of XCT for the imaging of the internal structures of geomaterials has become increasingly more prevalent (Cnudde & Boone 2013; Ketcham & Carlson 2001; Mees et al. 2003). A combination of hardware developments allowing improved image resolution, increased computing power for processing large data volumes, as well as scientists and engineers continually looking for new technology to answer their many questions have all contributed to this. The recent review paper by Cnudde and Boone (2013) summarises some of the many applications of this technology in the field of geosciences such as: 3D pore characterisation, 3D grain analysis, fracture analysis, multi scale imaging, ore analysis, monitoring structural dynamic processes, fluid flow analysis and morphological characterisation of fossils. A more recent paper by Kyle and Ketcham (2015) demonstrated the application of high resolution XCT imaging of drill core to provide insight to ore body origin and evaluation.

Although, many of the above mentioned examples have extracted some quantitative attributes from the XCT volumes (e.g. component volume fraction and pore analysis) to date there appears to have been no dedicated and systematic study on how to quantitatively describe the 3D internal structure. In geosciences this is more commonly known as texture - the interrelationship between mineral grains. Traditionally, image texture analysis is done using 2D photographic images which can be used to provide a rapid, economic, objective and consistent inspection method of material (Contreras et al. 2014; Donskoi et al. 2007; Gonçalves and Leta 2010; Hartner et al. 2011; Hinds et al. 2014; Partio et al. 2002; Pérez-Barnuevo et al. 2013; Pirard 2004). However, there are significant and unavoidable stereological implications when only considering 2D information (Pirard et al. 2007). Therefore, 3D quantitative mineralogical and textural analysis of objects is advantageous, especially for a methodology that lends itself to automation and the possibility of "computer vision"(Patel and Chatterjee 2014; Sanford et al. 2013; Thompson and Cabrol 2009).

The critical review of the literature in Chapter 2 identified the 2D grey level co-occurrence matrices (GLCM,(Haralick et al. 1973)) as the method of interest in this study for the quantitative textural analysis of rock drill core. The overarching motivation for the application of the GLCM in this study is that it uses grey level information, the primary output of 3D XCT scanning (Haralick et al. 1973; Carlson 2006). Although 3D GLCM of XCT scans has been applied in the medical field (Dhara et al. 2012; Gao et al. 2011), the software code is not readily and freely available.

This chapter is broadly divided into three sections covering the necessary theory and software development (Section 4.2), the extent to which mineralogical and textural information is captured by the 3D GLCM (results and combined discussion) (Section 4.3) and finally the potential applications of the methodology within the broader field of geosciences (Section 4.4). The complete set of results including the software code is provided in the Appendix. The above mentioned information that is presented in this chapter is aimed at addressing the first objective of this study "*to develop a methodology for the mineralogical and textural analysis of geomaterials using XCT coupled with 3D GLCM*".

4.2 Principles and Development of the 3D GLCM Code

4.2.1 Principles of 3D GLCM

A GLCM is a summary of the spatial relationship between grey values in an image. As described in chapter 2, Haralick mathematically described 2D images as a function of two variables (x, y), stored digitally as a 2D array in computation (see section 2.4.4).

It therefore follows that 3D XCT images may be defined as a function of three variables (x, y, z), stored as 3D data arrays in computation. If Lx = {1, 2, ,*Nx*}, Ly = {1, 2, ,*Ny*} and Lz = {1, 2, ,*Nz*} are the spatial domains for X, Y and Z, then Lx × Ly× Lz represents the image voxel resolution. Similarly, the image I is then a function which assigns some grey value $\mathrm{g} \in \{1, 2, Ng\}$ to each of the voxel resolutions cells;

$$I: Lx \times Ly \times Lz \rightarrow g \qquad [2]$$

This approach incorporates a modified definition of the pixel pair displacement d, where $d = (dx, dy, dz)$. Figure 4-2 provides a simple illustration (akin to a Rubix cube) of the interrelationship of the 3D XCT image voxels where a grey level g is assigned to each of the voxels. Figure 4-2 graphically illustrates the spatial configuration of a reference voxel highlighted in grey and its 26 neighbouring voxels. There are 13 unique voxel pair direction relationships that need to be considered by 3D GLCM analysis.

Conventionally, there are 14 statistical equation features that can be calculated for a GLCM. Only four of these features have a direct relation to the texture, whereas the remaining ten provide insight into

the transition between grey value populations (Haralick et al. 1973). For the purpose of this study, the textural features given in Table 4.1 are considered.

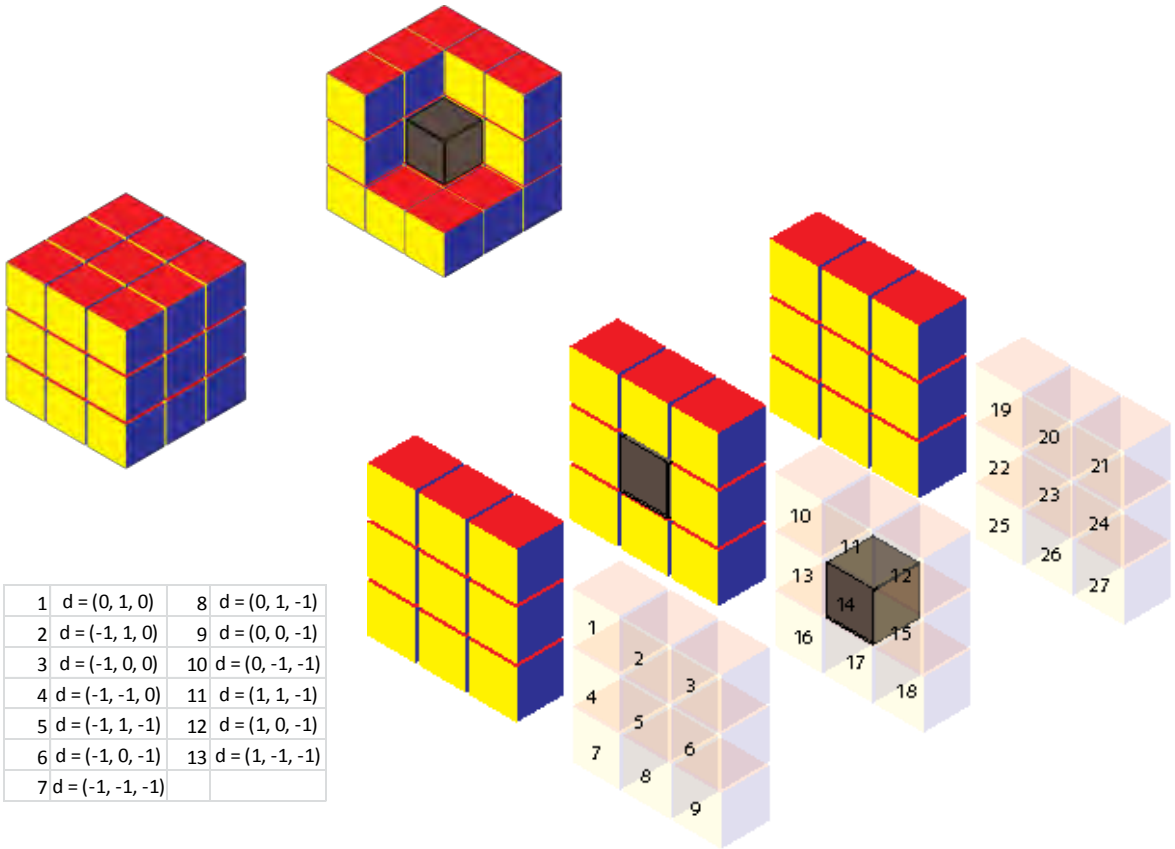

1	d = (0, 1, 0)	8	d = (0, 1, -1)
2	d = (-1, 1, 0)	9	d = (0, 0, -1)
3	d = (-1, 0, 0)	10	d = (0, -1, -1)
4	d = (-1, -1, 0)	11	d = (1, 1, -1)
5	d = (-1, 1, -1)	12	d = (1, 0, -1)
6	d = (-1, 0, -1)	13	d = (1, -1, -1)
7	d = (-1, -1, -1)		

Figure 4-1: a) 3D cube illustrating the spatial relationship between a central voxel with its neighbouring voxels which make up a 3D XCT image. b) 26 voxel pair directions and directions with displacements d. Adapted from Eichkitz et al. (2013).

:

Table 4-1: Summary of the standard GLCM statistical descriptors of interest in this study (μx, μy, σx and σy are averages and standard deviations).

Homogeneity	
The amount of grey value transitions. The higher the grey vaue transition, the closer the value is to 0, the lower the grey value transitions the closer the value is to 1. It does this by measuring how extensive the GLCM distribution is from the diagonal.	$f_1 = \sum_{g_i=1}^{N_g} \sum_{g_j=1}^{N_g} \{P(g_i, g_j)\}^2$
Contrast	
The amount of local variation in an image. A high Contrast measure means a high local variation.	$f_2 = \sum_{n=0}^{N_g-1} n^2 \left\{ \sum_{\lvert g_i - g_j \rvert = n} P(g_i, g_j) \right\}$
Correlations	
The joint probability occurrence of the specified pixel pairs.	$f_3 = \frac{\sum_{g_i=1}^{N_g} \sum_{g_j=1}^{N_g} P(g_i, g_j) - \mu_x \mu_y}{\sigma_x \times \sigma_y}$
Energy	
The sum of squared elements in the GLCM.	$f_4 = \sum_{g_i=1}^{N_g} \sum_{g_j=1}^{N_g} (g_i - \mu)^2 P(g_i, g_j)$

4.2.2 Development of 3D GLCM code

MATLAB, considered the programming platform for technical computing in engineering and science, was the chosen graphical user interface (GUI) for script and algorithm development in this study (Hansen et al. 2013; Fernández-Martínez et al. 2008; Giroux et al. 2007). The fundamentals of the code were developed in the Engineering department at Stellenbosch University. The scripts were run on the large data sets on the Chimera high performance computing servers accessible to engineering staff and students at the University of Cape Town. The analysis is computation intensive and cannot be performed on a standard desktop computer. MATLAB has a pre-existing 2D GLCM function that

was used as the basis of the development of the script to analyse XCT data. Computing efficiency was considered a significant priority for the script development. Consequently, 16-bit grey level XCT images (G = 65536) were downscaled to 8-bit grey level intensities to improve computational performance. Similarly, the script was written such that it required only a single image stack, thereafter matrix calculations were used to reconstruct a new set of image slices at a different unique planar orientation to the original image stack. In order to maintain a constant size and resolution for each of the images, a region of interest with dimensions 2000 images x 600 pixels x 600 pixels was constructed. The scale of each pixel in each image was 20µm.

As described in section 4.2.1, mathematically an image is a 2D array or matrix. MATLAB was used to extract either columns, rows or individual values from the matrices, then used to populate blank matrices. The 3D GLCM code (See Appendix) works in a similar way, by extracting rows and columns from each image in an image stack in a variety of 3D orientations. The original image stack as well as the new images produced by the MATLAB code are analysed by the GLCM. The resultant GLCM for the 13 unique directions (D1 to D13) was thereafter saved as a Portable Networks Graphic (PNG) image file.

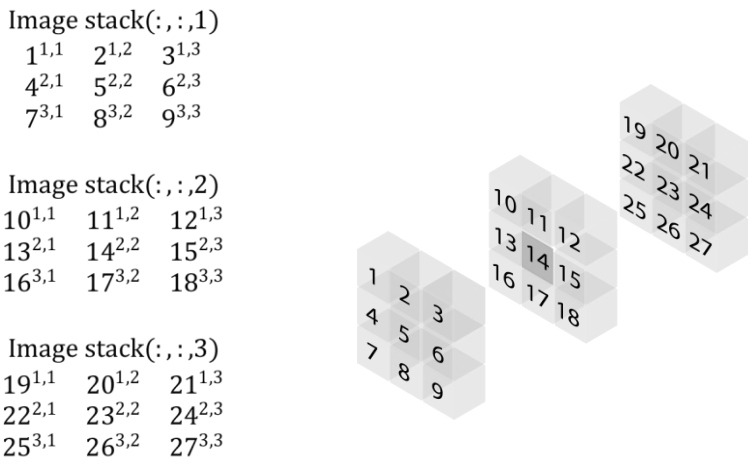

Figure 4-2: Graphical illustration of images presented as matrices saved in an image stack in the MATLAB directory and a 3D graphical illustration showing relative order in which the images have been stored. The 2D image data is stored as a 3Ddata set.

The three above matrices (Figure 4-3) mathematically represent the images presented in figure 4-1 that make up the 3D cube. These matrices, along with others, will be used to explain the basic workings of the MATLAB script. The script is designed to extract information from an image stack of 2D images that represent a 3D image volume. For this example the matrices have been named “Image stack (:,:,1), (:,:,2) and (:,:,3)” where the numbers 1,2 and 3 represent the order in which the images occur in 3D. The colon in the brackets considers all the rows and columns in an image respectively, row or column numbers can be used instead of colons in order to extract specific pixel values. This is very useful when generating new images from the original image stack (Figure 4-4)

The code generates a matrix of zeros, the resolution of which is based on the number of rows or columns and the number of images in the image stack as can be seen if figure 4-4. In this case there

are three images, each with three rows and three columns. The blank image will then be populated with the first row of each image. This means that the number of columns in an original image will be used as the number of columns in the blank image. The number of rows in the blank image is determined by the number of images in the image stack since the first row of every image in the stack is used to populate the blank image rows. This new image represents the voxel grey values at right angles to the original image stack. Once the blank image has been populated with the first row of every image in the image stack, it can then be inserted into a new image stack (Blank stack(:,:,1), (:,:,2) and (:,:,3)) to form the first image called Blank stack (:,:, 1) as illustrated In figure 4-5.

In addition, further scripts were written to allow for the extraction of the conventional GLCM statistics stored as excel files (see Table 4-1), as well as a 'colour intensity heat map' stored as a PNG image file allowing better visualization of the individual GLCM.

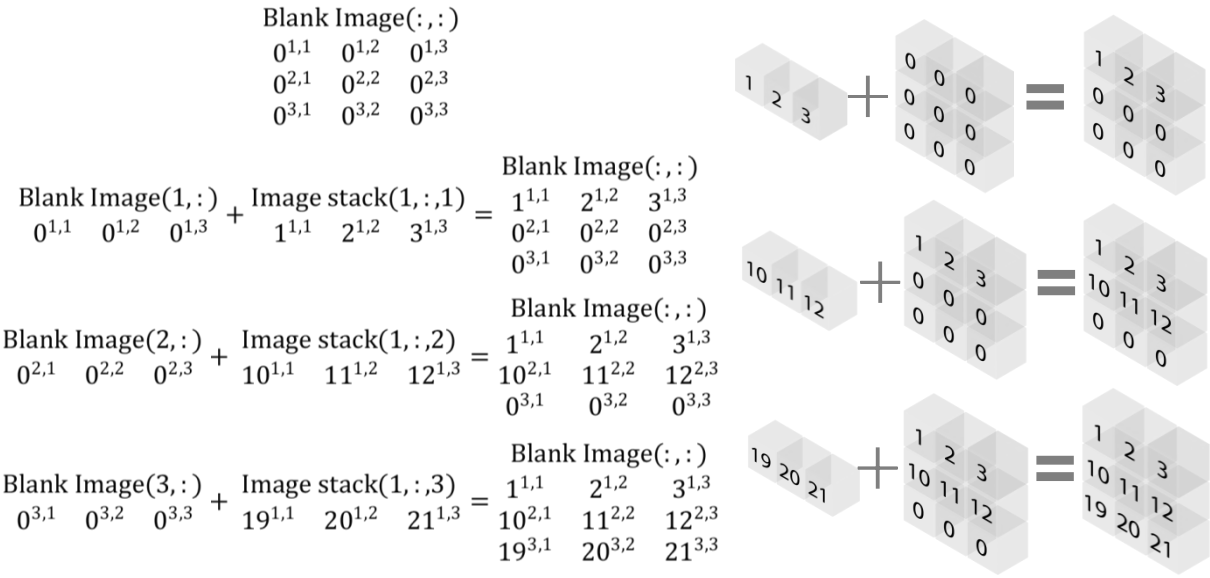

Figure 4-3: Graphical illustration of one of the matrix calculations used in MATLAB to generate a new image at right angles to the original image stack. This happens multiple times until all the pixel values from the original image stack have been used to create new images.

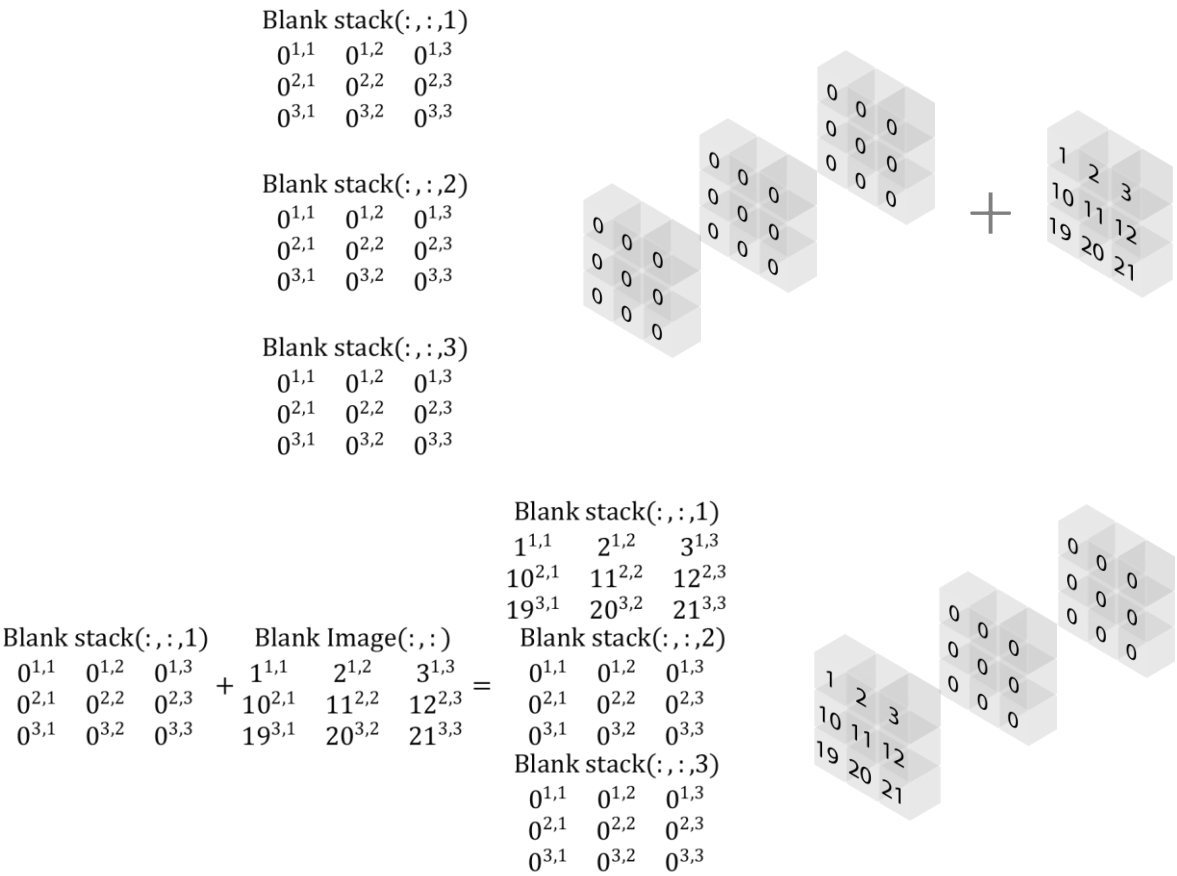

Figure 4-4: Graphical illustration showing the simplified matrix calculation in MATLAB to populate a blank image stack with the newly generated images in order at right angles to the original image stack.

4.3 XCT and 3D GLCM Results

4.3.1 Imaging the 3D internal structure of rocks with XCT

Based on the preliminary simple geological descriptions of the ten Nkomati rock samples as given in Chapter 3, section 3.2.1, two samples of interest (drill core 3 and 5, Figure 3-1) were selected to facilitate the development of a methodology for the 3D mineralogical and textural analysis of geomaterials. Image sections extracted through the centre of the XCT volumes for these two samples are shown in figure 4-6. As part of the XCT post processing procedure, XCT volumes were normalised such that phases with the lowest density will have equivalent grey level values in both samples, the same was done for the high density material. Mineral densities are tabulated in chapter 3 in section 3.2.1, table 3-4.

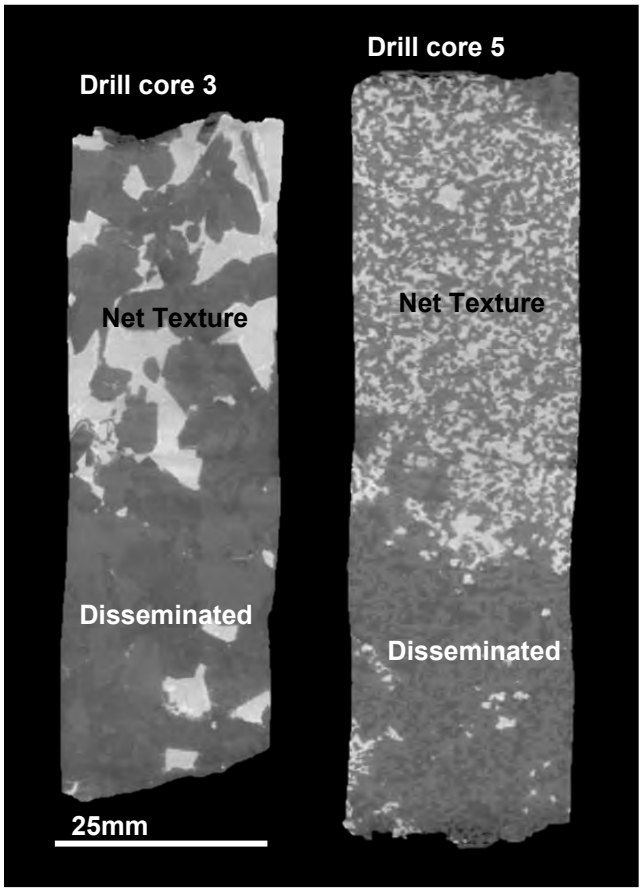

Figure 4-5: XCT image sections of drill core samples # 3 and # 5.

Both core samples have a similar distribution of grey levels, noticeably; dark grey (minerals with a low density), medium grey (minerals with a moderate density), to bright grey (minerals with a high density representing base metal sulfide and oxide minerals). This indicates that overall the bulk grey level mineralogy is comparable. However, it is clearly apparent that the texture varies between the two samples in figure 4-5. Drill core 3 is coarse grained and displays a weak net-texture (bright grey phases are connected in a net like pattern) in its upper half and a disseminated texture (bright grey phases are not connected) in its lower half. Drill core 5 is medium grained displaying a strong net texture in its top two thirds and a disseminated texture in its bottom third. For both samples, there is a concentration of the bright grey phases in the upper half of the core. In drill core 3, these bright grey phases represent the so-called sulfide 'net texture'. For both samples, these bright grey phases (sulfide and oxide minerals) comprise ~40% of the vertical cross sectional area, and the dark - medium grey phases comprise the other ~ 60% of the vertical cross sectional area.

4.3.2 Coupling 3D statistical GLCM data with XCT scanning of rock samples

The resultant 3D GLCM were accordingly determined by running the MATLAB code through the defined sections of XCT image stacks sections of drill cores 3 and 5 in 13 unique directions. Figure 4-6 presents the 13 GLCM presented as the conventional greyscale GLCM distributions. The focus of this study will be on one of the 13 unique GLCM directions for simplicity.

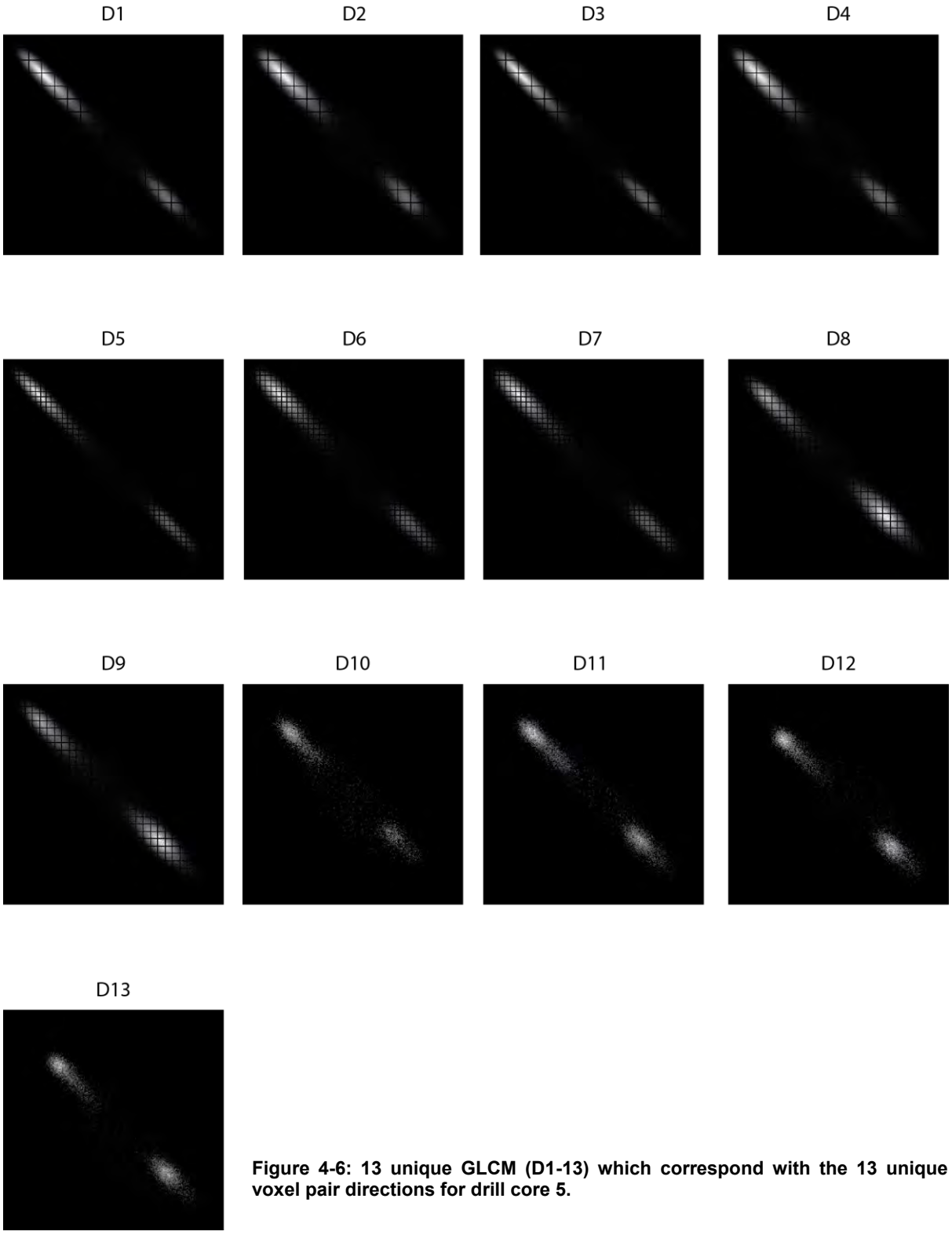

Figure 4-6: 13 unique GLCM (D1-13) which correspond with the 13 unique voxel pair directions for drill core 5.

Figure 4-7 and 4-8 present the four GLCM statistical graphs of the equations presented in section 4.2.1(Table 4-1). The statistical graphs provide clues on the position of textural changes within the drill core. The variations in the statistical values along the drill core should typically correspond to changes in texture. There was a weak correlation between statistical values and texture types. This may be due to noise in the statistical data as will be discussed later.

There are noticeable differences when comparing the statistical values from figure 4-7 and figure 4-8, the correlation is higher in figure 4-7 ranging from 0.990 to 0.996, while lower in figure 4-8 ranging from 0.970 to 0.991. Energy refers to the sum of squares calculated for the matrices, the values for energy are overall lower in figure 4-7 ($5x10^{-4}$ to $2x10^{-3}$) and are overall higher in figure 4-8 ($5x10^{-4}$ to $2.25x10^{-3}$). The homogeneity value is a number between 0 and 1, with 0 being a nonhomogeneous image and 1 being a homogeneous image. Homogeneity values in figure 4-7 ($2.85\ x10^{-3}$ to $3.5\ x10^{-3}$) are similar to the values in figure 4-8 ($2.7\ x10^{-3}$ to $3.7\ x10^{-3}$). Contrast is a measure of the local variation in the image. Contrast is higher overall in figure 4-7 (20 to 55) than in figure 4-8 (15 to 95). This suggests there is a lower overall local variation in figure 4-7. What is also apparent is the trend throughout each of the drill core with respect to the GLCM statistics. Figure 4-7 demonstrates values that fluctuate fairly consistently throughout the core as opposed to the well-defined change in statistical values in figure 4-8. This change in statistical values, or lack thereof, must be attributed to changes in texture along the drill core which is evident upon visual inspection of each drill core and their respective section images and GLCMs.

Within these first ore statistics, there appears to be a set of second order frequency fluctuations, akin to ‘noise’. Figure 4-9 is a repeat of the GLCM energy graph from figure 4-7 and illustrates the amplitude of the unknown noise. The continuous black line in the illustration indicates the trend line of the energy statistics, highlighting the maximum amplitude (“roof”) of the noise at $2x10^{-1}$ and the minimum amplitude (“floor”) at $0.6x10^{-1}$ and $0.4x10^{-1}$ as indicated by the stippled lines. The origin of this noise may potentially be attributed to the downscaling of the primary XCT images from 16-bit to 8-bit.

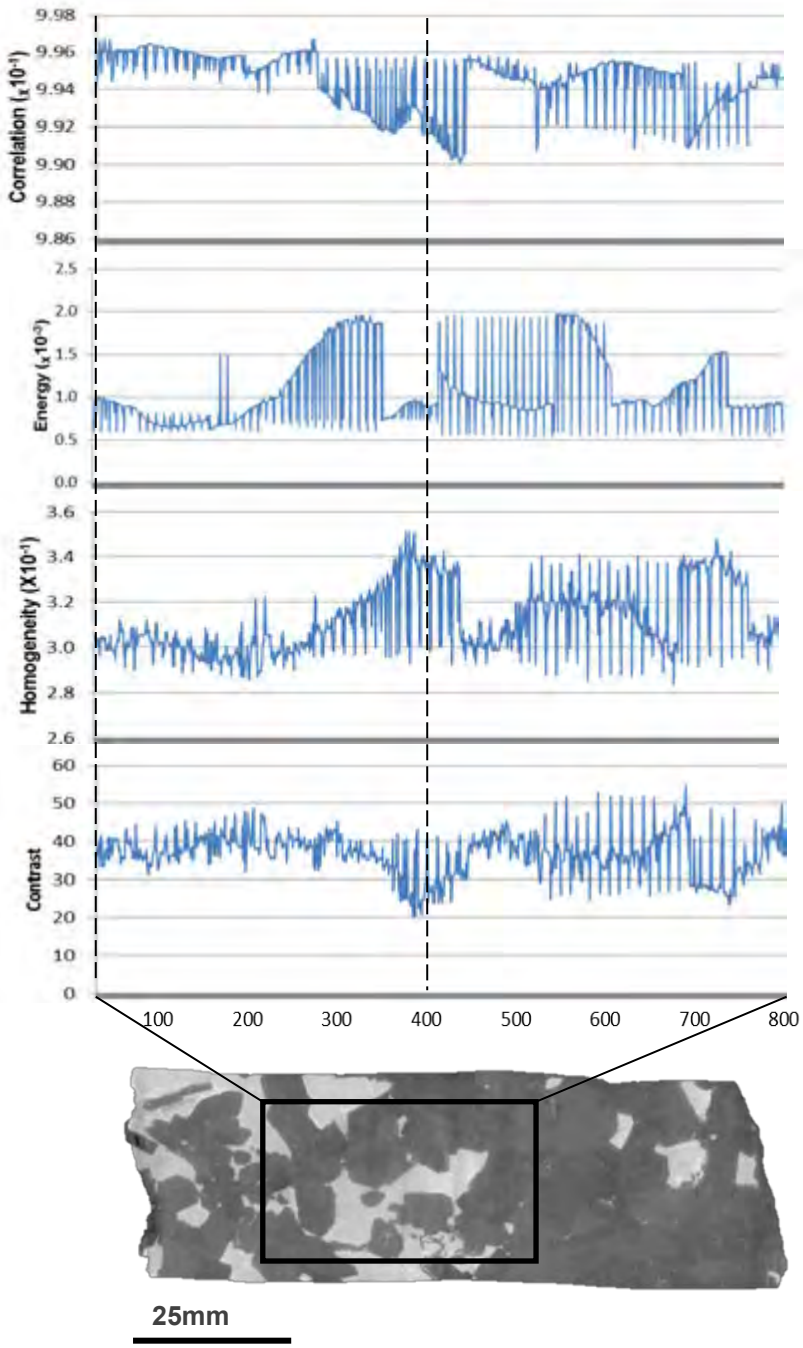

Figure 4-7: Graphical illustration presenting the GLCM statistical variation throughout drill core 3 as demonstrated by the XCT image on the lower left. The four main conventional GLCM statistics have been considered here. These are: correlation, energy, homogeneity and contrast. The stippled line indicates the position of the inspected XCT image slice and its corresponding GLCM presented as a heat map.

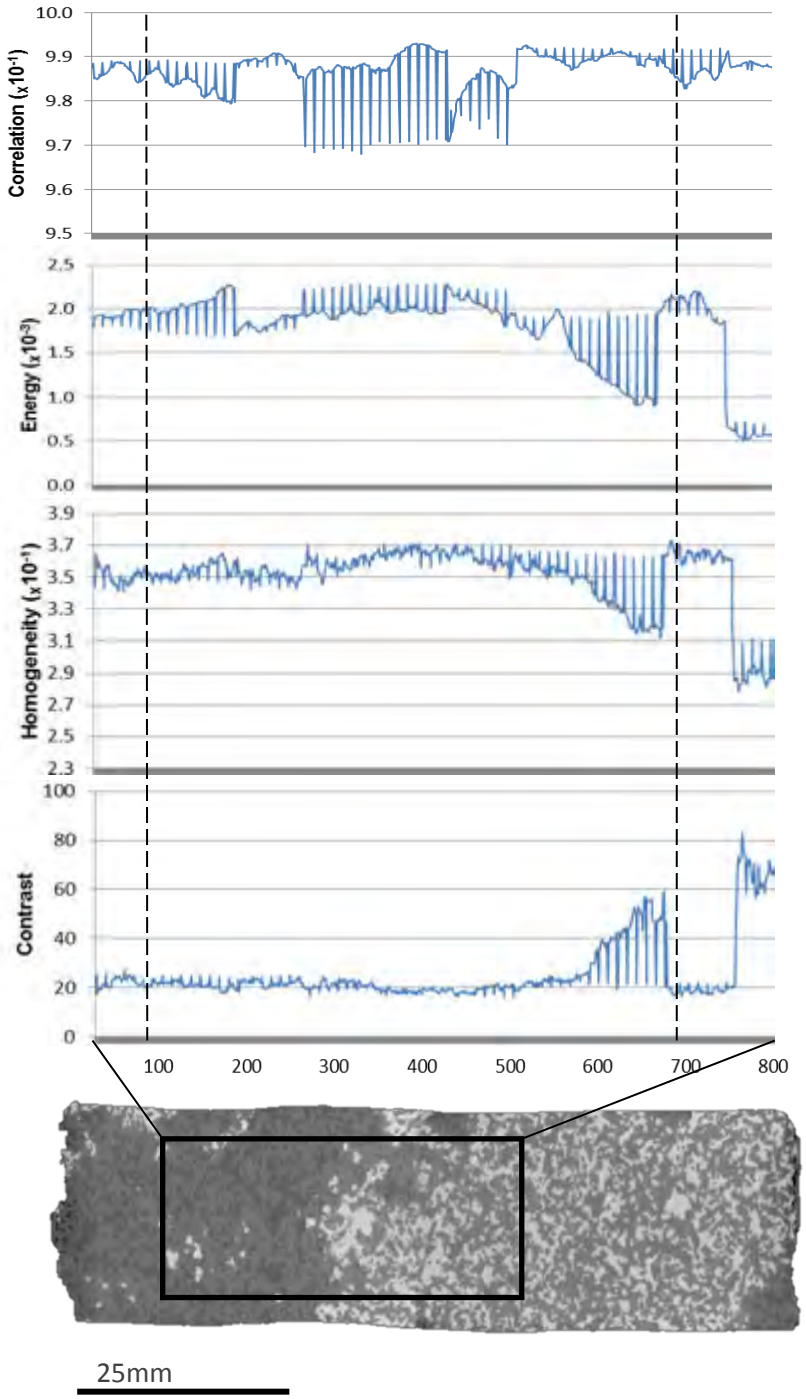

Figure 4-8: Graphical illustration presenting the GLCM statistical variation throughout drill core 5 as demonstrated by the XCT image on the lower left. The four main conventional GLCM statistics have been considered here. These are: correlation, energy, homogeneity and contrast. The stippled line indicates the position of the inspected XCT image slice and its corresponding GLCM presented as a heat map.

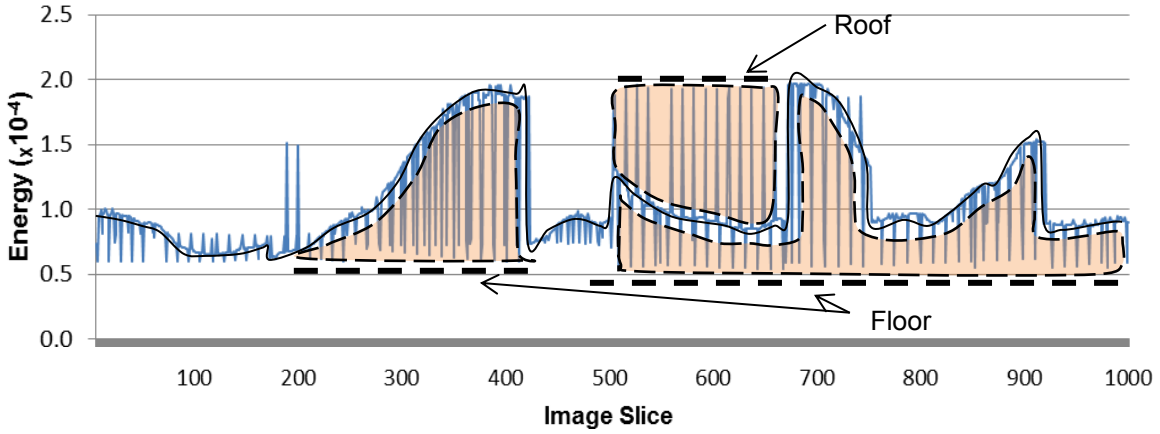

Figure 4-9: Graphical illustration using Energy GLCM statistical graph of drill core #3 to highlight the frequent error produced by the GLCM statistical feature calculations.

4.3.3 Mineralogical and Textural Interpretation of 3D GLCM

The GLCM image texture analysis for variable input data developed by Haralick et al. in 1973 has been used extensively in numerous fields of study, such as: in autonomous planetary exploration vehicles for the analysis of geomaterials for geological identification and path planning (Lu et al. 2009; Mathur 2012; Sharif et al. 2015; Yazdanpanah et al. 2015); in seismic based attribute identification (Eichkitz et al. 2013); in medical and biomedical applications for the identification of tumours, broken bones and other (Chai et al. 2011; Dhara et al. 2012; Dong et al. 2011; Khuzi et al. 2009; Mostaço-Guidolin et al. 2013; Nurtanio et al. 2013); in the food science for the discrimination of fat and meat (Kim et al. 1998); in the study of bubbles in froth flotation (Liu et al. 2005) and in the study of rocks for classification and rock identification through the use of a reference library of known samples (Friedrich, 2008; Patel and Chatterjee 2014; Partio et al. 2002). The focus of this section, is to determine whether meaningful mineralogical and textural information (directly or indirectly), and the changes thereof, can be derived from the 3D GLCM for XCT data in a basic and repeatable manner.

Figure 4-10 and 4-11 display the same two drill core samples, XCT image sections (the location of which correspond to the stippled lines on the statistical graphs of figure 7 and 8 respectively) and GLCM distributions of the 2D XCT image sections displayed as heat maps. Since the images analysed have been downscaled to 8 bit images that are comprised of grey values that range from 0 to 255, the GLCM only considers pixel pair interactions within this range. The matrices have two axes, the vertical axis represents the reference pixel value and the horozontal axis represents the neighbouring pixel value. There are four quadrants in the matrices, but only two quadrants reflecting meaningful information, namely the bottom right quadrant (hereafter referred to as the high density quadrant) and the top left quadrant (hereafter referred to as the low density quadrant). The distribution of the matrices lies along the diagonal between these two quadrants and can show varying degrees of

continuity or discontinuity. The red or 'hot' peaks of the distribution indicate the dominant grey value population within the XCT slice, thus representing the dominant mineral density information. Variable amounts of peak broadening are apparent in the GLCM illustrated in figures 4-10 and 4-11.

A brief inspection of the GLCM heat maps in figure 4-10 and 4-11 shows the variability of the position and the intensity of the peaks both between the two main quadrants, and within the individual quadrants themselves. This detail ultimately provides an indication of the simple mineralogy of the samples. For example: Figure 4-10a contains ~40 % bright grey (dense mineralogy) and ~60% dark grey (less dense mineralogy). Figure 4-10b contains ~20% bright grey (dense mineralogy) and ~80% dark grey (less dense mineralogy). The accompanying GLCM for figure 4-10a given in figure 4-10c contains two peaks in the GLCM: one is stretched out along the diagonal in the high density quadrant with a peak grey value of ~180, and the other is in the low density quadrant with a peak grey value of ~40. The peak in the low density quadrant is larger (more red or 'hot') than that in the high density quadrant indicating a greater abundance of mineralogy of a grey level of ~ 40 (low density mineralogy). Conversely the peak in the high density quadrant is smaller (more blue or 'cooler') indicating a lesser abundance of material with a grey level of ~ 180 (dense mineralogy). Similarly, the accompanying GLCM for figure 4-10b given in 4-10 d has two peaks. The dominant peak in the low density (top left) quadrant has a grey value of ~40, indicating the abundance of the less dense mineralogy The smaller and less well developed peak in the high density quadrant (bottom right) has a grey value of ~ 200 (indicating the less abundant dense mineralogy) in this XCT slice.

An equivalent interpretation of the GLCM can be done for figure 4-11: Figure 4-11a has only minor amounts of light grey phases which is captured by the virtual non-existence of a peak of grey value ~ 225 in the high density (bottom right) quadrant of 4-11c. Two distinct, high intensity (red) peaks however are apparent in the low density (top left) quadrant with grey levels of ~ 40 and 60 respectively. This indicates the presence of two populations of less dense material in the XCT scan, corresponding to the dark grey (low density mineralogy) and medium grey (moderate density mineralogy) present in the XCT slice in figure 4-11c.

The information stored in the GLCM not only provides information relating to simple bulk mineralogy, but also on the interrelationship between the grey values, i.e. grain boundary interactions. This detail ultimately provides an indication of the texture of the sample. For example: the minerals in the XCT slices in Figure 4-10a and b clearly have similar grain sizes (~ 10,000 μm), despite having varying grey levels. It therefore follows that the position of the peaks differs somewhat, but more importantly that the width of the diagonal distribution is similar when considered at right angles to the diagonal originating from the centre of the peaks. This similarity in the width of the distribution from the peaks indicates that the GLCM are accounting for the similar grain size.

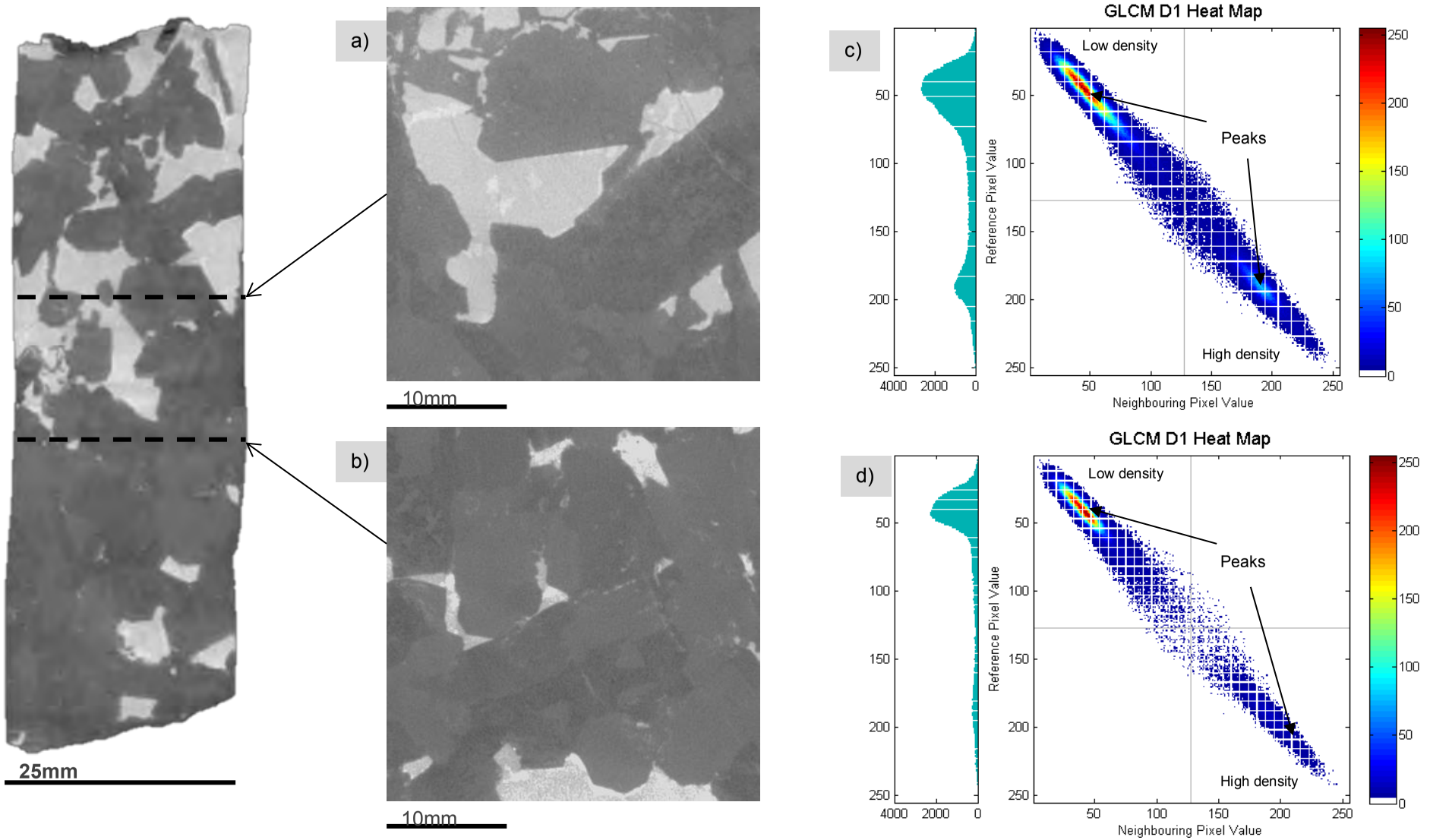

Figure 4-10: Graphical illustration presenting the GLCM statistical variation throughout drill core 3 as demonstrated by the XCT image on the lower left. The four main conventional GLCM statistics have been considered here. These are: correlation, energy, homogeneity and contrast. The stippled line indicates the position of the inspected XCT image slice and its corresponding GLCM presented as a heat map.

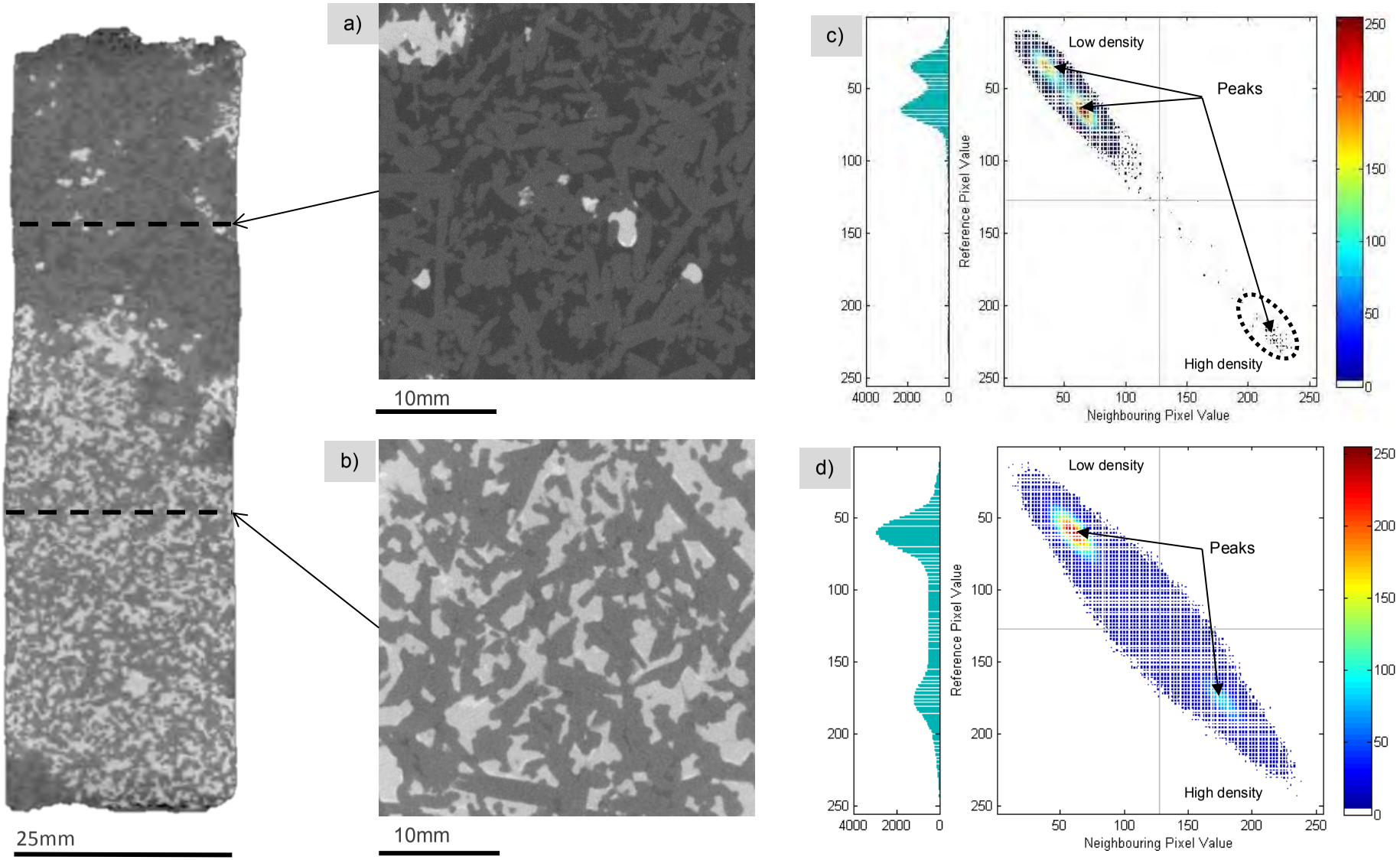

Figure 4-11: Graphical illustration presenting the GLCM statistical variation throughout drill core 5 as demonstrated by the XCT image on the lower left. The four main conventional GLCM statistics have been considered here. These are: correlation, energy, homogeneity and contrast. The stippled line indicates the position of the inspected XCT image slice and its corresponding GLCM presented as a heat map.

In contrast, Figure 4-10a is coarse grained, and figure 4-11b is medium grained. Both images display relatively similar abundances of the more dense mineralogy and less dense mineralogy. The comparison of their respective GLCM should then provide insight as to how the matrices record the different grain sizes without the effect of changing mineralogy. When comparing the two GLCM (figure 4-10c and 4-11d), the two peaks in both matrices show similar positioning of the peaks but display a very different distribution away from the diagonal. Figure 4-10c has a narrow or tight distribution and figure 4-11d has a wide distribution. A narrow distribution indicates that there is little interaction between the dominant grey values present in the image which means that there is little grain boundary interaction between the dominant grey level phases. A wide distribution indicates that there is a high amount of grey value interaction between the dominant grey values in the image and thus there is a high amount of grain boundary interaction between the dominant grey level phases. This illustrates how the change in mineral grain size will affect the GLCM distribution.

Two neighbouring pixels with different grey values can only be located along mineral grain boundaries. Therefore the GLCMs provide information on grain boundary interactions between phases of different grey levels, i.e. of different minerals. The relationship between the grain size of the minerals and their grain boundary interaction can be explained by the following equation:

$$A \propto \frac{1}{P} \qquad (4.1)$$

Where the surface area (A) of a mineral in 2D is indirectly proportional to its perimeter (P). This means that as the grain size decreases the surface area of the mineral increases and hence the degree of grain boundary interaction increases. The inverse is true for a coarse grained texture. In a 3D framework - the decreasing grain size results in a decrease in the individual grain volume, then the surface area to volume ratio increases hence resulting in an increase in the degree of grain boundary surface area interactions between the mineral populations. Therefore, a small grain size will have a broad GLCM distribution perpendicular to the diagonal and the inverse is true for a coarse grain size.

In some cases the distribution with the matrices can be continuous or discontinuous. A continuous distribution (figure 4-10c and 4-11d) indicates a high amount of grey values that is present between the dominant bright and dark grey values in the image. This may be more typical in images that contain relatively equal amounts of both dark and bright grey values (equal amount high and low density mineralogy). A discontinuous distribution (Figure 4-10d and 4-11c) indicates that there are grey values between the two dominant grey values that are not present within the image. This may be more typical in images that contain high amounts of one dominant grey value with minor amounts of other grey values.

The correlation between the GLCM and the statistical values is not very distinct, although there are a few things that are notable, three of the energy values 0.7 $x10^{-3}$, 0.9 $x10^{-3}$ and 0.5 $x10^{-3}$ correspond with GLCMs that have two well defined peaks in opposite quadrants (Figure 4-10c and d, and 4-11d), while the remaining energy value is 1.9 and corresponds with a GLCM that has two well-defined

peaks in the same quadrant (Figure 4-11c). Similarly, contrast values also show three matrices having similar values; 38, 36 and 33 (Figure 4-10c and d, and 4-11c) while the fourth value is 90 (Figure 4-11d). This is not the same grouping as was previously identified for energy. The contrast value appears to be related to the spread of the distribution from the peaks within the matrices. In 4-11d the distribution in board corresponding to a high contrast value, while in the remaining matrices the distribution is narrow with low contrast values. The statistics presented in table 4-2 and 4-3 are first order statistics used extensively in the literature to measure texture in images and have no units (Khuzi et al. 2009).

Table 4-2: Summary of the general characteristics and GLCM statistical values of core samples 3 and 5 as well as the dominant grey level variation and peak grey level counts. Single GLCM statistical values calculated for each XCT image.

Image slice	Figure 4-10a)	Figure 4-10b)	Figure 4-11a)	Figure 4-11b)
Grey level variation (Volume %)	bright ~ 40% dark ~ 60%	bright ~ 20% dark ~ 80%	bright ~ 5% dark ~ 95%	bright ~ 40% dark ~ 60%
Peak grey value (High peaks in matrices)	bright ~ 180 dark ~ 40	bright ~ 200 dark ~ 40	bright ~ 225 dark ~ 40 & 60	bright ~ 175 dark ~ 60
Peak value count (Histogram x-axis)	bright ~ 1000 dark ~ 2900	bright ~ 250 dark ~ 3000	bright ~ 100 dark ~ 2300 & 1900	bright ~ 650 dark ~ 3000
Texture	coarse grained, disseminated	coarse grained, disseminated	medium grained, disseminated	medium grained net-texture
Correlation ($x10^{-1}$)	9.6	9.9	9.8	9.8
Energy ($x10^{-3}$)	0.7	0.9	1.9	0.5
Homogeneity ($x10^{-1}$)	3	3	3	2
Contrast	38	36	33	90

Table 4-3: Summary of Minimum, Maximum and Mean GLCM statistical values of core samples 3 and 5

Drill Core Volume	Drill core 3			Drill core 5		
	Minimum	**Maximum**	**Mean**	**Minimum**	**Maximum**	**Mean**
Correlation ($x10^{-1}$)	9.90	9.97	9.95	9.68	9.93	9.87
Energy ($x10^{-3}$)	0.79	1.92	1.26	0.46	2.28	1.55
Homogeneity ($x10^{-1}$)	2.84	3.51	3.11	2.59	3.68	3.32
Contrast	20.41	54.45	37.66	16.22	94.41	35.24

The GLCM are able to provide simple mineralogical and textural information. For the ore type presented in this section the analysis of one pixel pair direction sufficiently represent the rocks character. This is due to the random nature of the texture within the rocks. For ore types that have

preferred textural orientations such as banded iron formation, the use of additional directions would prove valuable however this has not been shown and will be a further recommendation. For example, the pixel pair directions that cross cut the preferred oriented texture will provide contrasting data to that of pixels pair directions that run the length of the preferred oriented texture.

4.4 Potential Applications in Science and Industry

Improvements in imaging technology and computing efficiency have opened up the possibility to capture, process and analyse images for various purposes. In recent years there have been breakthrough technologies and advancements in two key areas: (1) the development of new imaging techniques and the refinement of pre-existing imaging tools, and (2) the development of computer vision systems that use the information stored in images to recognise objects or trends in processing systems.

In computation the recognition of an object in an image is crucial in decision making. As presented in the literature review in chapter 2, there are various was in which this information can be measured and calculated. Image analysis by GLCM is one of many ways to decouple the complex nature of the information stored in images, specifically to discern and recognise variations in the texture of the objects imaged (Haralick et al. 1973). This technology has been applied in a variety of applications (Gadkari 2004; Liu et al. 2005; Mathur 2012; Nurtanio et al. 2013; Partio et al. 2002).

Pore characterisation of oil reservoir rock is a crucial tool in the estimation of oil reserves. In this regards the value adding aspects of the XCT scanner to this industry has been responsible for most of the historical development of the scanners. The analysis of these geomaterials by XCT is favourable since it allows for the qualitative and quantitative inspection of void volume, porosity size and shape, as well as interconnectivity in 3D (Carlson, 2006; and references therein). The use of a 3D GLCM image analysis tool would prove invaluable to this billion dollar industry. Textural attributes in the host rock would behave in much the same way as that defined in this chapter. Changes in the texture of this rock will indicate changes in porosity which may indicate oil and gas flow characteristics. The application to measure and record texture may also allow for the recognition of favourable texture and rock types.

The 3D GLCM methodology presented may also be applied to other 3D image data sets. Eichkitz et al. (2013) designed a similar analysis for the identification of geological features such as channel structures using 3D seismic data and 3D analysis by GLCM. Seismic data is also used in the oil industry for resource location and reserve estimation.

The On-board Autonomous Science Investigation System (OASIS) of some autonomous planetary exploration vehicle or rovers allow for the collection of geological samples for the measurement of their mineralogical properties (Maki et al. 2012; Castano et al. 2007). Some of these systems capture, process and produce GLCM analyses of 2D images of their surroundings to identify obstacles and

ground surface (Mathur 2012). Sharif et al. (2015) used GLCM distribution, produced from the 2D conventional GLCM application of photographs of rocks taken aboard rover based planetary exploration vehicles, to classify the rock types that the rover would encounter along its exploration route. The GLCM distributions were considered as unique patterns for each rock texture type with some overlaps while using Bayesian probability calculation to classify the rock types. However, as discussed earlier, stereology has an effect on the quality of the image processing results, especially when analysing rock samples remotely as these rovers would. Many of these rovers are kitted with XRF and EDS (LIBS on Mars rover Curiosity) instrumentation for the identification of chemical compositions in sample material. This can be used for mineral identification, and when coupled with the methodology proposed in this chapter (a new technique to collect mini core samples) will not only provide appropriate information for accurate textural identification and recognition, but also to provide an important array of spatial association information for better comparison with earth originated counterparts.

The methodology proposed in this chapter may add significant value to processing plants that process complex materials such as recycling plants. Computer vision based systems for recycling already exist (Kleber et al. 2015). The material processed in a recycling plant is composed of various components such as copper wiring, plastic casing, glass screens and bottles. The texture of such material would have a high degree of variability (i.e. broken cell phones would exhibit a unique internal texture to that of plastic containers and electric wires). The application of a XCT scanner and the proposed methodology to analyse texture in 3D, implemented through a computer vision system would add significant value to a recycling operation. Specifically by identifying material types and density differences prior to processing to perform sorting tasks.

The most significant value adding use for this proposed technique will be on a mine site. This is typically due to the large capital investment that goes into mining (from feasibility right though to rehabilitation with the goal to maximise profit margins in a sustainable manner) and the need to strengthen geological knowledge for better planning and processing. The pre-characterisation of ore material will provide logistical and planning advantage before and during mining operations. Determining mineralogy and texture presents the opportunity to characterise ore in terms of hardness and predictive comminution performance, as well as problematic minerals in flotation. This is the focus of Chapter 5.

Chapter 5 : Case Study Application of 3D GLCM Textural Analysis Using Nkomati Ore Samples

5.1 Introduction

To date there is no appropriate methodology for the use of an XCT on a mine site. Mining activities typically process thousands of tons of material each month driven by the global demand for valuable commodities. As discussed in chapter 4, mining activities are challenged by various factors. These are: increasing energy costs, environmental limitations, fluctuating commodity prices, unexpected ore body variation and an increase in ore body and processing circuit complexity among other things (Northey et al. 2014; West 2011; Morrell 2009; Prior et al. 2012). In minerals processing, a simple mineralogical and textural ore body allows for simple of process refinement due to low geological variation and complexity. In contrast, for a highly variable mineralogical and textural ore body process refinement becomes a challenge. Having a good understanding of what enters the processing circuit and how its character influences comminution and concentrator performance is the first step in overcoming these challenges. To do this requires an innovative geometallurgical approach which includes a well thought out sampling and analysis protocol that is cost effective, rapid, repeatable and consistent. The results of which should guide the appropriate mine planning and plant optimisation strategies.

X-ray tomography and 3D GLCM texture analysis, offers a hybrid opportunity to provide rapid upfront information for better mine planning and minerals processing, The XCT scanner is a non-destructive 3D image acquisition tool that can be used, in conjunction with 3D GLCM texture algorithms, to analyse and recognise textural and mineralogical patterns of drill core. The primary evaluation of an ore body hinges on the data collected from surface study techniques of the surface of drill cores during exploration.

The information presented in this chapter is aimed at addressing the second objective, "*to assess the application of XCT coupled with 3D GLCM for the quantitative textural analysis of drill core: Case study of the Nkomati nickel sulfide ore."* This chapter is broadly divided into three sections: the first

section for the characterisation of the Nkomati samples, the second addresses the application of the GLCM on the different textural groupings of the Nkomati samples; and the third to a discussion on the potential application of this methodology in geometallurgy.

5.2 Characterisation of Nkomati Samples

In order to avoid using subjective geological classifications (Andrew, 2012) as the basis for a textural classification scheme in this study, a metallurgical approach is used in this study. To this end, the shape of the particle size distribution of a rod mill product will be used to classify the samples. These groupings will form the basis of further mineralogical classification using 2D QEMSCAN (auto-SEM) and 3D XCT before the application of the GLCM.

5.2.1 Particle size distribution

The particle size distribution is one of the key parameters which is universally measured within the field of comminution. An ore type will produce different particle size distributions when comminuted with different breakage mechanisms (Taşdemir and Taşdemir 2009; Powell et al. 2015 and references therein). However, when the comminution conditions are maintained constant, then the particle size distribution is an indication of the ore hardness which is a function of its mineralogy and texture.

In this study, the PSD of each sample after milling in a bench scale rod mill is illustrated in Figure 5-1., and the % material passing 90µm, 200µm and 3mm is summarised in Table 5-1. The comminution parameters have been kept constant as detailed in chapter 3. The coarsest PSD is presented by ore samples 7, 8 and 9 (coloured in green) which indicate the hardest material with ~ 20% of the material having a particle size larger than 3mm. The PSD of these samples is very close to one another. Ore samples 3, 4, 5 and 6 (coloured in blue) display an intermediate PSD with ~ 10% of the material greater than 3mm. The PSD of these samples is not quite as close to one another or tight as samples 7, 8 and 9 (coloured in green). Ore samples 1 and 2 (coloured in yellow) have a fine PSD indicating it is the softest of the ores with only ~ 20% of material greater than 200µm. The gangue sample which is late stage diabase dyke cross cutting the ore body presents the overall finest PSD with 83% of the material finer than 200µm. This PSD does not conform to the general shape of the other 9 samples which may be due to the post ore body deposit nature of the diabase dyke. The composition of this diabase gangue sample will be quite different to the ore due to a number of factors: differences in primary magma composition of the intrusive dykes, temperature and pressure influencing the cooling rate and likely to result in a different mineralogy and texture (Hornsey, 2000). However, since the diabase is dispersed throughout the ore body it is likely to be present within the run of mine material sent to the mill for processing. The groups defined in this section will be used throughout the remaining chapter as a reference to ore character and variability.

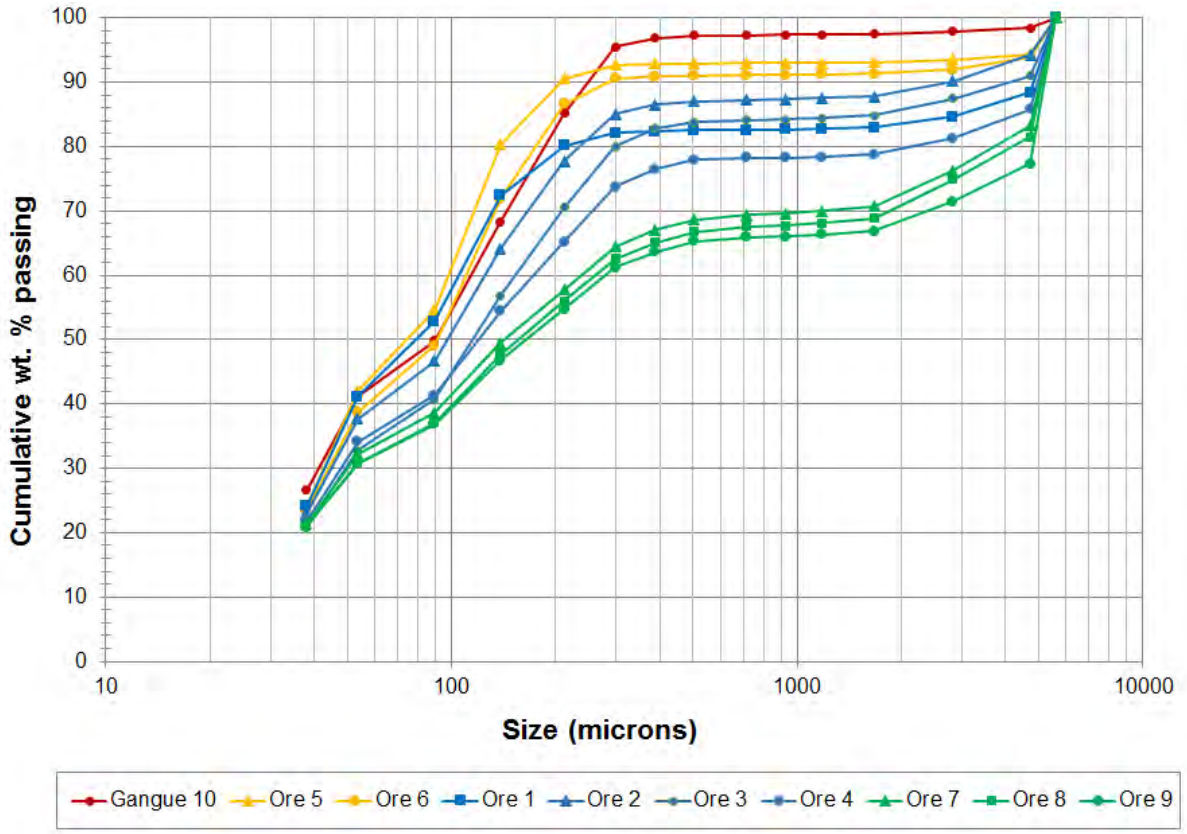

Figure 5-1: Particle size distribution of the ten Nkomati samples, showing a classification into four groupings based on differences in the shape of the PSD.

Table 5-1: Summary of sample set PSD.

Sample	% passing 90 µm	% passing 200 µm	% passing 3 mm
Ore 1	53	79	85
Ore 2	47	76	91
Ore 3	41	69	88
Ore 4	40	64	82
Ore 5	54	89	94
Ore 6	49	85	92
Ore 7	38	57	77
Ore 8	37	55	76
Ore 9	37	54	72
Gangue 10	50	83	98

5.2.2 Mineralogical characterisation of the Nkomati ore

This section is aimed at establishing a working knowledge of the mineralogical characteristics of the Nkomati samples using QEMSCAN for the interpretation of the 3D XCT data.

Figure 5-2 presents a vertical section through the centre of each Nkomati drill core sample which runs the full length of the cores. One of the disadvantages of XCT is that it only provides information on variations in mineral density (Van Geet et al. 2001; Videla et al. 2007) and therefore a working knowledge of the mineralogy obtained using complimentary techniques is essential. This is common practice in process mineralogy studies, especially those working with XCT data (Ghorbani et al. 2011; Nwaila, 2014).

Four drill cores from each of the groups defined from the PSD (figure 5-1) were chosen and horizontally sectioned (annotated as the stippled lines in figure 5-2) for QEMSCAN field image analysis (drill core 3, 5, 8 and the gangue sample) as a means to validate the XCT grey level data. Drill core 3 is from the intermediate PSD grouping (blue). Drill core 5 is from the finest PSD grouping (yellow). Drill core 8 is from the coarsest PSD grouping (green). The gangue drill core has been given its own group and has a relatively fine PSD (red).

Figure 5-3 presents four images of drill core 3, three of the images are QEMSCAN field images and one corresponding XCT image section located and extracted from the XCT volume. The detailed QEMCSCAN image (Figure 5-3a) presents the individual minerals and their locations on the polished surface of drill core 3. This information has been simplified in figure 5-3b where minerals of similar density have been grouped together (Table 5-2). There are three mineral groupings, namely; base metal sulphides and oxides, silicate (SG > 3) and other silicates (SG < 3). Although pentlandite has been included in the base metal sulphides and oxides group in table 5-2, it has not been grouped in figure 5-3b since pentlandite is the valuable target mineral. Figure 5-3c is a BSE QEMSCAN field image of the same surface of drill core 3. The BSE image is grey scale and, depending on the grey level, provides an indication of mineral density. The bright grey values correspond with high density mineralogy, whereas the dark grey values correspond with the low density mineralogy. This is validated by the comparison between figure 5-3b and 5-3c, where the mineral density groups correspond spatially with the bright and dark grey BSE mineralogy. Finally the XCT image in figure 5-3d can be directly correlated with the BSE image (figure 5-3c) as having similar grey value spatial distribution. However, the XCT image has better discrimination between pentlandite and the remaining base metal sulphides and oxides. The brightest grey values in the XCT image correspond spatially with the location of pentlandite in figure 5-3b.

Figure 5-4 presents a series of sectional images taken from each core: a QEMSCAN field image providing simple false colour mineralogy, a QEMSCAN BSE field image and an XCT image slice. The QEMSCAN BSE image and XCT slice can be correlated with one another given the information is derived from similar physical and chemical attributes of the material. Subtle variations in grey level are a function of the brightness, contrast and standardisation of the two techniques.

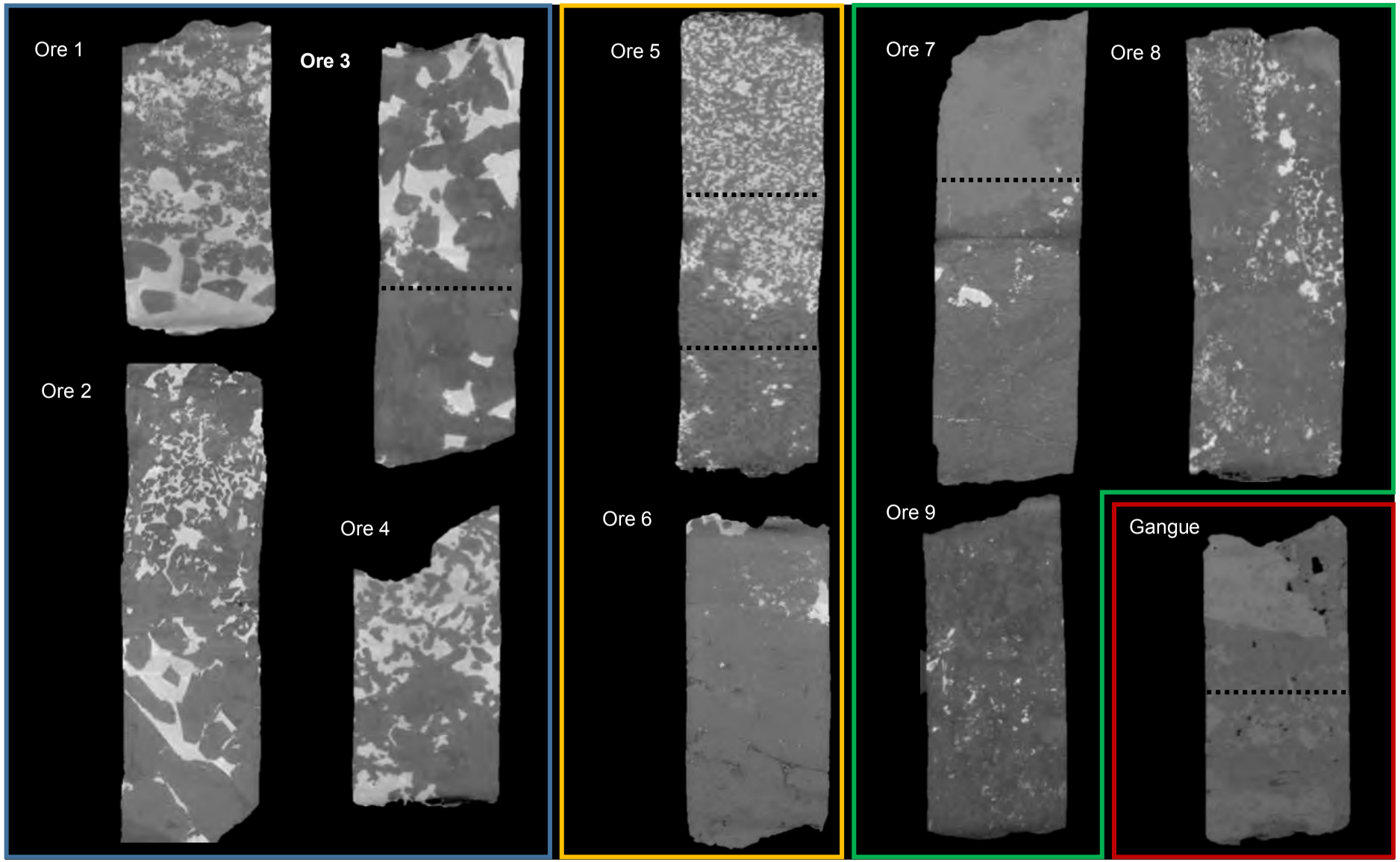

Figure 5-2: XCT image section of the 10 drill core samples. The 5 stippled lines indicate sectional planes that were cut and polished for later QEMSCAN analysis.

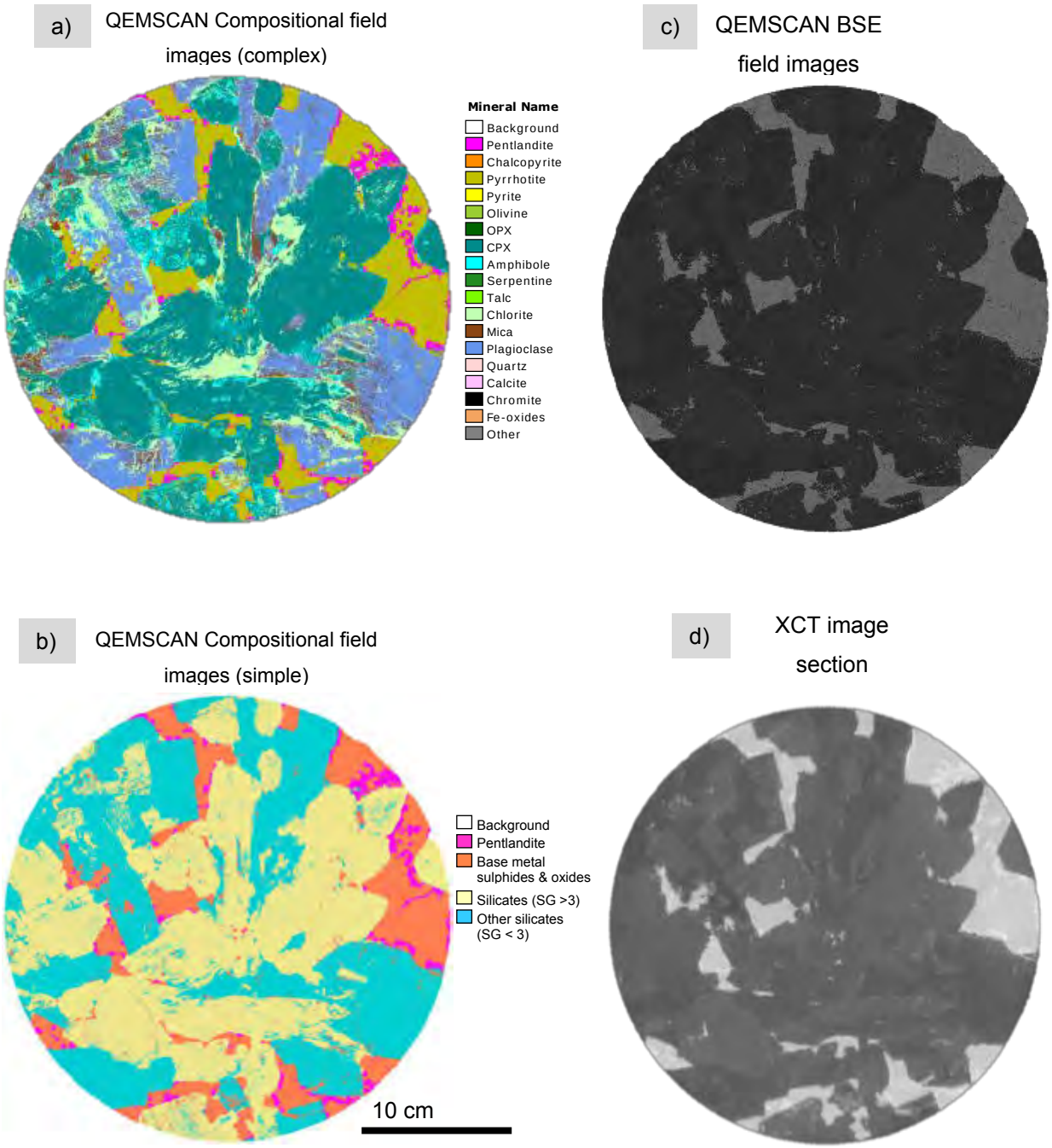

Figure 5-3: Comparison between a) QEMSCAN compositional field image (detailed), b) QEMSCAN compositional field image (simple), c) QEMSCAN BSE field image and d) XCT image slice. All of which are for a surface of drill core 3.

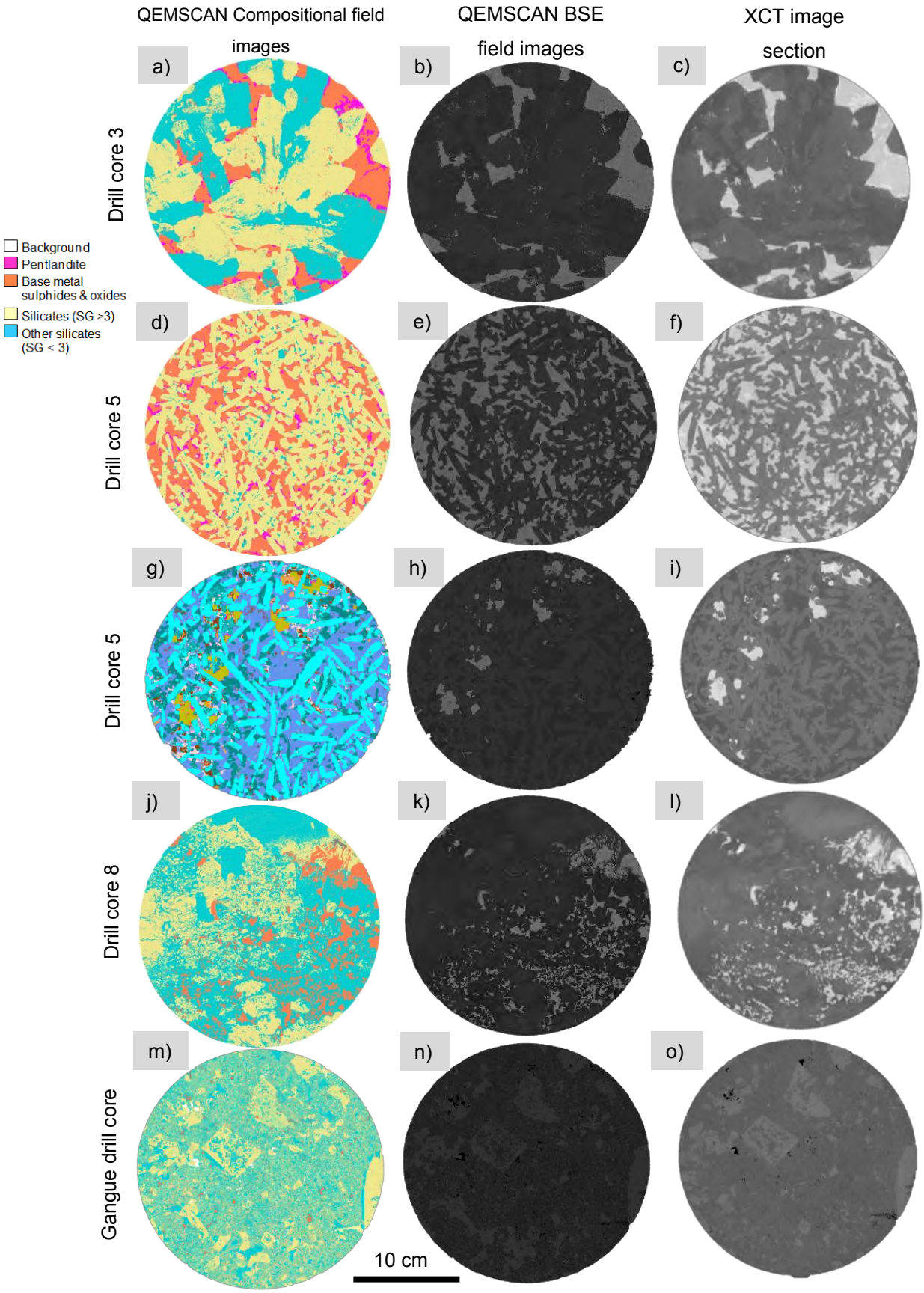

Figure 5-4: Drill core section analysed by QEMSCAN and XCT providing; Compositional field image, BSE field images and XCT grey level density images.

Table 5-2: Summary of mineralogical content of QEMSCAN drill core sections and mineral grouping based on specific gravity of each mineral.

Mineral	Wt. % of each QEMSCAN field image					Mineral Group	SG	Mohs scale
	Core 3	Core 5i	Core 5ii	Core 8	Gangue			
Pentlandite	3.8	6.8	0.5	2.4	<0.1	Base metal sulphides & oxides	4.1 – 4.9	3.5 -4
Chalcopyrite	0.7	1.3	0.8	0.2	<0.1			3.5 - 4
Pyrrhotite	19.4	43.8	6.2	14.8	<0.1			3.5 – 4.5
Pyrite	<0.1	<0.1	<0.1	<0.1	<0.1			6 - 6.5
Chromite	<0.1	<0.1	<0.1	<0.1	1.2			5.5
Fe-oxides	0.2	1.7	2.5	3.4	7.3			5 - 5.5
Olivine	<0.1	0.2	0.1	4.9	<0.1	Silicates (SG >3)	3.0 - 3.6	6.5 - 7
Orthopyroxene	0.3	0.4	0.1	8.4	5.7			5.5 - 6
Clinopyroxene	38.4	32.1	32.8	11.0	22.5			5 - 6
Amphibole	4.8	0.4	0.3	9.8	3.9			5.5 - 6
Mica	3.3	1.0	4.8	1.7	0.4	Other silicates (SG < 3)	2.5 - 2.7	2
Plagioclase	17.1	3.7	45.9	6.4	4.1			6 – 6.5
Quartz	<0.1	<0.1	4.3	<0.1	<0.1			7
Serpentine	<0.1	<0.1	<0.1	28.0	25.3			2 - 5
Talc	<0.1	0.1	0.1	0.5	22.0			2
Chlorite	11.4	0.3	0.5	6.9	5.1			2
Calcite	<0.1	<0.1	0.2	0.7	3.8			3
Other	0.2	8.4	0.2	0.3	0.2			

(Charikinya et al. 2015, see section 3.4.1). The modal mineralogy for each of the drill core QEMSCAN field images as well as mineral grouping according to specific gravity (SG) is given in table 5-2. Appropriate groupings according to SG correlate with the spatial location of false colour QEMSCAN minerals and XCT grey value mineral phases (as was done for figure 5-3) since mineral discrimination in the XCT images is based on mineral density.

Drill Core Mineralogy

From the XCT images in figure 5-2 it is clear that there are two distinct grey level populations, and based on this it is possible to discern between the two mineral groups that contribute to each grey

level population. There is a bright grey level mineral population (dense minerals) and a dark grey level mineral population (less dense minerals). Within the two grey level mineral populations there is further grey level discrimination, with two dark grey value mineral phases. The QEMSCAN BSE images shows two dominant grey value intensities, within the darker grey levels there are two grey values intensities. In the XCT images the grey level intensities correspond directly with the BSE images, except there is better discrimination between bright grey value intensities. The brightest grey value minerals in the XCT images correspond spatially with pentlandite in the QEMSCAN images. The sectional images in figure 5-4 can be used to identify which minerals are represented by which grey levels in the XCT images since these XCT images are the images that will be used to identify simple mineralogy and texture in the 3D GLCM analysis.

In the QEMSCAN field image of drill core 3 (figure 5-3a) the most dominant mineral is clinopyroxene (CPX) (38.4 wt%) a primary silicate mineral. Amphibole (4.8 wt%) is an alteration product of pyroxenes, formed through the uralitization process. Plagioclase (17.1 wt%) is also present in high amounts in this drill core and is a primary silicate mineral. Chlorite (11.4 wt%) is an alteration product of plagioclase, formed through a process called saussuritization. Mica (3.3 wt%) is present in small amounts. These minerals spatially correspond with the darker of the two dark grey level intensities in (b) and (c). The bright grey value intensities in the BSE correspond with the sulphide and oxide mineralogy in (b). Similarly, pentlandite (3.8 wt%) corresponds with the brightest grey level intensity in (c) and the remaining BMS (20.1 wt%) and oxide (0.2 wt%) correspond with the darker of the bright grey level intensities. In figure 5-4 the sectional QEMSCAN field image of drill core 5 (d) displays the presence of high modal amounts of BMS (51.9 wt%), orthopyroxene (OPX) (0.4 wt%) and clinopyroxene (CPX) (32.1 wt%) with minor amounts of plagioclase (3.7 wt%).

In the sectional QEMSCAN field image of drill core 5 (g) it is clear that there is an increase in the amount of plagioclase (45.9 wt%) and a minor increase in alteration minerals from that in (d) and a substantial decrease in the amount of BMS (7.5 wt%). The change in modal mineralogy between the compositional field images (d) and (g) is clearly apparent in the BSE images (e) and (h). In the BSE image (h) there is less bright (BMS and oxide) grey levels and the dark (silicate and other) grey levels are predominant. Within the predominant darker grey levels there are two intensities, the darker corresponding with the plagioclase and quartz while the lighter corresponds with clinopyroxene and orthopyroxene. Similarly, the XCT image (i) shows the same grey level intensity trends with better discrimination between pentlandite and the remaining BMS (pyrrhotite, chalcopyrite and pyrite).

The QEMSCAN field image of drill core 8 (j) displays a high modal amount of serpentine (28.0 wt%) and actinolite (9.8 wt%), due to the replacement of CPX, OPX and plagioclase, indicating a high degree of alteration. The image also displays moderate amounts of BMS (17.4 wt%), olivine (4.9 wt%), OPX (8.4 wt%), CPX (11.0 wt%) and plagioclase (6.4 wt%) with minor amounts of calcite (0.7 wt%), mica (1.7 wt%), and chlorite (6.9 wt%). As in the previous sample images, the mineralogical information in (j) can be represented by the grey level data in the BSE image (k) with better grey level discrimination in the XCT image (l).

There are no sulphides minerals present in the gangue drill core QEMSCAN field image (m) in figure 5-4. This is due to the nature of the sample being comprised entirely of gangue mineralogy. The sample is predominantly composed of CPX (22.5 wt%), OPX (5.7 wt%), serpentine (25.3 wt%) and talc (22.0 wt%). The sample contains high amounts of calcite (3.8 wt%) and oxides (8.5 wt%) relative to the ore samples. There are two dominant dark grey values that correspond to the CPX and altered silicates (brighter grey values) and the highly altered OPX (darker grey values). Similarly, the XCT image (o) shows the same grey level intensity trends. By visual inspection of the section in figure 5-4 it is clear that the grey level information in the XCT images, which is consistent over a number of samples, provides information of a simple mineralogy.

Drill core Texture

Using a combination of the QEMSCAN and XCT data to describe mineralogy as given above, a similar qualitative description of the texture of the different groups of drill cores can be done using conventional rock textural descriptors in geology.

Drill cores 1-4 in figure 5-2 reveals that the dense material phase (BMS & oxides) is coarse grained (2-10mm) and demonstrates a net texture. This is a common sulphide texture. The less dense material (Silicates (SG >3)) displays 2-8mm grains surrounded by dense material (BMS & oxides). In figure 5-4 section (a) of drill core 3 shows coarse grained sulphides displaying a net texture. The silicate mineralogy displays a high degree of alteration with irregular grain boundaries. There is a strong spatial association between OPX and actinolite, and between plagioclase and chlorite. Pentlandite is strongly associated with Pyrrhotite.

Drill core 5 in figure 5-2 displays two textures, the top of the core contains a high amount of dense mineralogy (BMS & oxides) which is net textured and the bottom of the core which has a low amount of dense mineralogy (BMS & oxides). The approximate grain size is 1-3mm. In figure 5-4 drill core 5 (d) (top of drill core) has medium grained sulphides which are net textured. In drill core 5 (g) (bottom of drill core) the low sulphide content shows a disseminated texture. Actinolite is present in both image section (d) and (g) as long well shaped crystals that are randomly oriented. The lack of alteration in drill core 5 and the presence of well-formed crystal shapes indicate a primary texture. Pentlandite is strongly associated with pyrrhotite in both (d) and (g).

In figure 5-2 drill core samples 6, 7, 8 and 9 show visual similarities. Each displays a low quantity of dense mineralogy (BMS & oxides) that is medium to fine grained (1-5mm) and is disseminated. Ore 7 shows a concentration of dense mineralogy (BMS & oxides) in its centre with its lower and upper most portions comprised of ultra-fine grained silicate mineralogy. This appears quite similar to ore 6. Ore 8 and 9 also show concentrations or clustering of dense mineralogy (BMS & oxides) spread throughout the drill core.

The QEMSCAN image of drill core 8 (j) in figure 5-4, show the most textural complexity in comparison to the prior QEMSCAN images (a), (d) and (g). The mineral grains have variable size but are predominantly small and have irregular shapes. The sulphide minerals are fine grained and demonstrate a bleb texture.

The gangue sample has a bimodal mineral grain size distribution this is clear in both figures 5-2 and 5-4 (m, n and o). CPX is present as the largest of the grain sizes. The rest of the mineralogy is fine grained. The larger CPX crystals, although demonstrating partial replacement, have moderately formed grain boundaries and are surrounded by fine grained partially replaced OPX and serpentine. There is also a considerable amount of calcite which is spatially associated with CPX.

In summary, there are four PSD groupings (ore 1-4 intermediate PSD, ore 5-6 fine PSD, ore 7-9 coarse PSD and gangue fine PSD). According to the density mineralogy presented in the XCT images the drill cores; ore 1-5 has high amounts of dense mineralogy (BMS & oxides) and similar low density materials (Silicates & other (SG < 3.6)), ore 6-9 has low amounts of dense mineralogy (BMS & oxides) but can be subdivided again into ore 6 and 7 with clustered dense mineralogy (BMS & oxides) and lack of the low density materials (Silicates (SG < 3.6)), and ore 8 and 9 have evenly distributed dense mineralogy (BMS & oxides) with the presence of the low density materials (Silicates & other (SG < 3.6)).

Texturally the samples can be grouped accordingly: ores 1-4 displaying a coarse grain size and net texture, ore 5 displaying a medium grain size with both net and disseminated textures, ores 6 and 7 displaying a clustered dense mineralogy (BMS & oxides) surrounded by fine grained (the lighter of the two dark grey levels) less dense materials (Silicates (SG > 3)), ore 8 and 9 displaying a fine grained disseminated dense mineralogy (BMS & oxides). Individual mineral hardness is a contributing factor to the overall hardness of the ore samples. An ore sample composed of softer minerals will be a softer sample overall. Mica (2, Mohs scale), chlorite (2, Mohs scale) and talc (1, Mohs scale) are soft minerals, while pentlandite, chalcopyrite and pyrrhotite have an intermediate hardness, and oxides, OPX, CPX and actinolite are hard minerals. However, texture also has a contribution towards ore hardness. A sample demonstrating a coarse grain size may be softer than another finer grained sample with the same mineralogy. The over printing of primary texture by alteration textures may also contribute to ore hardness (Stanton and Willey, 1970). As written in Craig and Vaughan (1994), “Defects, particularly the linear regions of mismatching of the crystal lattice known as dislocations are introduced by mechanical deformation (a process known as work hardening).” This may explain why the samples that contain high amounts of soft mineralogy (drill core 8 from the green PSD group)(samples with secondary alteration) have the coarsest PSD (indicating a high hardness or resistance to breakage).

The information provided about the mineralogy and texture of the samples allows for groupings that are similar to the PSD groupings. However there are discrepancies, since it would be expected that the mineralogy and texture for each of the samples would correlate more strongly with the PSD groupings. For the first PSD grouping (ore1-4) the mineralogy and texture have been grouped as

similar as well and provides a strong correlation. For fine grained PSD (ore 5-6) the sample fall into different mineralogical and textural classes. Given the nature of the samples described in chapter 3, suggesting that ore 6 is composed of foliations. The drill core sample may have only sampled one of the layers which may be the cause of the error or lack of correlation (i.e. the drill core is not necessarily representative of the bulk sample used for the determination of the PSD). The coarse grained PSD (ores 7-9) show a correlation with the mineralogical and textural description, since all the samples have only minor disseminated fine grained dense mineralogy (BMS & oxides) as well as the presence of the least dense material (Silicates (SG < 3)).

5.3 GLCM Characterisation of Drill Core Textures

The following section presents the GLCM textural statistics and distribution results for a sample from each of the PSD groupings. The data is presented in the same format as that in chapter 4. The number of images used was limited to 800 due to the size of the smallest XCT drill core image and is used as the minimum number of images for all samples to ensure reproducibility. Figure 5-5 to figure 5-8 present the 3D GLCM data of a drill core from each PSD grouping. Complimentary data of each drill core can be found in the appendices.

The statistical GLCM graphs in figure 5-5, of drill core 2 from the intermediate PSD group (blue group), indicate a fairly consistent texture throughout the image. There is a slight increase in the contrast and correlation statistics from the first image to the 800th image. Similarly, there is a slight decreasing trend in energy and homogeneity. The image sections (a) and (b) display a coarse mineral grain size of between 5-10mm with (b) having a slightly smaller grain size. The dense mineralogy (BMS & oxides) appears as elongate minerals and accounts for 30% of the modal mineralogy. Pentlandite, the brightest grey level mineral, is present near and along the edge of the dense mineralogy (BMS & oxides) in contact with the low density material (Silicates (SG < 3.6)). The dense mineralogy (BMS & oxides) in both images display distinct grain boundaries and a net texture. The GLCM distribution in (c) and (d) are similar. Both show two peaks at grey levels of 50 and 200, the peak at a grey level of 50 being red indicating a high modal amount of low density material (Silicates (SG < 3.6)). Both distributions are narrow which indicates a low amount of grey level interaction between the two peak grey level intensity ranges. This indicates that the sample is dominated by a coarse mineral grain size. There is slightly less discontinuity in (b) than that in (c) which indicates that the grains in the corresponding section (b) is smaller than that in (a).

The statistical GLCM graphs in figure 5-6, of drill core 5 from the fine grained PSD grouping (yellow group), indicate a gradual but distinct change in texture after the 500th image. The values show a gradual decrease in energy and homogeneity between image 500 and image 800 while contrast is increasing in this interval. There is an anomaly between 680 and 770 where the statistics move to initial values. Two sectional images were selected based on these trends, the 100st (a) and 790th (b) image. The section (a) displays well-formed mineral grain boundaries with grain sizes that range from

1mm to 5mm with an overall coarse grain size. There is a low amount of dense mineralogy (BMS & oxides) at approximately 5%. There is a clearly discernible difference in grey levels between the two low density material (Silicates (SG < 3.6)) where the least dense material (Silicates (SG < 3)) displays elongate mineral grain shapes. In section (b) there is a high amount of dense mineralogy (BMS & oxides) present at approximately 40% with minor amounts of pentlandite (the brightest grey level mineral). The low density material (Silicates (SG < 3.6)) displays only one discernible grey level. The dense mineralogy (BMS & oxides) displays a net texture.

The GLCM distribution in figure 5-6 (c) displays three peaks, two are in the low density quadrant and one in the high density quadrant (indicated by the stippled ellipse). The two peaks in the low density quadrant are larger than that in the high density quadrant. This indicates that the GLCM is registering the two low density materials (Silicates (SG < 3.6)) in (a) and the small amount of dense mineralogy (BMS & oxides). The histogram showing the total value counts of each row in the matrix indicates that the peak grey values are 40, 60 and 225. The distribution between these two peaks is not separate however there is a distinct gap between the two peaks in the low density quadrant and the high density quadrant peak. The distribution of the two peaks in the low density quadrant is wide relative to the distance between the two peaks. This indicates a high grey level interaction between the two low density materials (Silicates (SG < 3.6)) and hence a medium to fine grain size. The GLCM (d) of (b) displays two peaks, one in the low density quadrant at a grey level of 60 and one in the high density quadrant at a grey level of 180.

The statistical GLCM graphs in figure 5-7 show random variation across the 800 images of drill 8 from the coarse PSD group (green group). The contrast values show the most a small local variation but remain consistent overall. The correlation trend line shows a high random variation. All of the four graphs show a change at the 290th image while energy and correlation show a change at the 530th image. Two image sections (a) and (b) have been selected to analyse the drill cores texture and mineralogy. In (a) the 1st image section from the region of interest displays two clearly visible dark grey level areas, the brighter of the two is coarse grained and the darker is medium to fine grained. Bright grey level minerals can also be seen in this image and are present as fine grains that are disseminated in texture. In (b) the 620th image section there are two low density materials (Silicates (SG < 3.6)), both present in equal amounts and are medium to fine grained. It also contains appreciable amounts of bright grey mineralogy.

The GLCM distribution in figure 5-7 (c) displays only one peak in the low density quadrant at a grey level of 35, however it is spread out along the diagonal towards the bottom right of the matrix. As indicated by the histogram there is a steady decrease in the counts registered by the GLCM from the low density quadrant to the high density quadrant. Even though there is no peak in the high density quadrant the presence of a distribution indicates the presence of bright grey level mineralogy. The distribution is wide indicating a high degree of grain boundary interaction and hence a fine grain size. In the GLCM distribution (d) there is one peak in the low density quadrant at a grey level of approximately 50 with the distribution extending into the top right corner of the matrix. The distribution

is narrow suggesting a coarse grained low density material (Silicates (SG < 3.6)). There is a detection of bright mineralogy in the GLCM (d) since there are bright minerals in the section (b).

The statistical GLCM graphs in figure 5-8, of the gangue drill core from the fine grained PSD grouping (red group), show minimal variation across the 800 images with a distinct change in the statistical values after the 300th image and 760th image. Contrast shows a high degree of local variation throughout the region of interest. Two image sections have been selected from the 3D GLCM analysis. In (a) the 1st image section displays two clearly low density materials (Silicates (SG < 3.6)) which have an approximate grain size of 1-5mm. There are no bright minerals in the section which is to be expected since this sample is entirely comprised of gangue mineralogy. The less dense material (Silicates (SG > 3)) displays well-formed grain boundaries which are surrounded by the least dense material (Silicates (SG < 3)). In (b) the 780th image section there are two low density materials (Silicates (SG < 3.6)), the less dense material (Silicates (SG > 3)) has a grain size of 25mm or more and appears to have minor amounts of the least dense material (Silicates (SG < 3)) present within the grain. The least dense material (Silicates (SG < 3)) also displays a large grain size of approximately 20mm as well as being fine grained. In both sectional images the grain boundaries are distinctly shape with some of the minerals forming sharp corners.

The GLCM distribution in figure 5-8 (c) displays only two peaks with one in the low density quadrant at a grey level of 120 and the other in the high density quadrant at a grey value of 155. These two peaks are positioned close to one another near the centre of the matrix with a tail of the distribution extending discontinuously into the top left corner of the matrix. The distribution has a moderate slope or width from the peaks which is an indication of a medium grain size. The tail in the low density quadrant may suggest the presence of pores in the sample since the tail ends at the low grey level value of 10 indicating a low density. In the GLCM distribution (d) there are two peaks with both in the low density quadrant at grey levels of approximately 85 and 110. Similar to the distribution in (c), two peaks are positioned close to one another in the low density quadrant with a tail of the distribution extending discontinuously into the top left corner of the matrix. The width of this distribution is smaller than that of (c) which is an indication of a coarse grain size.

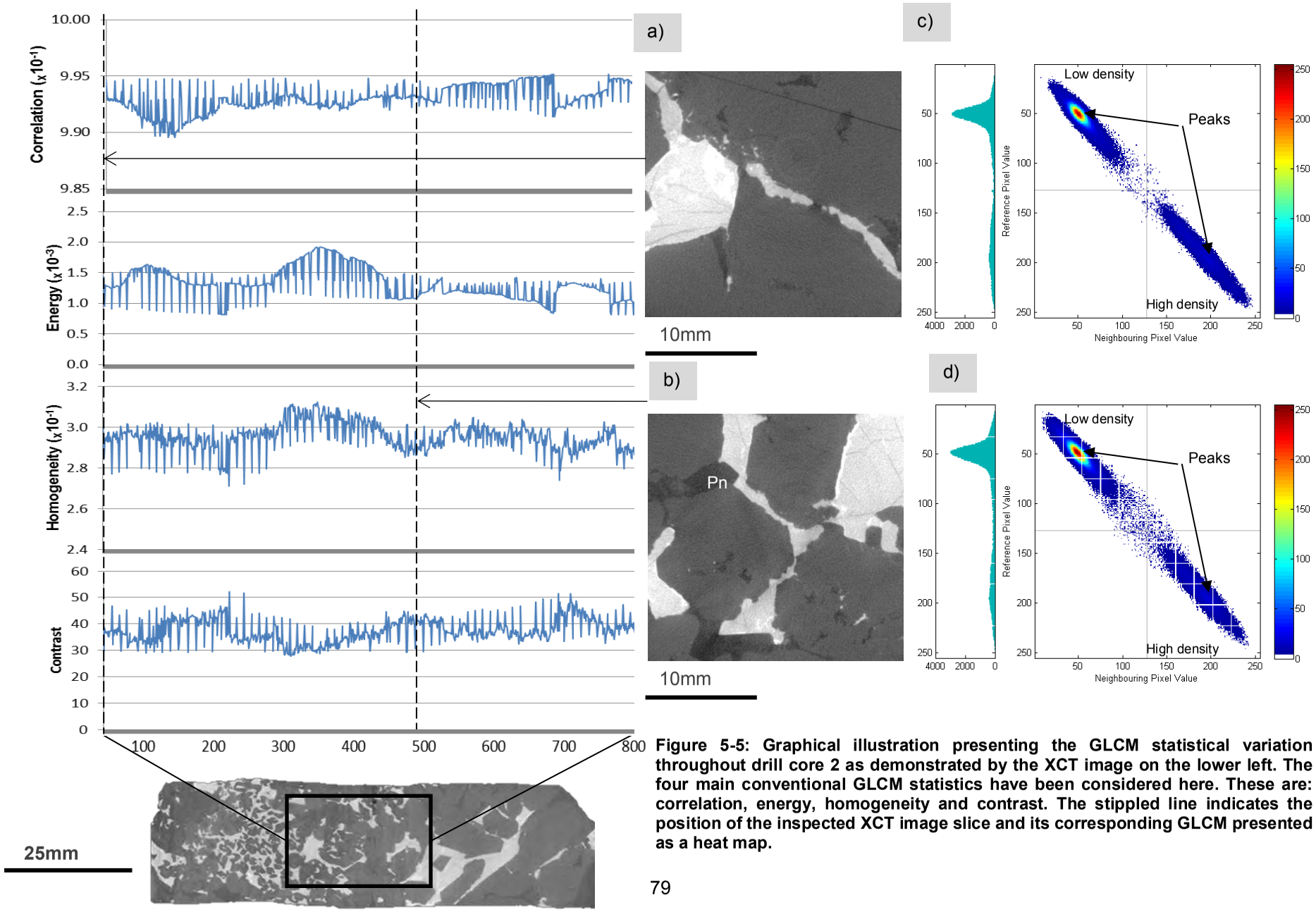

Figure 5-5: Graphical illustration presenting the GLCM statistical variation throughout drill core 2 as demonstrated by the XCT image on the lower left. The four main conventional GLCM statistics have been considered here. These are: correlation, energy, homogeneity and contrast. The stippled line indicates the position of the inspected XCT image slice and its corresponding GLCM presented as a heat map.

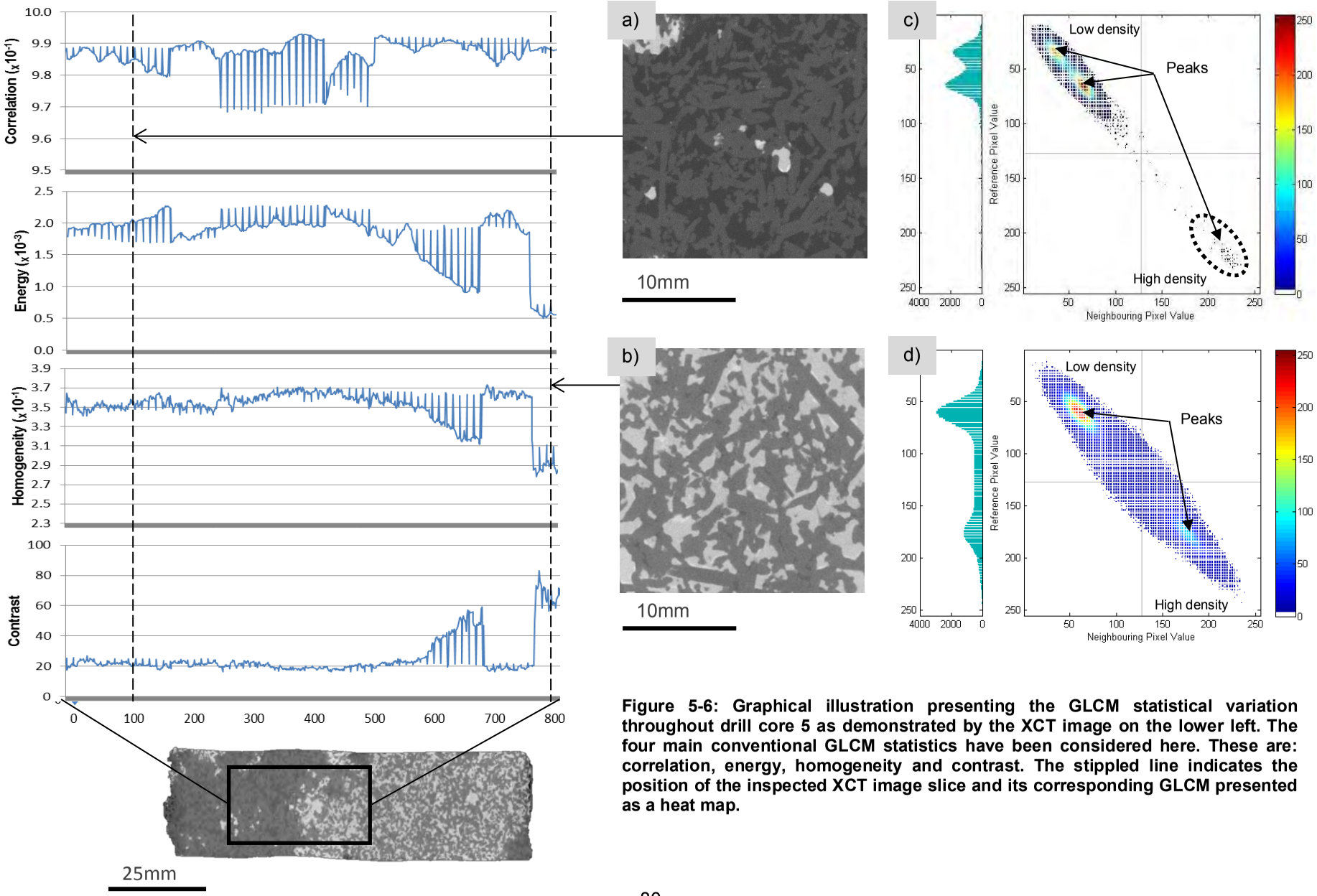

Figure 5-6: Graphical illustration presenting the GLCM statistical variation throughout drill core 5 as demonstrated by the XCT image on the lower left. The four main conventional GLCM statistics have been considered here. These are: correlation, energy, homogeneity and contrast. The stippled line indicates the position of the inspected XCT image slice and its corresponding GLCM presented as a heat map.

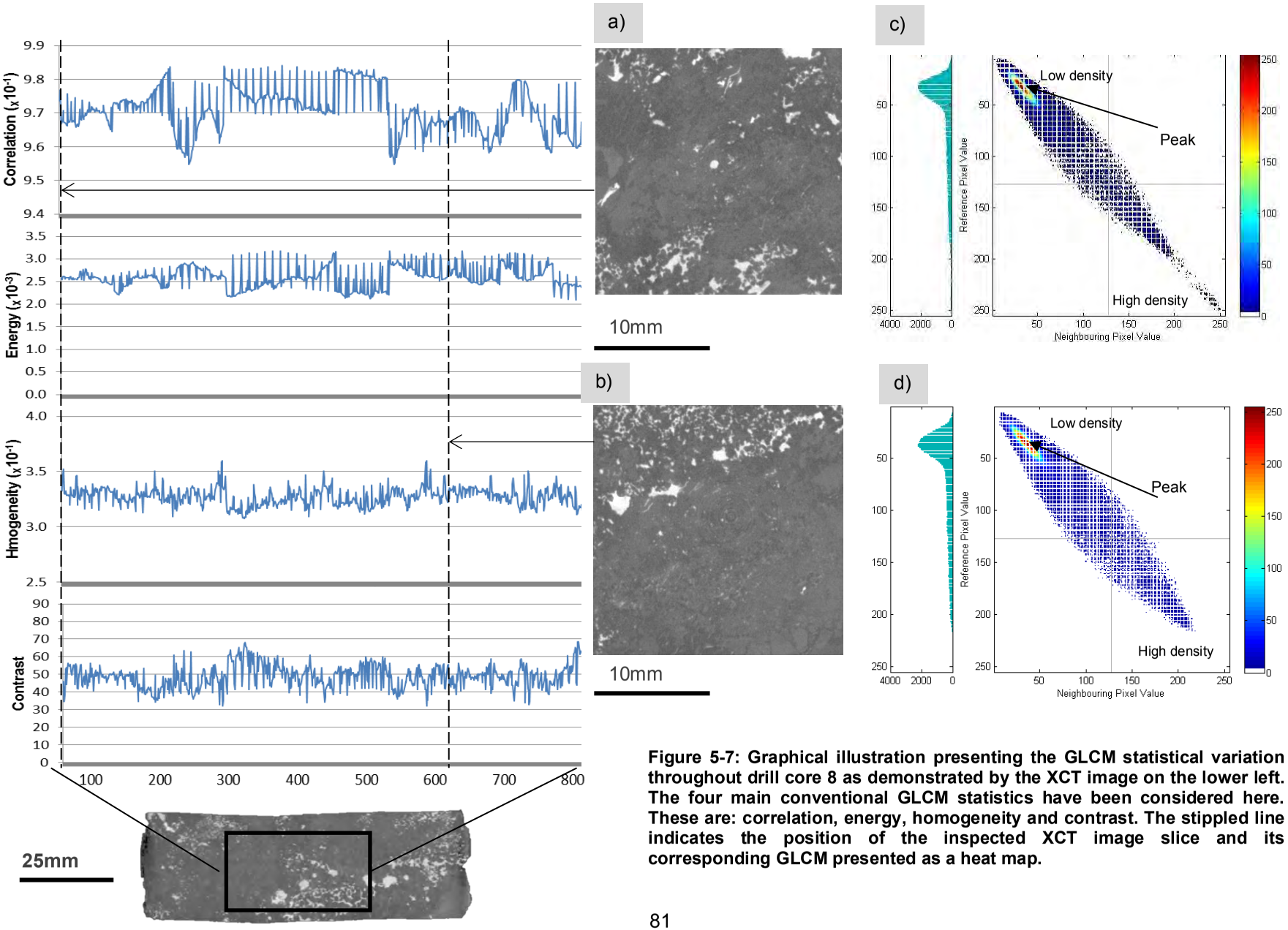

Figure 5-7: Graphical illustration presenting the GLCM statistical variation throughout drill core 8 as demonstrated by the XCT image on the lower left. The four main conventional GLCM statistics have been considered here. These are: correlation, energy, homogeneity and contrast. The stippled line indicates the position of the inspected XCT image slice and its corresponding GLCM presented as a heat map.

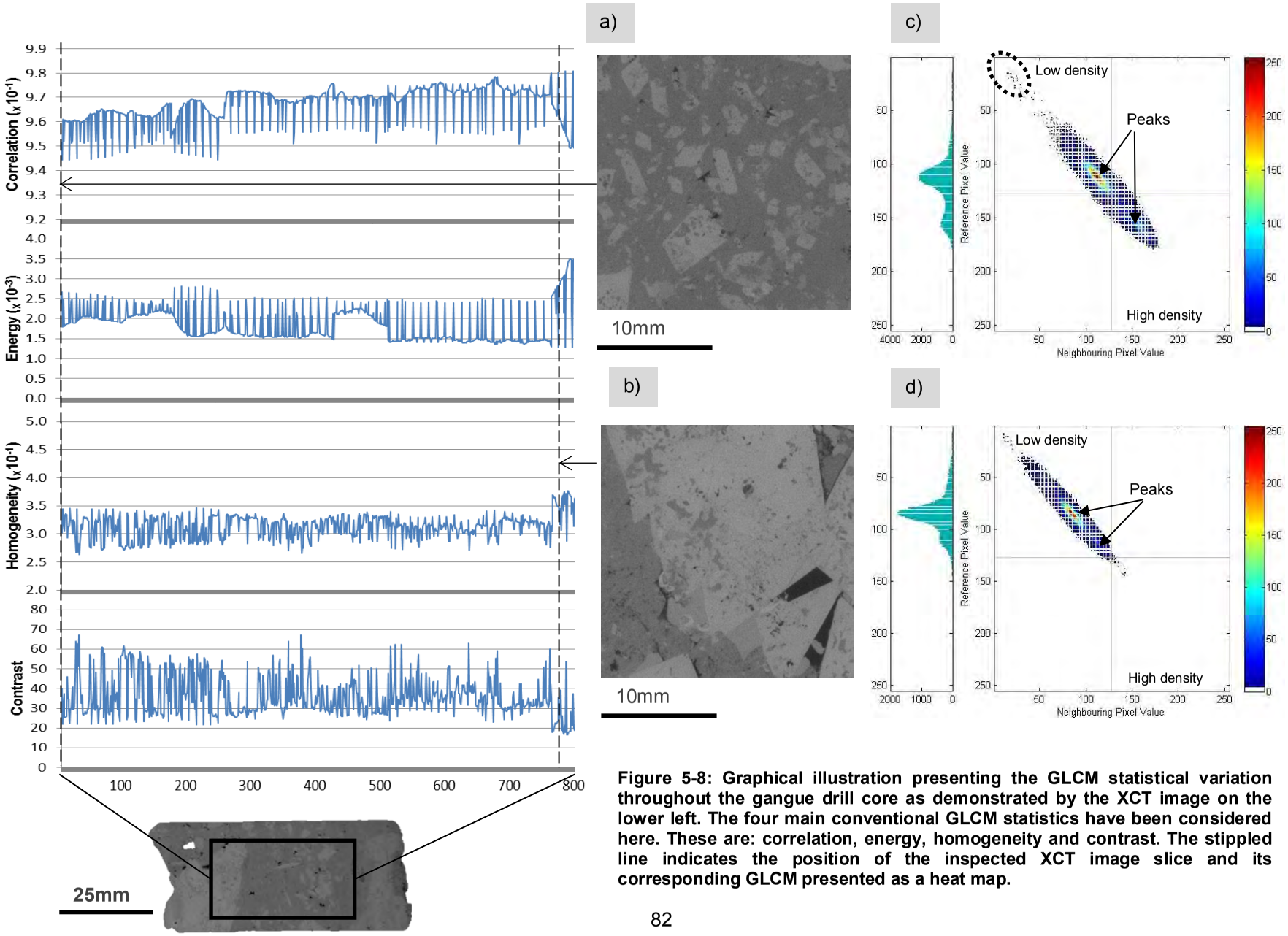

Figure 5-8: Graphical illustration presenting the GLCM statistical variation throughout the gangue drill core as demonstrated by the XCT image on the lower left. The four main conventional GLCM statistics have been considered here. These are: correlation, energy, homogeneity and contrast. The stippled line indicates the position of the inspected XCT image slice and its corresponding GLCM presented as a heat map.

5.4 Mineralogical and Textural Summary of Nkomati Drill Core 3D GLCM Results

The objective of the analysis by 3D GLCM is to provide rapid and consistent quantitative information on ore texture and simple mineralogy. The potential advantage of this approach is the ability to provide a measurable relationship between metallurgical performance and ore character.

From the presentation and discussion of the results in section 5.3 it is apparent that the GLCM provide two key pieces of information, simple mineralogy and ore texture. Figure 5-9 and 5-10 presents a summarised graphical presentation of the drill core sections analysed by GLCM and have been colour coded according to their corresponding PSD trends. There are four PSD trends (Fine - Yellow, Intermediate - Blue, Coarse - Green and a gangue - Red).

The fine PSD group shows the most variation between the GLCM. This may be due to the high variation of the textures seen between the four sectional images in figure 5-10 of ore 5 and 6, respectively. It may be that the high degree of textural and mineralogical variation is complimentary in comminution, although this is highly speculative and needs to be tested further. The intermediate PSD group shows a strong unique GLCM distribution where each of the GLCM registers two dominant grey level intensity peaks. The coarse PSD group also displays a distinct GLCM distribution with only one of the matrices (the second matrix of ore 7, figure 5-10) substantially different from the rest. In the inspection of the sectional image (the first matrix of ore 7, figure 5-10) it is clear that this image displays almost no bright grey level mineralogy whereas the others in this PSD grouping do have minor amounts of bright level minerals. Finally, the GLCM for the gangue sample show a unique distribution unlike any of the other PSD groupings.

The GLCM trends are therefore unique for each of the PSD trends with some groups displaying stronger GLCM similarity than others. For each of the ore samples the matrices define at least two peaks that are positioned apart and often in opposite quadrants, quite different as compared to the gangue sample where the peaks are closer together and tend toward the low density quadrant. The ability to analyse the texture of an internal image section make this quantitative analysis of texture innovative. This 3D analysis removes error associated with stereology and allows for the accurate analysis of ore. There are some unknown anomalies that occur within the GLCM matrices and statistics which may require further testing to fully understand, the noise identified in the statistical graphs for example. However, the information presented section 5.3 has clearly indicated that the GLCM are unique for the PSD groups, and that in theory the GLCM analysis of simple mineralogy and texture may be used to provide rapid and upfront information on mineral behaviour in beneficiation.

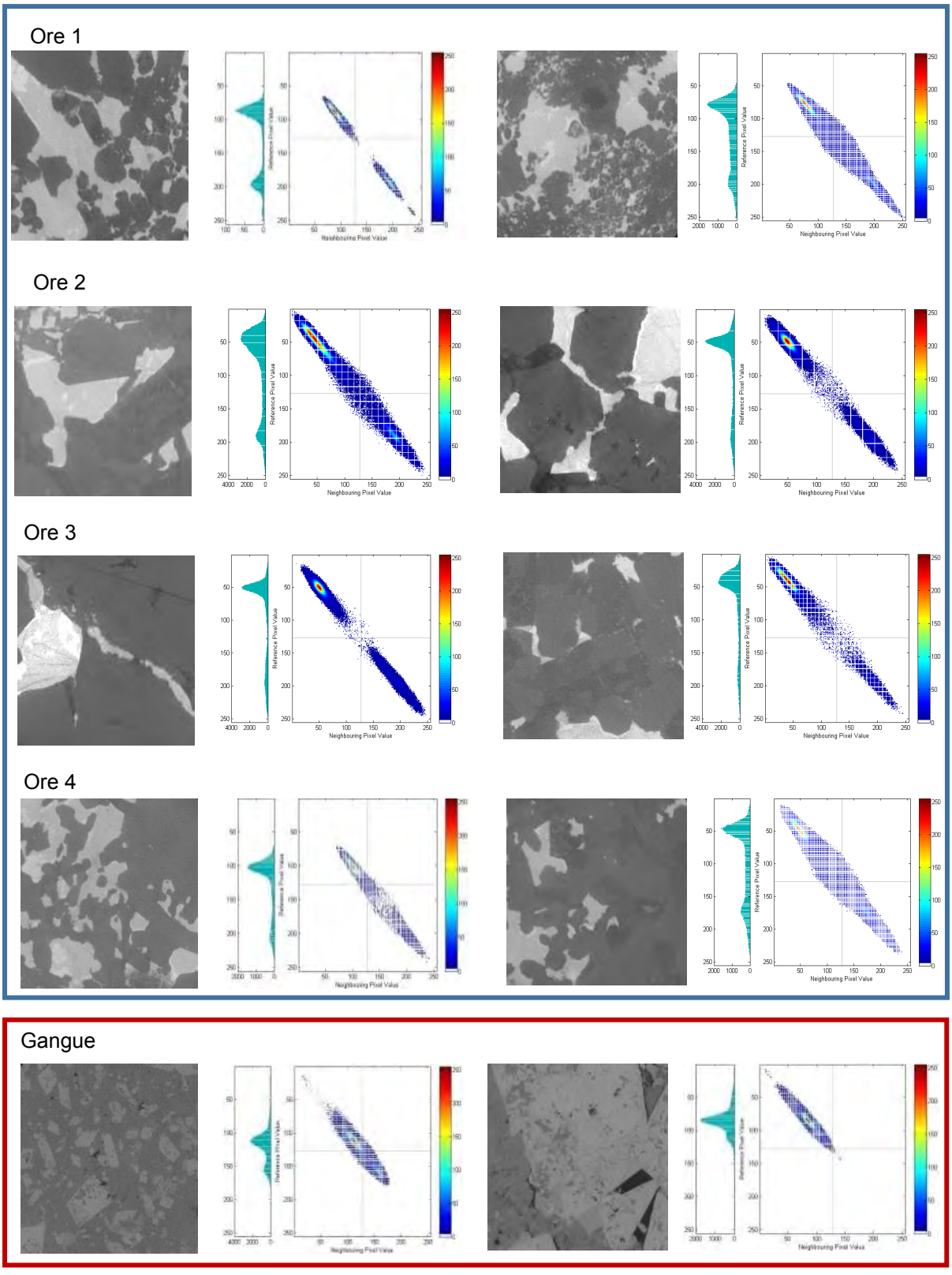

Figure 5-9 : The first series of XCT image sections of drill core 1, 2, 3, 4 and the gangue sample, and their respective GLCM distributions.

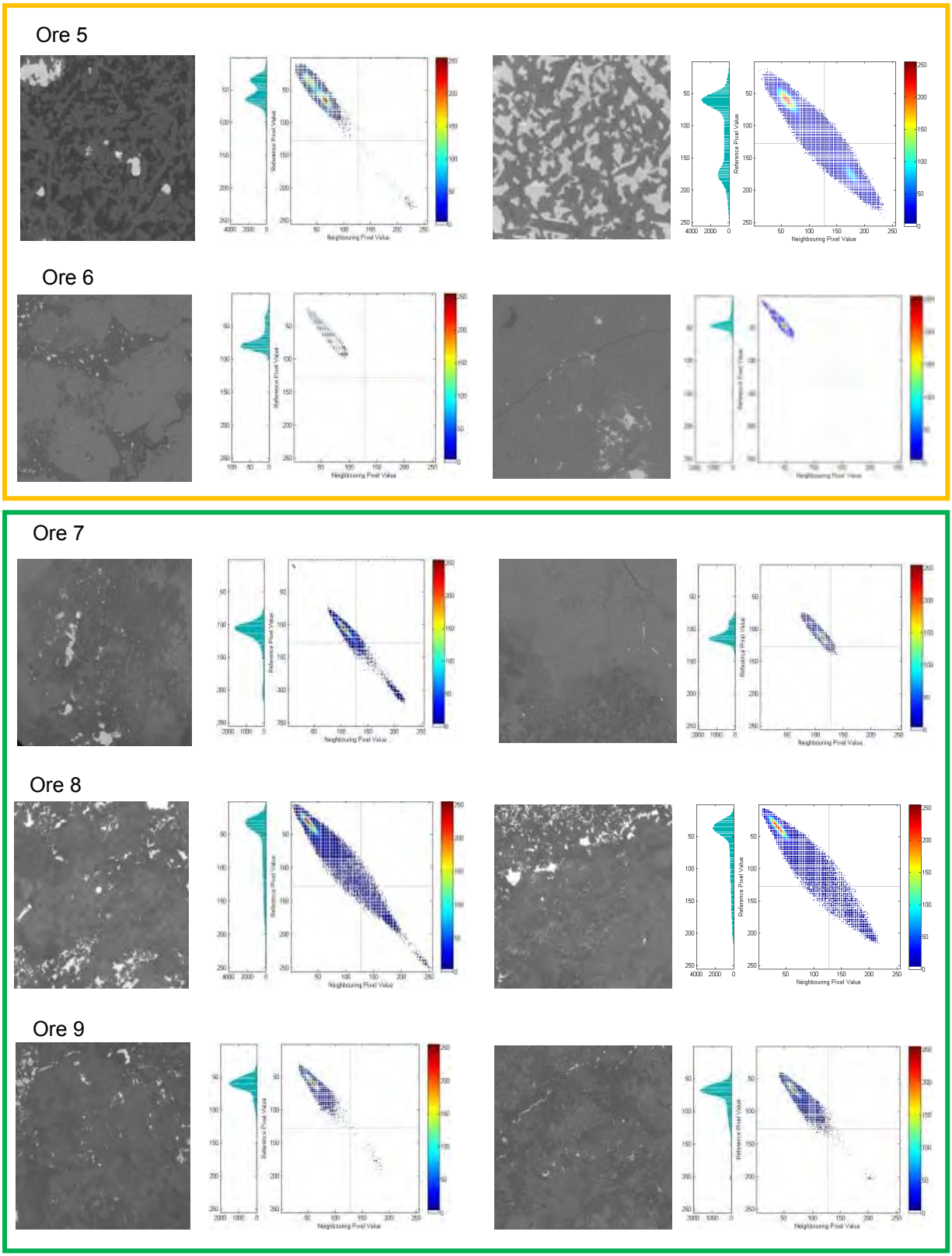

Figure 5-10: The second series of XCT image sections of drill core 5, 6, 7, 8 and 9 and their respective GLCM distributions.

The developed GLCM methodology has demonstrated the ability to analyse texture in 3D and repeatedly produce unique distribution within the matrices for each ore type. As a follow on from the earlier quote by Craig and Vaughan, (1994), samples that contain more evidence of metamorphic alteration have been through a work hardening process. Therefore ore sample with more alteration minerals and textures may be harder than ore samples with primary minerals and textures. This may provide some reasoning for the distinct PSD grouping and the relatively positive correlation with their textures.

Mineralogically, drill core 3 has a moderate amount of BMS, silicates with SG>3 (olivine, ortho and clino-pyroxene, amphibole) and other silicates with SG<3 (mica, plagioclase, quartz, serpentine, talc, chlorite and calcite). Drill core 5 has two areas of bulk mineralogy, one with high amounts of BMS and one with low amounts while both regions have low amounts of other silicates with SG<3 and moderate amounts of silicates with SG>3. Drill core 8 has a low amount of BMS, moderate amount of silicates with SG>3 and the highest amount of other silicates with SG<3 (serpentine). The gangue drill core is composed of post Nkomati origin mineralogy district with a lack of BMS and a high amount of silicates with SG>3 (CPX) and high amounts of other silicates with SG<3 (talc and serpentine).

Texturally, dill core 3 has a coarse grain size with poorly defined grain boundaries. Drill core 5 has moderate mineral grain sizes with well-formed needle like amphibole minerals. Drill core 8 has an overall fine grain size with poorly defined grain boundaries. Gangue drill core has a distinct bimodal distribution with large pyroxene minerals and a fine grained matrix of predominantly serpentine and talc mineralogy.

The successful application of 3D GLCM to quantify the texture present within this sample set now provides the motivation for further mineralogical and textural investigation of the Nkomati MMZ ore to fully and representatively characterise the ore body.

5.5 Potential Application in the Mining Industry

A key motivating factor for this project was to deliver innovative technology to the mining sector that can potentially lead to improved economic sustainability of mining activities. In the mining industry thousands of tonnes of ore are processed monthly, the content of which is statistically evaluated through rigorous samples techniques and campaigns (Farrell et al. 2011; Afewu and Lewis 1998; Lotter 1995). Some of the characterisation is done manually or descriptively by geologist. As introduced in section 4.1, increasing speed and accuracy in production is in demand which strengthens the need for automation through computer vision based tools (Brosnan and Sun 2002). The mining industry faces numerous challenges in today's economic climate such as increasing energy cost, environmental limitations, fluctuating commodity prices, unexpected ore body variation and an overall increase in ore body and processing circuit complexity (Northey et al. 2014; West 2011; Morrell 2009; Prior et al. 2012). In order to minimize energy costs, reduce environmental

impact, maximize final product quality and fully characterise variation that may cause complication in minerals processing, there needs to be a more transparent flow of relevant data. One way of achieving this is by replacing the slow and sometimes contradicting human interpretation of ore character with a computer vision based system that is rapid with consistent results. Apart from pre-existing hyperspectral imaging techniques, 3D data provides the opportunity to access true ore character information. Better data allows for better understanding, in the mining sector correct characterisation of ore begins with understanding mineralogy and texture, which ultimately leads to better understanding of ore types and their response to minerals processing.

In this study, results have shown that the 3D textural analysis method is sensitive to changes in mineralogy and texture within ore displaying fairly consistent results. The ability to quantify ore texture provides the opportunity, when coupled with a computer vision system, to produce rapid, robust and repeatable results for decision making in mining. Therefore this project provides a platform for further development into a computer vision tool. To do this the information must be linked to comminution and processing performance, a recommendation for future studies.

The data from such a system should measure the character of the ore that goes into the process, how this character affects process performance, and the character of the material that comes out of the process. Once processing performance and ore character have been established, then the ore character can be used as a proxy. There are already a few computer vision systems in place that use parameter and image processing to provide valuable insight into minerals processing performance such as the analysis of froth to determine bubble size, shape and burst rate (Morar et al. 2012; Liu et al. 2005; Marais and Aldrich 2011), factors that influence the efficiency of froth flotation. The newly developed 3D GLCM is another innovative analysis technique that is the first step towards meeting the demand to analyse more geomaterials in a shorter space of time and with a lower cost, which is also repeatable and consistent. This technology, when implemented on a mine-site, has the potential to provide rapid information upfront to geologists, mining engineers and metallurgist for rapid decision making in geometallurgy.

There are two main areas where the 3D GLCM texture analysis technique can be implemented in mining. These are during exploration for the analysis of drill core and during minerals processing for the analysis of ore entering the processing circuit. Since the technique is non-destructive all the drill core samples can be quantitatively analysed for trends in mineralogy and texture. This repeatable and consistent information, possibly the first of its kind of drill core, can be compared to bench, pilot and eventually full scale conventional metallurgical test work. Trends in mineralogy, texture and metallurgical response may potentially be linked. Once ore has been characterised in this manner, future rapid information obtained from this analysis may be used to predict ore behaviour in minerals processing. Further research could extend its impact by analysing material traveling on conveyer belts on path to the mill to measure the effects of mineralogy and texture on throughput, recovery, flotation performance and even perform autonomous ore sorting.

.

Chapter 6 : Conclusions and Recommendations

6.1 Conclusions

The importance of ore texture and its variability affecting metallurgical performance has long been recognised. Therefore, the first objective of this thesis was “to develop a methodology for the mineralogical and textural analysis of geomaterials using XCT coupled with 3D GLCM”. The second objective of this thesis was “to assess the application of XCT coupled with 3D GLCM for the quantitative textural analysis of drill core: Case study of the Nkomati nickel sulphide ore”.

A methodology for the 3D quantitative and textural analysis of drill core was accordingly developed in Chapter 4 in fulfilment of the first objective. The method was based on using 3D XCT to image the internal structure of drill core. Thereafter, appropriate software code was written on a MATLAB platform for the 3D quantitative analysis of drill core. This involved extending the well-known 2D grey level co-occurrence matrices into a 3D script suitable for image analysis of XCT grey level volumes. A series of XCT image sections from each drill core were sorted digitally as multi-dimensional arrays in computation. This pixel information was rearranged according to specific geometric dimensions for the GLCM analysis of all 13 unique pixel pair directions. This method is not subject to stereological error.

The GLCM were thereafter interpreted with the focus on what mineralogical and textural information could be drawn from them, rather than just using conventional GLCM statistics. Although the GLCM statistics indicated some sensitivity to textural variations, this could not be simply correlated with qualitative mineralogical and textural information. Further investigation showed that the position and intensity of the GLCM peaks in a colour heat map correlated with the relative grey level populations in the XCT data (a function of mineral density): peaks representing dense mineral phases were located in the bottom right hand quadrant and peaks representing light mineral phases were located in the top left quadrant. The width of the GLCM peaks away from the diagonal showed a correlation with mineral grain size dependent on the degree of grain boundary interaction between neighbouring pixels. A narrow distribution indicated a coarse grain size population, whereas a broad distribution indicated a fine grain size population. This appears to be the first time that such mineralogical and textural information has been interpreted and described for the GLCM in the geosciences.

Potential opportunities for the application of this approach where XCT and 3D GLCM information could provide value in the broader field of geosciences were highlighted: The analysis of oil reservoir material by XCT is favourable since it allows for the qualitative and quantitative inspection of void

volume, porosity size and shape, as well as interconnectivity in 3D. The proposed methodology would allow for the characterisation and recognition of reservoir rock texture with the potential for automation.

The application of XCT coupled with 3D GLCM for the 3D quantitative textural analysis of drill core was investigated using a case study from the Nkomati nickel mine in Chapter 5 in fulfilment of the second objective. Ten samples from the Nkomati MMZ deposit ranging from low, moderate and high sulphide content and representing a range of styles of sulfide mineralization were investigated. The samples were subdivided into four textural groups on the basis of their particle size distribution from laboratory scale rod milling: coarse PSD, intermediate PSD, fine PSD and gangue sample PSD. This geometallurgical approach was used in preference to subjective and qualitative geological descriptions. The 3D GLCM were thereafter successfully run on XCT volumes of 25 mm diameter drill cores extracted from the ten Nkomati samples in the D1 unique direction. Complimentary QEMSCAN mineralogical data was used facilitate the interpretation of the grey level XCT data. In the case of Nkomati, the GLCM peaks in the bottom right (high density quadrant) correlated with the relative abundance of the sulphides (pyrrhotite, pentlandite and chalcopyrite) and oxide minerals. Two peaks could be defined in the low density quadrant (top left) that correlated with the relative abundance of silicate minerals with SG greater than 3 (olivine, orthopyroxene, clinopyroxene, actinolite), and silicate minerals with an SG less than 3 (mica, plagioclase, quartz, serpentine, talc, chlorite, calcite). The GLCM distributions were also able to capture changes between coarse and fine grained Nkomati samples. Comparison of the GLCM across the four textural groups and 10 samples, showed a low degree of similarity for the fine PSD group (possibly due to sample representativeness), whereas results for the intermediate PSD, coarse PSD and gangue group each demonstrated unique GLCM distributions.

The methodology developed in this thesis has the potential to run as an automated, online, rapid, routine, non-destructive computer vision tool for drill core logging on a mine site. The mining industry typically processes thousands of tonnes of ore per month. The challenge for such an operation is to rapidly provide statistically representative data capturing the mineralogical and textural variability of the ore body which can be incorporated into the geometallurgical block model. Ultimately this quantitative mineralogical and textural data should be coupled to metallurgical performance (PSD of mill, crusher and flotation feeds and products as well as throughput, recovery and energy consumption) to fully embrace the concept of a comprehensive ore body geometallurgical model.

6.2 Recommendations

The true impact of such an analysis may only be realized in many years to come. To ensure timely further development of this methodology the following recommendations are given:

- **Further script development for increased computing performance:** The script developed in this study is suited for relatively small data sets and could be further modified for parallel computing. This will improve processing performance and allow for the analysis to be conducted on computers with lower computing power. The use of a C++ dashboard could make data management more user friendly. Further testing of the 3D code with images that have been uncropped will significantly decrease post XCT image processing time. In addition, the XCT software package Avizo Fire allows for the MATLAB scripts as plugins enabling image reconstruction and image analysis to be done with the same software. This may take the technology closer to automation.
- **Establishing the robustness of the GLCM:** Further investigation is needed to establish the minimum number of GLCM unique directions (D1 to D13) needed to quantify ore texture. This will significantly reduce the computing capacity needed for the quantitative textural analysis. Focus should be given to samples and ore types that showcase greater textural variability (e.g. distinct foliations or laminated textures) where more than one unique direction (D1 to D13) may be needed for quantitative textural analysis.

- **Determining the quantitative relationship between ore texture and metallurgy:** The next challenge is to comprehensively link the information produced by this quantitative textural measure of ore texture to the behaviour of ore in different metallurgical processes. The ultimate goal of which is to provide metallurgical engineers with proxy data that may act as a basis of which to monitor processing performance.

- **Pilot scale testing, automation and mine site development:** The technology can be further developed by totally redesigning the XCT apparatus. The design could be similar to that of figure 1-4 but scaled down for the continual analysis of drill core. This, geometrically, would allow for scale up routine analysis of drill core. Initial pilot scale testing may further prove the technology and allow for automation test work, given the size of the sample sets. The use of such a technique on a mine site depends upon demonstrated proven 3D XCT GLCM technology that adds significant value to a mining operation (that also covers the cost to run the machinery) to improve profit margins and increase sustainability.

- **Application in the broader geosciences:** The presentation of this methodology into the broader geosciences should be enabled by publication of the coupled XCT and 3D GLCM code into the peer reviewed scientific literature (*Journal paper in preparation for submission to Computers and Geosciences*). A proven 3D textural analysis technology has significant potential to add value in the geoscience and mining industry. The automation of oil reservoir characterisation based on quantitative textural measures to recognize favorable reservoir conditions is just but one example.

References

Afewu, K.I. and Lewis, G.O., 1998. Sampling of run-of-mine mill feed - A practical approach. *The Journal of the Southern African Institute of Mining and Metallurgy*, pages.299–306.

AMR Intergrated Annual Report, 2014. Intergrated Annual Report 2014 African Rainbow Minerals Platinum,

Andersen, J.C.Ø. Rollinson, G.K. Snook, B. Herrington, R. and Fairhurst, R.J., 2009. Use of QEMSCAN® for the characterization of Ni-rich and Ni-poor goethite in laterite ores. *Minerals Engineering*, 22, pages.1119–1129.

Andrew, C., 2012. The Science of Subjectivity. *Geological Society of America*, 40, pages.95–96.

Baker, D.R. Mancini, L. Polacci, M. Higgins, M.D. Gualda, G. a. R. Hill, R.J. and Rivers, M.L., 2012. An introduction to the application of X-ray microtomography to the three-dimensional study of igneous rocks. *Lithos*, 148, pages.262–276.

Baum, W., 2014. Ore characterization, process mineralogy and lab automation a roadmap for future mining. *Minerals Engineering*, 60, pages.69–73.

Brosnan, T. and Sun, D.-W., 2002. Inspection and grading of agricultural and food products by computer vision systems—a review. *Computers and Electronics in Agriculture*, 36, pages.193–213.

Bulled, D., 2007. Flotation Circuit Design for Adanac Moly Corp using a Geometallurgical Approach. *SGS Technical Bulletin*, pages.1–10.

Carlson, W.D., 2006. Three-dimensional imaging of earth and planetary materials. *Earth and Planetary Science Letters*, 249, pages.133–147.

Castano, R. Estlin, T. Anderson, R. Gaines, D. Castano, A. Bornstein, B. Chouinard, C. and Judd, M., 2007. OASIS: Onboard Autonomous Science Investigation System for Opportunistic Rover Science. *Journal of Field Robotics*, 24, pages.379–397.

Chai, H.Y. Wee, L.K. Swee, T.T. Salleh, S.H. Ariff, A.K. and Kamarulafizam, 2011. Gray-level co-occurrence matrix bone fracture detection. *American Journal of Applied Sciences*, 8, pages.26–32.

Charikinya, E. Bradshaw, S. and Becker, M., 2015. Characterising and quantifying microwave induced damage in coarse sphalerite ore particles. *Minerals Engineering*, 82, pages.14–24.

Chetty, D. Gryffenberg, L. Lekgetho, T. and Molebale, I., 2009. Automated SEM study of PGM distribution across a UG2 flotation concentrate bank: implications for understanding PGM floatability. *The Southern African Institute of Mining and Metallurgy*, pages.587–593.

Cnudde, V. and Boone, M.N., 2013. High-resolution X-ray computed tomography in geosciences: A review of the current technology and applications. *Earth-Science Reviews*, 123, pages.1–17.

Cockburn, G., 2013. Challenges and successes at the Nkomati Nickel JV : pit-to-product process improvements. *The Southern African Institute of Mining and Metallurgy, Base Metals Conference*, pages.151–168.

Contreras, R.J. Fréderic, V.L. Jean-françois, D. Marek, S. Štěpánek, M.F. and Pirard, E., 2014. Effect of Raw Material Properties on the Kinetics of Iron Ores Granulation. *Metec and 2nd Estad*, pages.15–19.

Craig, J.R., 2001. Ore-mineral textures and the tales they tell. *Canadian Mineralogist*, 39, pages.937–956.

Craig, J.R. and Vaughan, D.J., 1994. Ore Microscopy and Ore Petrography 2nd ed., *John Wiley & Sons, Inc.*

Van Dalen, G. and Koster, M.W., 2012. 2D & 3D particle size analysis of micro-CT images. *Bruker-microCT UserMeeting 2012*, pages.16–31.

Denison, C. Carlson, W.D. and Ketcham, R.A., 1997. Three-dimensional quantitative textural analysis of metamorphic rocks using high-resolution computed X-ray tomography: Part I. Methods and techniques. *Journal of Metamorphic Geology*, 15, pages.29–44.

Deveci, H. Akcil, A. and Alp, I., 2004. Bioleaching of complex zinc sulphides using mesophilic and thermophilic bacteria: Comparative importance of pH and iron. *Hydrometallurgy*, 73, pages.293–303.

Dhara, A.K. Mukhopadhyay, S. and Khandelwal, N., 2012. 3D Texture Analysis of Solitary Pulmonary Nodules using Co-occurrence Matrix from Volumetric Lung CT Images. *Preceedings of Spie - The International Society for Optical Engineering*, pages.1–5.

Dhawan, N. Safarzadeh, M.S. Miller, J.D. Moats, M.S. Rajamani, R.K. and Lin, C.-L., 2012. Recent advances in the application of X-ray computed tomography in the analysis of heap leaching systems. *Minerals Engineering*, 35, pages.75–86.

Dominy, S. Platten, I. Howard, L. Elangovan, P. Armstrong, R. Minnitt, R.C.A. and Abel, R.L., 2011. Characterisation of gold ores by X-ray computed tomography–Part 2: Applications to the determination of gold particle size and distribution. *The First AusIMM Interational Geometallugy Conference*, pages.5–7.

Dong, K. Feng, Y. Jacobs, K.M. Lu, J.Q. Brock, R.S. Yang, L. V. Bertrand, F.E. Farwell, M. a and Hu, X.-H., 2011. Label-free classification of cultured cells through diffraction imaging. *Biomedical optics express*, 2, pages.1717–26.

Donskoi, E. Suthers, S.P. Fradd, S.B. Young, J.M. Campbell, J.J. Raynlyn, T.D. and Clout, J.M.F., 2007. Utilization of optical image analysis and automatic texture classification for iron ore particle characterisation. *Minerals Engineering*, 20, pages.461–471.

Dunham, S. and Vann, J., 2007. Geometallurgy , Geostatistics and Project Value — Does Your Block Model Tell You What You Need to Know ? *Project Evaluation Conference*, pages.19–20.

Eichkitz, C.G. Amtmann, J. and Schreilechner, M.G., 2013. Calculation of grey level co-occurrence matrix-based seismic attributes in three dimensions. *Computers & Geosciences*, 60, pages.176–183.

Fandrich, R. Gu, Y. Burrows, D. and Moeller, K., 2007. Modern SEM-based mineral liberation analysis. *International Journal of Mineral Processing*, 84(1-4), pages.310–320.

Farrell, J.N. Miller, A.D. and Gaze, R.L., 2011. Geometallurgical Sampling and Resource Estimation for Magnetite Deposits. *The Flirst AusIMM International Geometallurgy Conference*, pages.5–7.

Fernández-Martínez, J.L. Fernández-Alvarez, J.P. and Pedruelo-González, L.M., 2008. MTCLAB: A MATLAB®-based program for traveltime quality analysis and pre-inversion velocity tuning in 2D transmission tomography. *Computers and Geosciences*, 34, pages.213–225.

Friedrich, J.M., 2008. Quantitative methods for three-dimensional comparison and petrographic description of chondrites. *Computers and Geosciences*, 34, pages.1926–1935.

Gadkari, D., 2004. Image Quality Analysis Using GLCM. *MSc Thesis, University of Central Florida*.

Gao, X. Qian, Y. Loomes, M. Comley, R. Barn, B. Chapman, A. and Rix, J., 2011. Retrieval of 3D Medical Images via Their Texture Features. *International Journal of Advances in Software*, 4, pages.499–509.

Gaspar, O. and Pinto, A., 1991. The ore textures of the neves-Corvo volcanogenic massive sulphides and their implications for ore beneficiation. *Mineralogical Magazine*, 55, pages.417–422.

Gauert, C., 2001. Sulphide and oxide mineralisation in the Uitkomst Complex, South Africa: origin in a magma conduit. *Journal of African Earth Sciences*, 32, pages.149–161.

Gauert, C.D.K. De Waal, S. a. and Wallmach, T., 1995. Geology of the ultrabasic to basic Uitkomst complex, eastern Transvaal, South Africa: an overview. *Journal of African Earth Sciences*, 21, pages.553–570.

Gazo, R. and Benes, B., 2013. Computed Tomogrophy Log Scanning: An Industrial Application. *The 4th International Scientific Conference on Hardwood Processing*, pages.140–147.

Van Geet, M. Swennen, R. and Wevers, M., 2001. Towards 3-D petrography: Application of microfocus computer tomography in geological science. *Computers and Geosciences*, 27, pages.1091–1099.

Ghorbani, Y. Becker, M. Petersen, J. Mainza, A.N. and Franzidis, J.-P., 2013. Investigation of the effect of mineralogy as rate-limiting factors in large particle leaching. *Minerals Engineering*, 52, pages.38–51.

Ghorbani, Y. Becker, M. Petersen, J. Morar, S.H. Mainza, A. and Franzidis, J.-P., 2011. Use of X-ray computed tomography to investigate crack distribution and mineral dissemination in sphalerite ore particles. *Minerals Engineering*, 24, pages.1249–1257.

Giroux, B. Gloaguen, E. and Chouteau, M., 2007. bh_tomo-a Matlab borehole georadar 2D tomography package. *Computers and Geosciences*, 33, pages.126–137.

Godel, B., 2006. 3-D Distribution of Sulphide Minerals in the Merensky Reef (Bushveld Complex, South Africa) and the J-M Reef (Stillwater Complex, USA) and their Relationship to Microstructures Using X-Ray Computed Tomography. *Journal of Petrology*, 47, pages.1853–1872.

Godel, B. Barnes, S.J. Barnes, S.-J. and Maier, W.D., 2010. Platinum ore in three dimensions: Insights from high-resolution X-ray computed tomography. *Geology*, 38, pages.1127–1130.

Gonçalves, L.B. and Leta, F.R., 2010. Macroscopic Rock Texture Image Classification Using a Hierarchical Neuro-Fuzzy Class Method. *Mathematical Problems in Engineering*, pages.1–24.

Gottlieb, P. Wilkie, G. Sutherland, D. and Ho-Tun, E., 2000. Using quantitative electron microscopy for process mineralogy applications. *Journal of Mineralogy*, pages.24–25.

Gu, Y. and Rd, I., 2003. Automated Scanning Electron Microscope Based Mineral Liberation Analysis. , 2, pages.33–41.

Hansen, T.M. Cordua, K.S. Looms, M.C. and Mosegaard, K., 2013. SIPPI: A Matlab toolbox for sampling the solution to inverse problems with complex prior information: Part 2-Application to crosshole GPR tomography. *Computers and Geosciences*, 52, pages.481–492.

Haralick, R.M. Shanmugam, K. and Dinstein, I., 1973. Textural Features for Image Classification. *IEEE Transactions on Systems, Man, and Cybernetics*, 3, pages.610–621.

Hartner, R. Walters, S. and Berry, R., 2011. Optical and SEM based microscopy integration for optimisation of geometallurgical modelling and ore deposit characterisation. *The First AusIMM Interational Geometallugy Conference*, pages.5–7.

Hinds, O. Duller, R.A. Walker, R.P. Wells, B.T. and Worden, R.H., 2014. Enhanced Two Dimensional Grain Size Analysis through the Use of Calibrated Digital Petrography *. , pages.1–7.

Hornsey, R.A., 2000. The Genesis and Evolution of the Nkomati Mine Ni-sulphide Deposit, Mpumalanga Province, South Africa.

Howard, L.E. Elangovan, P. Dominy, S.C. Armstrong, R. and Hezel, D., 2011. Characterisation of Gold Ores by X-Ray Computed Tomography – Part 1 : Software for Calibration and Quantifi cation of Mineralogical Phases. , pages.5–7.

Jankovic, A., 2003. Variables affecting the fine grinding of minerals using stirred mills. *Minerals Engineering*, 16, pages.337–345.

Ketcham, R. a. and Carlson, W.D., 2001. Acquisition, optimization and interpretation of X-ray computed tomographic imagery: applications to the geosciences. *Computers & Geosciences*, 27, pages.381–400.

Khuzi, A.M. Besar, R. Wan Zaki, W. and Ahmad, N., 2009. Identification of masses in digital mammogram using gray level co-occurrence matrices. *Biomedical imaging and intervention journal*, 5, pages.e17.

Kim, N. Amin, V. Wilson, D. Rouse, G. and Udpa, S., 1998. Ultrasound image texture analysis for

characterizing intramuscular fat content of live beef cattle. *Ultrasonic imaging*, 20, pages.191–205.

Kleber, F. Pramerdorfer, C. Wetzinger, E. and Kampel, M., 2015. Optical Sensor Evaluation for Vision Based Recognition of Electronics Waste. *Journal of Environmental Science and Development*, (12), pages.929–933.

Knight, R. Hoal, K.O. and Abraham, A.P.G., 2011. Three-Dimensional Geometallurgical Data Integration for Predicting Concentrate Quality and Tailings Composition in a Massive Sulfi de Deposit. , pages.227–232.

Kodali, P. Dhawan, N. Depci, T. Lin, C.L. and Miller, J.D., 2011. Particle damage and exposure analysis in HPGR crushing of selected copper ores for column leaching. *Minerals Engineering*, 24, pages.1478–1487.

Kyle, J.R. and Ketcham, R.A., 2015. Application of high resolution X-ray computed tomography to mineral deposit origin, evaluation, and processing. *Ore Geology Reviews*, 65, pages.821–839.

Kyle, J.R. Mote, A.S. and Ketcham, R. a., 2008. High resolution X-ray computed tomography studies of Grasberg porphyry Cu-Au ores, Papua, Indonesia. *Mineralium Deposita*, 43, pages.519–532.

Li, C. Ripley, E.. Maier, W.. and Gomwe, T.E.., 2002. sulfur isotopic compositions of the Uitkomst Ni–Cu sulfide ore-bearing complex, South Africa: evidence for sulfur contamination and multiple magma emplacements. *Chemical geology*, 188, pages.149–159.

Liebezeit, V. Smith, M. Ehrig, K. Kittler, P. Macmillan, E. and Lower, C., 2011. Geometallurgy Data Management – A Signifi cant Consideration. *The First AusIMM Interational Geometallugy Conference*, pages.5–7.

Lin, C.L. and Miller, J.D., 1996. Cone beam X-ray microtomography for three-dimensional liberation analysis in the 21st century. *International Journal of Mineral Processing*, 47, pages.61–73.

Liu, J.J. MacGregor, J.F. Duchesne, C. and Bartolacci, G., 2005. Flotation froth monitoring using multiresolutional multivariate image analysis. *Minerals Engineering*, 18, pages.65–76.

Lotter, N.O., 1995. Review of evaluation models for the representative sampling of ore. *The Journal of the Southern African Institute of Mining and Metallurgy*, pages.149–156.

Lotter, N.O. Kormos, L.J. Oliveira, J. Fragomeni, D. and Whiteman, E., 2011. Modern Process Mineralogy: Two case studies. *Minerals Engineering*, 24, pages.638–650.

Lu, L.L.L. Ordonez, C. Collins, E.G. and DuPont, E.M., 2009. Terrain Surface Classification for Autonomous Ground Vehicles Using a 2D Laser Stripe-Based Structured Light Sensor. *IEEE/RSJ International Conference on Intelligent Robots and Systems*, pages.1–8.

Maki, J. Thiessen, D. Pourangi, A. Kobzeff, P. Litwin, T. Scherr, L. Elliott, S. Dingizian, A. and Maimone, M., 2012. The Mars Science Laboratory engineering cameras. *Space Science Reviews*, 170, pages.77–93.

Marais, C. and Aldrich, C., 2011. The estimation of platinum flotation grade from froth image features by using artificial neural networks. *Journal of the South African Institute of Mining …*, 111, pages.11–14.

Mathur, P., 2012. Terrain Classification for Traversability Analysis for Autonomous Robot Navigation in Unknown Natural Terrain. *International Journal of Engineering Science and Technology*, 4, pages.38–49.

Mishra, G. Viljoen, K.S. and Mouri, H., 2013. Influence of mineralogy and ore texture on pentlandite flotation at the Nkomati nickel mine, South Africa. *Minerals Engineering*, 54, pages.63–78.

Morar, S.H. Harris, M.C. and Bradshaw, D.J., 2012. The use of machine vision to predict flotation performance. *Minerals Engineering*, 36, pages.31–36.

Morrell, S., 2009. Predicting the overall specific energy requirement of crushing, high pressure grinding roll and tumbling mill circuits. *Minerals Engineering*, 22, pages.544–549.

Mostaço-Guidolin, L.B. Ko, A.C.-T. Wang, F. Xiang, B. Hewko, M. Tian, G. Major, A. Shiomi, M. and Sowa, M.G., 2013. Collagen morphology and texture analysis: from statistics to classification.

Scientific reports, 3, pages.1–10.

Northey, S. Mohr, S. Mudd, G.M. Weng, Z. and Giurco, D., 2014. Modelling future copper ore grade decline based on a detailed assessment of copper resources and mining. *Resources, Conservation and Recycling*, 83, pages.190–201.

Nurtanio, I. Astuti, E.R. Ketut Eddy Pumama, I. Hariadi, M. and Purnomo, M.H., 2013. Classifying cyst and tumor lesion using Support Vector Machine based on dental panoramic images texture features. *IAENG International Journal of Computer Science*, 40, pages.29–37.

Nwaila, G., 2014. Application of HPGR and X-Ray CT to investigate the potential of Witwatersrand gold ore for heap leaching : A process mineralogy approach. *MSc Thesis, University of Cape Town*.

Nyambayo, C.K., 2014. The use of mixed thiol collectors in the flotation of Nkomati sulfide ore. *MSc Thesis, University of Cape Town*.

Ojala, T. Pietikäinen, M. and Harwood, D., 1996. A comparative study of texture measures with classification based on featured distributions. *Pattern Recognition*, 29, pages.51–59.

Oyarzún, M. and Arévalo, A., 2011. Rock Texture and BWi Relationships , El Teniente Ore Deposit , Chile. *The First AusIMM Interational Geometallugy Conference*, pages.5–7.

Parbhakar-Fox, A.K. and Bradshaw, D.J., 2013. Cost-Effective Means for Identifying Acid Rock Drainage Risks – Integration of the Geochemistry- Mineralogy-Texture Approach and Geometallurgical Techniques. *2nd AusIMM International Geometallurgy Conference*, pages.143–154.

Parbhakar-Fox, A.K. Edraki, M. Walters, S. and Bradshaw, D., 2011. Development of a textural index for the prediction of acid rock drainage. *Minerals Engineering*, 24, pages.1277–1287.

Partio, M. Cramariuc, B. Gabbouj, M. and Visa, A., 2002. Rock texture retrieval using gray level co-occurrence matrix. *The Proceedings of the 5th Nordic Signal Conference*, pages.1–5.

Pascoe, R.D. Power, M.R. and Simpson, B., 2007. QEMSCAN analysis as a tool for improved understanding of gravity separator performance. *Minerals Engineering*, 20, pages.487–495.

Patel, A.K. and Chatterjee, S., 2014. Computer vision-based limestone rock-type classification using probabilistic neural network. *Geoscience Frontiers*, pages.1–9.

Pease, J.D. Young, M.F. Curry, D. and N.W., J., 2004. Improving Fines Recovery by Grinding Finer. *The MetPlant AusIMM Conference*, pages.1–17.

Pérez-Barnuevo, L. Pirard, E. and Castroviejo, R., 2013. Automated characterisation of intergrowth textures in mineral particles. A case study. *Minerals Engineering*, 52, pages.136–142.

Pillay, K. Becker, M. Chetty, D. and Thiele, H., 2011. The Effect of Gangue Mineralogy on the Density Seperation of Low Grade Nickel Ore. *Thesis, University of Pretoria*.

Pirard, E., 2004. Multispectral imaging of ore minerals in optical microscopy. *The Mineralogical Magazine*, 68, pages.323–333.

Pirard, E. Lebichot, S. and Krier, W., 2007. Particle texture analysis using polarized light imaging and grey level intercepts. *International Journal of Mineral Processing*, 84, pages.299–309.

Powell, M.S., 2013. Utilising orebody knowledge to improve comminution circuit design and energy utilisation. *The second AUSIMM international geometallurgy conference*, pages.27–35.

Powell, M.S. Mainza, A.N. Hilden, M.H. and Yahyaei, M., 2015. Full Pre-Crush to SAG Mills – The Case for Changing this Practice. *International Semi-Autogenous Grinding and High Pressure Grinding Roll Technology*, pages.1–22.

Prior, T. Giurco, D. Mudd, G. Mason, L. and Behrisch, J., 2012. Resource depletion, peak minerals and the implications for sustainable resource management. *Global Environmental Change*, 22, pages.577–587.

Rollinson, G.K. Andersen, J.C.Ø. Stickland, R.J. Boni, M. and Fairhurst, R., 2011. Characterisation of non-sulphide zinc deposits using QEMSCAN®. *Minerals Engineering*, 24, pages.778–787.

Roux, S.G. Le. Plessis, A. Du and Rozendaal, A., 2015. The quantitative analysis of tungsten ore using X-ray microCT - Case study. *Computers and Geosciences*, 85, pages.75–80.

Sanford, R.L. Meredith, D.L. and Spears, D.R., 2013. Computer vision applications in mineral processing research. , pages.2013–2019.

Schwartz, G.M., 1951. Classification and definitions of textures and mineral structures in ores. *Economic Geology*, 46, pages.578–591.

Sharif, H. Ralchenko, M. Samson, C. and Ellery, A., 2015. Autonomous rock classification using Bayesian image analysis for Rover-based planetary exploration. *Computers & Geosciences*, 83, pages.153–167.

Stanton, R.L. and Willey, H.G., 1970. Natural work-hardening in galena, and its experimental reduciton. *Economic Geology*, 65, pages.182–194.

Stradling, A., 2011. Geometallurgical Modelling – A Mineral Processor ' s Prespective. *The First AusIMM International Geometallurgy Conference*, pages.33–34.

Taşdemir, A. and Taşdemir, T., 2009. A Comparative Study on PSD Models for Chromite Ores Comminuted by Different Devices. *Particle & Particle Systems Characterization*, 26, pages.69–79.

Thompson, D. and Cabrol, N., 2009. Fast onboard texture analysis for planetary exploration. *IJCAI Workshop on Artificial Intelegance in Space*, pages.1–8.

Tuceryan, M. and Jain, A., 1998. The Handbook of Pattern Recognition and Computer Vision, *World Scientific Publishing Co.*

Vacchetti, L. Lepetit, V. and Fua, P., 2004. Combining Edge and Texture Information for Real-Time Accurate 3D Camera Tracking. *Third IEEE and ACM International Symposium on Mixed and Augmented Reality*, pages.48–57.

Videla, A.R. Lin, C.L. and Miller, J.D., 2007. 3D characterization of individual multiphase particles in packed particle beds by X-ray microtomography (XMT). *International Journal of Mineral Processing*, 84, pages.321–326.

Vizcarra, T.G. Wightman, E.M. Johnson, N.W. and Manlapig, E.V., 2010. The effect of breakage mechanism on the mineral liberation properties of sulphide ores. *Minerals Engineering*, 23, pages.374–382.

De Waal, S. a. Maier, W.D. Armstrong, R. a. and Gauert, C.D.K., 2001. Parental Magma and Emplacement of the Stratiform Uitkomst Complex, South Africa. *The Canadian Mineralogist*, 39, pages.557–571.

Wang, L. and He, D.-C., 1990. Texture classification using texture spectrum. *Pattern Recognition*, 23, pages.905–910.

West, J., 2011. Decreasing Metal Ore Grades: Are They Really Being Driven by the Depletion of High-Grade Deposits? *Journal of Industrial Ecology*, 15, pages.165–168.

Wightman, E.M. and Evans, C.L., 2013. Representing and interpreting the liberation spectrum in a processing context. *Minerals Engineering*, pages.1–5.

Williams, N.R. and Holtzhausen, S., 2001. The impact of ore characterization and blending on metallurgical plant performance. *Journal of the South African Institute of Mining and Metallurgy*, 101, pages.437–446.

Yazdanpanah, A.P. Regentova, E.E. and Bebis, G., 2015. Real-Time Horizon Line Detection based on Fusion of Classification and Clustering. *International Journal of Computer Applications*, 121, pages.5–11.

Appendices

Appendix I: Table of elemental composition comparing elemental data from XRF with that of QEMSCAN for QEMSCAN data validation. Presented in chapter 3 section 3.4.1 as a parity chart.

Element	Entity	Combined	-1000/+106	-106/+75	-75/+53	-53/+25	-25/+0
Al	QEMSCAN	1.62	1.54	1.46	1.63	1.86	1.68
	XRF	2.61	2.53	2.58	2.76	3.02	2.49
Ca	QEMSCAN	4.82	4.96	5.22	5.08	4.66	4.54
	XRF	3.67	3.63	3.93	3.78	3.50	3.74
Cr	QEMSCAN	1.62	0.74	1.93	4.08	4.10	1.11
	XRF	1.33	0.72	1.66	2.75	3.51	0.80
Fe	QEMSCAN	10.23	8.32	11.62	12.77	11.93	11.38
	XRF	7.31	6.38	7.97	8.57	9.22	7.33
Mg	QEMSCAN	11.01	12.21	10.00	8.93	9.30	10.74
	XRF	9.51	10.12	8.99	8.43	8.26	9.58
Na	QEMSCAN	0.10	0.11	0.11	0.09	0.11	0.09
	XRF	0.31	0.34	0.30	0.30	0.31	0.28
Ni	QEMSCAN	0.37	0.13	0.30	0.50	0.50	0.66
	XRF	0.24	0.13	0.22	0.26	0.38	0.34
S	QEMSCAN	2.65	1.56	3.18	3.49	2.95	3.84
	XRF	2.48	1.96	2.70	3.15	2.88	2.87
Si	QEMSCAN	20.12	21.56	19.78	18.02	18.30	19.37
	XRF	18.56	19.83	18.11	17.20	15.76	18.40
Ti	QEMSCAN	0.33	0.42	0.32	0.26	0.22	0.27
	XRF	0.18	0.19	0.20	0.20	0.20	0.16

Appendix II: MATLAB code 1, calculating GLCM's in 13 directions for a XCT image stack.

```
% 3D GLCM calculation by manipulation of image XCT image stack.
% Created 2014 by Mitchel Jardine for fulfilment of masters thesis.

d = dir('*.png');
d = rmfield(d,'date');
d = rmfield(d, 'bytes');
d = rmfield(d, 'datenum');
d = rmfield(d, 'isdir');



Directory = d;



    for i = 1:length(d);
        name = getfield(d(i), 'name');
        x = imread(name);
%         bwx = rgb2gray(x);
        imageStack(:,:,i) = x;
    end
imageStack;


x = []


[r,c,z] = size(imageStack);


Max = [max(imageStack(:))+1];


%
```

```
%------------------- Image stack 1 (original) --------------------

    for ii = 1:z

        D1 = graycomatrix(imageStack(:,:,ii), 'offset', [0 1],
'GrayLimits', [], 'NumLevels', Max);

        imageStackGLCMsD1(:,:,ii)= D1;



        D2 = graycomatrix(imageStack(:,:,ii), 'offset', [-1 1],
'GrayLimits', [], 'NumLevels', Max);

        imageStackGLCMsD2(:,:,ii)= D2;



        D3 = graycomatrix(imageStack(:,:,ii), 'offset', [-1 0],
'GrayLimits', [], 'NumLevels', Max);

        imageStackGLCMsD3(:,:,ii)= D3;



        D4 = graycomatrix(imageStack(:,:,ii), 'offset', [-1 -1],
'GrayLimits', [], 'NumLevels', Max);

        imageStackGLCMsD4(:,:,ii)= D4;

    end




imageStackGLCMsD1;

imageStackGLCMsD2;

imageStackGLCMsD3;

imageStackGLCMsD4;




for iii = 1:z

    imwrite(uint8(255 * mat2gray(imageStackGLCMsD1(:,:,iii))),['D1_',
num2str(iii), '.png'])



    imwrite(uint8(255 * mat2gray(imageStackGLCMsD2(:,:,iii))),['D2_',
num2str(iii), '.png'])
```

```
    imwrite(uint8(255 * mat2gray(imageStackGLCMsD3(:,:,iii))),['D3_',
num2str(iii), '.png'])



    imwrite(uint8(255 * mat2gray(imageStackGLCMsD4(:,:,iii))),['D4_',
num2str(iii), '.png'])

end







imageStackGLCMsD1 = [];

imageStackGLCMsD2 = [];

imageStackGLCMsD3 = [];

imageStackGLCMsD4 = [];



% _____________________________________________________________________

 %------------------- Image stack 2 (regenerated) --------------------



newImageVertical = [];



for c2 = 1:c

    for z2 = 1:z
%Creates a string of pixel values along a defined vector.

        columnPixel = imageStack(:,c2,z2);

        newImageVertical = [newImageVertical, columnPixel];

    end

    newImageVerticalMultiMatrix(:,:,c2) = newImageVertical;
%the number of new images in this image stack depend on the number of pixel
columns in the original images.

    newImageVertical = [];

end

newImageVerticalMultiMatrix;


%Above for loop creates new image stack along a defined plane through


%the original image stack. In this case a vertical trending
```

```
%plane.


[Nr,Nc,Nz] = size(newImageVerticalMultiMatrix);

%N denotes a vertical trending plane through the original image

%stack


Max2 = [max(newImageVerticalMultiMatrix(:))+1];


    for iii = 1:Nz
%(Nc)dependened on the number of colums in the original image stack

        D5 = graycomatrix(newImageVerticalMultiMatrix(:,:,iii), 'offset',
[0 -1], 'GrayLimits', [], 'NumLevels', Max2);

        newImageVerticalMultiMatrixGLCMsD5(:,:,iii)= D5;



        D6 = graycomatrix(newImageVerticalMultiMatrix(:,:,iii), 'offset',
[-1 -1], 'GrayLimits', [], 'NumLevels', Max2);

        newImageVerticalMultiMatrixGLCMsD6(:,:,iii)= D6;



        D7 = graycomatrix(newImageVerticalMultiMatrix(:,:,iii), 'offset',
[1 -1], 'GrayLimits', [], 'NumLevels', Max2);

        newImageVerticalMultiMatrixGLCMsD7(:,:,iii)= D7;

    end


newImageVerticalMultiMatrixGLCMsD5;

newImageVerticalMultiMatrixGLCMsD6;

newImageVerticalMultiMatrixGLCMsD7;




for iii = 1:z

    imwrite(uint8(255 *
mat2gray(newImageVerticalMultiMatrixGLCMsD5(:,:,iii))),['D5_',
num2str(iii), '.png'])
```

```
    imwrite(uint8(255 *
mat2gray(newImageVerticalMultiMatrixGLCMsD6(:,:,iii))),['D6_',
num2str(iii), '.png'])


    imwrite(uint8(255 *
mat2gray(newImageVerticalMultiMatrixGLCMsD7(:,:,iii))),['D7_',
num2str(iii), '.png'])

end




newImageVerticalMultiMatrixGLCMsD5 = [];

newImageVerticalMultiMatrixGLCMsD6 = [];

newImageVerticalMultiMatrixGLCMsD7 = [];


newImageVerticalMultiMatrix = [];




%_____________________________________________________________________________

%------------------- Image stack 3 (regenerated) --------------------


newImageHorizontal = [];


for r2 = 1:r

    for z2 = 1:z

        rowPixel = imageStack(r2,:,z2);

        newImageHorizontal = [newImageHorizontal; rowPixel];

    end

    newImageHorizontal;

    newImageHorizontalMultiMatrix(:,:,r2) = newImageHorizontal;


    newImageHorizontal = [];
```

```
end

newImageHorizontalMultiMatrix;


[Mr,Mc,Mz] = size(newImageHorizontalMultiMatrix);

%N denotes a North/South trending Vertical plane through the original image

%stack


    for iiii = 1:Mz


        D8 = graycomatrix(newImageHorizontalMultiMatrix(:,:,iiii),
'offset', [1 -1], 'GrayLimits', [], 'NumLevels', Max2);

        newImageHorizontalMultiMatrixGLCMsD8(:,:,iiii)= D8;


        D9 = graycomatrix(newImageHorizontalMultiMatrix(:,:,iiii),
'offset', [1 1], 'GrayLimits', [], 'NumLevels', Max2);

        newImageHorizontalMultiMatrixGLCMsD9(:,:,iiii)= D9;


    end


newImageHorizontalMultiMatrixGLCMsD8;

newImageHorizontalMultiMatrixGLCMsD9;




for iii = 1:z

    imwrite(uint8(255 *
mat2gray(newImageHorizontalMultiMatrixGLCMsD8(:,:,iii))),['D8_',
num2str(iii), '.png'])


    imwrite(uint8(255 *
mat2gray(newImageHorizontalMultiMatrixGLCMsD9(:,:,iii))),['D9_',
num2str(iii), '.png'])

end
```

```
newImageHorizontalMultiMatrixGLCMsD8 = [];
newImageHorizontalMultiMatrixGLCMsD9 = [];

newImageHorizontalMultiMatrix = [];

% ____________________________________________________________________
  %------------------- Image stack 4 (regenerated) --------------------

max3 = [max(imageStack(:))+2];

newImage45 = [];
newImage45shift = [];



for iv = 1:z
    newImage45 = zeros(r+(c-1),c)-1;
    newImage45shiftMultiMatrix(:,:,iv) = newImage45;
    newImage45 = [];
end

for vii = 1:z
    for a = 1:c;
        b = a+(r-1);
        newImage45shiftMultiMatrix(a:b,a,vii) = imageStack(:,a,vii);
    end
end

newImage45shiftMultiMatrix;

newImage45 = [];
```

```
newImage45shift = [];



[R,C,Z] = size(newImage45shiftMultiMatrix);


newImage45shiftHorizontal = [];


for r3 = 1:R
    for z3 = 1:Z
        RowPixel = newImage45shiftMultiMatrix(r3,:,z3);
        newImage45shiftHorizontal = [newImage45shiftHorizontal; RowPixel];
    end
    newImage45shiftHorizontal;
    newImage45shiftHorizontalMultiMatrix(:,:,r3) =
newImage45shiftHorizontal;


    newImage45shiftHorizontal = [];
end


newImage45shiftHorizontalMultiMatrix;


[NR,NC,NZ] = size(newImage45shiftHorizontalMultiMatrix);


 for iiiii = 1:NZ


     D10 = graycomatrix(newImage45shiftHorizontalMultiMatrix(:,:,iiiii),
'offset', [1 -1], 'GrayLimits', [-1
(max(newImage45shiftHorizontalMultiMatrix(:)))], 'NumLevels', max3);
     newImageShift45HorizontalMultiMatrixGLCMsD10MinusOnes(:,:,iiiii)= D10;


     D11 = graycomatrix(newImage45shiftHorizontalMultiMatrix(:,:,iiiii),
'offset', [1 1], 'GrayLimits', [-1
(max(newImage45shiftHorizontalMultiMatrix(:)))], 'NumLevels', max3);
```

```
     newImageShift45HorizontalMultiMatrixGLCMsD11MinusOnes(:,:,iiiii)= D11;


    end


newImageShift45HorizontalMultiMatrixGLCMsD10MinusOnes(2:end,2:end,:);

newImageShift45HorizontalMultiMatrixGLCMsD11MinusOnes(2:end,2:end,:);


newImageShift45HorizontalMultiMatrixGLCMsD10MinusOnesFinal =
newImageShift45HorizontalMultiMatrixGLCMsD10MinusOnes(2:end,2:end,:);

newImageShift45HorizontalMultiMatrixGLCMsD11MinusOnesFinal =
newImageShift45HorizontalMultiMatrixGLCMsD11MinusOnes(2:end,2:end,:);


newImageShift45HorizontalMultiMatrixGLCMsD10 =
newImageShift45HorizontalMultiMatrixGLCMsD10MinusOnes(2:end,2:end,:);

newImageShift45HorizontalMultiMatrixGLCMsD10;

newImageShift45HorizontalMultiMatrixGLCMsD11 =
newImageShift45HorizontalMultiMatrixGLCMsD11MinusOnes(2:end,2:end,:);

newImageShift45HorizontalMultiMatrixGLCMsD11;


for iii = 1:z

    imwrite(uint8(255 *
mat2gray(newImageShift45HorizontalMultiMatrixGLCMsD10MinusOnesFinal(:,:,iii
))),['D10_', num2str(iii), '.png'])


    imwrite(uint8(255 *
mat2gray(newImageShift45HorizontalMultiMatrixGLCMsD11MinusOnesFinal(:,:,iii
))),['D11_', num2str(iii), '.png'])

end


newImageShift45HorizontalMultiMatrixGLCMsD10 = [];

newImageShift45HorizontalMultiMatrixGLCMsD11 = [];


newImageShift45HorizontalMultiMatrixGLCMsD10MinusOnesFinal = [];

newImageShift45HorizontalMultiMatrixGLCMsD11MinusOnesFinal = [];
```

```
newImageShift45HorizontalMultiMatrixGLCMsD10MinusOnes = [];
newImageShift45HorizontalMultiMatrixGLCMsD11MinusOnes = [];


newImage45shiftHorizontalMultiMatrix = [];
newImage45shiftMultiMatrix = [];
% ____________________________________________________________________________
  %------------------- Image stack 5 (regenerated) --------------------


newImage135 = [];
newImage135shift = [];



for iv = 1:z
    newImage135 = zeros(1300,700)-1;
    newImage135shiftMultiMatrix(:,:,iv) = newImage135;
    newImage135 = [];
end



for vii = 1:z;
    for a = 1:c;
        j = (c+1)-a;
          k = (r+c)-a;
%          k = (r*2)-a;
        newImage135shiftMultiMatrix(j:k,a,vii) = imageStack(:,a,vii);
    end
end


newImage135shiftMultiMatrix;


newImage135shiftHorizontal = [];
```

```
for r3 = 1:R

    for z3 = 1:Z

        RowPixel = newImage135shiftMultiMatrix(r3,:,z3);

        newImage135shiftHorizontal = [newImage135shiftHorizontal;
RowPixel];

    end

    newImage135shiftHorizontal;

    newImage135shiftHorizontalMultiMatrix(:,:,r3) =
newImage135shiftHorizontal;



    newImage135shiftHorizontal = [];

end

newImage135shiftHorizontalMultiMatrix;



[MR,MC,MZ] = size(newImage135shiftHorizontalMultiMatrix);



 for iiiiii = 1:MZ



    D12 = graycomatrix(newImage135shiftHorizontalMultiMatrix(:,:,iiiiii),
'offset', [1 -1], 'GrayLimits', [-1
(max(newImage135shiftHorizontalMultiMatrix(:)))], 'NumLevels', max3);

    newImageShift135HorizontalMultiMatrixGLCMsD12MinusOnes(:,:,iiiiii)=
D12;



    D13 = graycomatrix(newImage135shiftHorizontalMultiMatrix(:,:,iiiiii),
'offset', [1 1], 'GrayLimits', [-1
(max(newImage135shiftHorizontalMultiMatrix(:)))], 'NumLevels', max3);

    newImageShift135HorizontalMultiMatrixGLCMsD13MinusOnes(:,:,iiiiii)=
D13;

 end



newImage135shiftHorizontalMultiMatrix = [];

newImage135shiftMultiMatrix = [];
```

```
newImageShift135HorizontalMultiMatrixGLCMsD12MinusOnes(2:end,2:end,:);

newImageShift135HorizontalMultiMatrixGLCMsD13MinusOnes(2:end,2:end,:);



newImageShift135HorizontalMultiMatrixGLCMsD12MinusOnesFinal =
newImageShift135HorizontalMultiMatrixGLCMsD12MinusOnes(2:end,2:end,:);

newImageShift135HorizontalMultiMatrixGLCMsD13MinusOnesFinal =
newImageShift135HorizontalMultiMatrixGLCMsD13MinusOnes(2:end,2:end,:);




newImageShift135HorizontalMultiMatrixGLCMsD12 =
newImageShift135HorizontalMultiMatrixGLCMsD12MinusOnes(2:end,2:end,:);

newImageShift135HorizontalMultiMatrixGLCMsD12;

newImageShift135HorizontalMultiMatrixGLCMsD13 =
newImageShift135HorizontalMultiMatrixGLCMsD13MinusOnes(2:end,2:end,:);

newImageShift135HorizontalMultiMatrixGLCMsD13;



newImageShift135HorizontalMultiMatrixGLCMsD12MinusOnes = [];

newImageShift135HorizontalMultiMatrixGLCMsD13MinusOnes = [];



newImageShift135HorizontalMultiMatrixGLCMsD12MinusOnesFinal = [];

newImageShift135HorizontalMultiMatrixGLCMsD13MinusOnesFinal = [];



for iii = 1:MZ

    imwrite(uint8(255 *
mat2gray(newImageShift135HorizontalMultiMatrixGLCMsD12(:,:,iii))),['D12_',
num2str(iii), '.png'])



    imwrite(uint8(255 *
mat2gray(newImageShift135HorizontalMultiMatrixGLCMsD13(:,:,iii))),['D13_',
num2str(iii), '.png'])

end



newImage135 = [];

newImage135shift = [];
```

```
newImageShift135HorizontalMultiMatrixGLCMsD12 = [];
newImageShift135HorizontalMultiMatrixGLCMsD13 = [];
```

Appendix III: MATLAB code 2, producing a heat map of a selected GLCM.

```
% Heat map projection of GLCM's.
% Created 2015 by Mitchel Jardine for fulfilment of masters thesis.



d = dir('*.png');
d = rmfield(d,'date');
d = rmfield(d, 'bytes');
d = rmfield(d, 'datenum');
d = rmfield(d, 'isdir');



Directory = d;



    for i = 1:length(d);
        name = getfield(d(i), 'name');
        x = imread(name);
%         bwx = rgb2gray(x);
        imageStack(:,:,i) = x;
    end
imageStack;


% scaledimagestack =
I = imageStack(:,:,1);
II = (I<1)
III = (I<10)
IV = III-II
Add = uint8(IV)
Slice = I+(Add*5)
```

```
% determine the plots and plot possitions in the figure window
yhistAxes = axes('position',    [0.05 0.085 0.15  0.85]);
mainDataAxes = axes('position', [0.30 0.085 0.69  0.85]);
% imAxes = axes('position',       [0.60 0.05 0.80  0.85]);

%plot map
axes(mainDataAxes);
h = imagesc(Slice);
%each data point is exactly what it is without interpolation.

%Change colour map(makes the backgroud white)
j = jet; %colormap is an array of colours coded in RGD triplet
j(1,:) = [ 1 1 1 ]; %set the lowest colour form blue to white
colormap(j);
colorbar;
% use data cursor to check out the points on the map

%set the range that the data will be coloured
axHdl = get(h, 'Parent'); %get the axes parent handle of the surface
get(axHdl, 'CLim'); %check out the range of the coloured data
set(axHdl, 'CLim', [1,255]) %use the j colourmap to cover data values {

%Best option is;
data_max = max(max(Slice)); % D1 is 2D matrix, so it has a amx value
data_min = min(min(Slice)); %
set(axHdl,'CLim',[data_min, data_max]);

% both x and y range from 1 to 255
line([127.5 127.5],[0 255],'linewidth',0.5,'Color',[0.7 0.7 0.7]);
line([0 255],[127.5 127.5],'linewidth',0.5,'Color',[0.7 0.7 0.7]);
```

```
% labeling
ylabel('Reference Pixel Value')
xlabel('Neighbouring Pixel Value')
title(['GLCM D1 Heat Map'],'FontSize', 13)

% %Display average of each row on the left hand side
% for j=1:255
%     ave(j)=mean(Slice(j,find(Slice(j,:)~=0)));
% end

%Display total of each row on the left hand side
for j=1:255
    SUM(j)=sum(Slice(j,find(Slice(j,:)~=0)));
end

axes(yhistAxes); % move focus to this axes
barh(1:255,SUM,'facecolor',[0. 0.7 0.7], 'edgecolor',[1 1 1]);

set(gca,'xdir','reverse');
set(gca,'ydir','reverse');
ylim([0.5 255.5]);

% %get what you see in the window
% set(gcf,'position',[100 100 800 500]); % undock the figure window first
% figure_size = get(gcf,'position')
% set(gcf,'PaperPosition',figure_size/100);
% print(gcf,'-dpng','-r100',['./2D_heatmap'])
```

Appendix IV: MATLAB code 3, calculating the 4 conventional GLCM statistics for 1000 images in an image stack.

```
% GLCM statistics calculation: Energy, Contrast, Correlation, Homogeneity.
% Created 2015 by Mitchel Jardine for fulfilment of masters thesis.



clear all


d = dir('*.png');
d = rmfield(d,'date');
d = rmfield(d, 'bytes');
d = rmfield(d, 'datenum');
d = rmfield(d, 'isdir');


Directory = d;


x = [];


    for i = 1:length(d);
        name = getfield(d(i), 'name');
        x = imread(name);
        GLCMStack(:,:,i) = x;
    end
GLCMStack;


[r,c,z] = size(GLCMStack);
Max = [max(GLCMStack(:))+1];


statsD1Contrast = [];
statsD1StructContrast = [];
```

```
statsD1StructHomogeneity = [];

statsD1StructEnergy = [];

statsD1StructCorrelation = [];

GLCM = [];


for ii = 1:z

    GLCM = GLCMStack(:,:,ii);


    statsD1Contrast = graycoprops(GLCM,{'contrast'});

    statsD1StructContrast =[statsD1StructContrast, statsD1Contrast];


    statsD1Homogeneity = graycoprops(GLCM,{'homogeneity'});

    statsD1StructHomogeneity = [statsD1StructHomogeneity,
statsD1Homogeneity];


    statsD1Energy = graycoprops(GLCM,{'energy'});

    statsD1StructEnergy = [statsD1StructEnergy, statsD1Energy];


    statsD1Correlation = graycoprops(GLCM,{'correlation'});

    statsD1StructCorrelation = [statsD1StructCorrelation,
statsD1Correlation];


    ((100/z)*ii)

end




statsD1StructContrast2cell = struct2cell(statsD1StructContrast(:));

xlswrite('Stats.xls', statsD1StructContrast2cell(1:200), 'GLCMStats',
'B1');

xlswrite('Stats.xls', statsD1StructContrast2cell(201:400), 'GLCMStats',
'B2');

xlswrite('Stats.xls', statsD1StructContrast2cell(401:600), 'GLCMStats',
'B3');

xlswrite('Stats.xls', statsD1StructContrast2cell(601:800), 'GLCMStats',
```

```
'B4');


statsD1structHomogeneity2cell = struct2cell(statsD1StructHomogeneity(:));

xlswrite('Stats.xls', statsD1structHomogeneity2cell(1:200), 'GLCMStats',
'B6');

xlswrite('Stats.xls', statsD1structHomogeneity2cell(201:400), 'GLCMStats',
'B7');

xlswrite('Stats.xls', statsD1structHomogeneity2cell(401:600), 'GLCMStats',
'B8');

xlswrite('Stats.xls', statsD1structHomogeneity2cell(601:800), 'GLCMStats',
'B9');


statsD1structEnergy2cell = struct2cell(statsD1StructEnergy(:));

xlswrite('Stats.xls', statsD1structEnergy2cell(1:200), 'GLCMStats', 'B11');

xlswrite('Stats.xls', statsD1structEnergy2cell(201:400), 'GLCMStats',
'B12');

xlswrite('Stats.xls', statsD1structEnergy2cell(401:600), 'GLCMStats',
'B13');

xlswrite('Stats.xls', statsD1structEnergy2cell(601:800), 'GLCMStats',
'B14');


statsD1structCorrelation2cell = struct2cell(statsD1StructCorrelation(:));

xlswrite('Stats.xls', statsD1structCorrelation2cell(1:200), 'GLCMStats',
'B16');

xlswrite('Stats.xls', statsD1structCorrelation2cell(201:400), 'GLCMStats',
'B17');

xlswrite('Stats.xls', statsD1structCorrelation2cell(401:600), 'GLCMStats',
'B18');

xlswrite('Stats.xls', statsD1structCorrelation2cell(601:800), 'GLCMStats',
'B19');
```

Appendix V: Table of PSD of each sample, data is given as cumulative wt%.

Aperture (µm)	Ore 1 (Wt%)	Ore 2 (Wt%)	Ore 3 (Wt%)	Ore 4 (Wt%)	Ore 5 (Wt%)	Ore 6 (Wt%)	Ore 7 (Wt%)	Ore 8 (Wt%)	Ore 9 (Wt%)	Gangue (Wt%)
-38	24.1	23.1	20.9	21.8	24.1	23.4	21.3	21.0	21.0	26.6
+38/-75	41.1	37.7	32.8	34.1	42.0	38.7	32.2	30.8	30.8	41.1
+75/-106	52.8	46.7	40.8	41.4	54.6	49.1	38.6	37.1	36.9	49.8
+106/-180	72.4	64.1	56.8	54.4	80.3	71.9	49.5	47.7	46.8	68.3
+180/-250	80.2	77.7	70.5	65.2	90.6	86.6	57.7	56.0	54.7	85.1
+250/-355	82.1	85.0	80.1	73.7	92.7	90.6	64.4	62.6	61.2	95.5
+355/-425	82.3	86.5	82.8	76.5	92.9	90.9	67.1	65.1	63.7	96.9
+425/-600	82.5	87.0	83.8	77.9	92.9	91.0	68.6	66.8	65.3	97.2
+600/-850	82.5	87.3	84.1	78.2	93.0	91.1	69.4	67.6	65.9	97.3
+850/-1000	82.6	87.4	84.2	78.3	93.0	91.1	69.5	67.7	66.1	97.3
+1000/-1400	82.7	87.5	84.4	78.4	93.0	91.2	70.0	68.1	66.3	97.4
+1400/-2000	82.9	87.8	84.8	78.7	93.1	91.3	70.7	68.9	66.8	97.4
+2000/-4000	84.7	90.2	87.4	81.3	93.5	91.9	76.3	74.9	71.4	97.9
+4000/-5600	88.4	94.2	90.9	85.7	94.3	93.9	83.2	81.5	77.3	98.4
+5600	100.0	100.0	100.0	100.0	100.0	100.0	100.0	100.0	100.0	100.0

Appendix VI: The following 10 appendices are the GLCM results for each of the drill core samples as discussed in chapter 5.

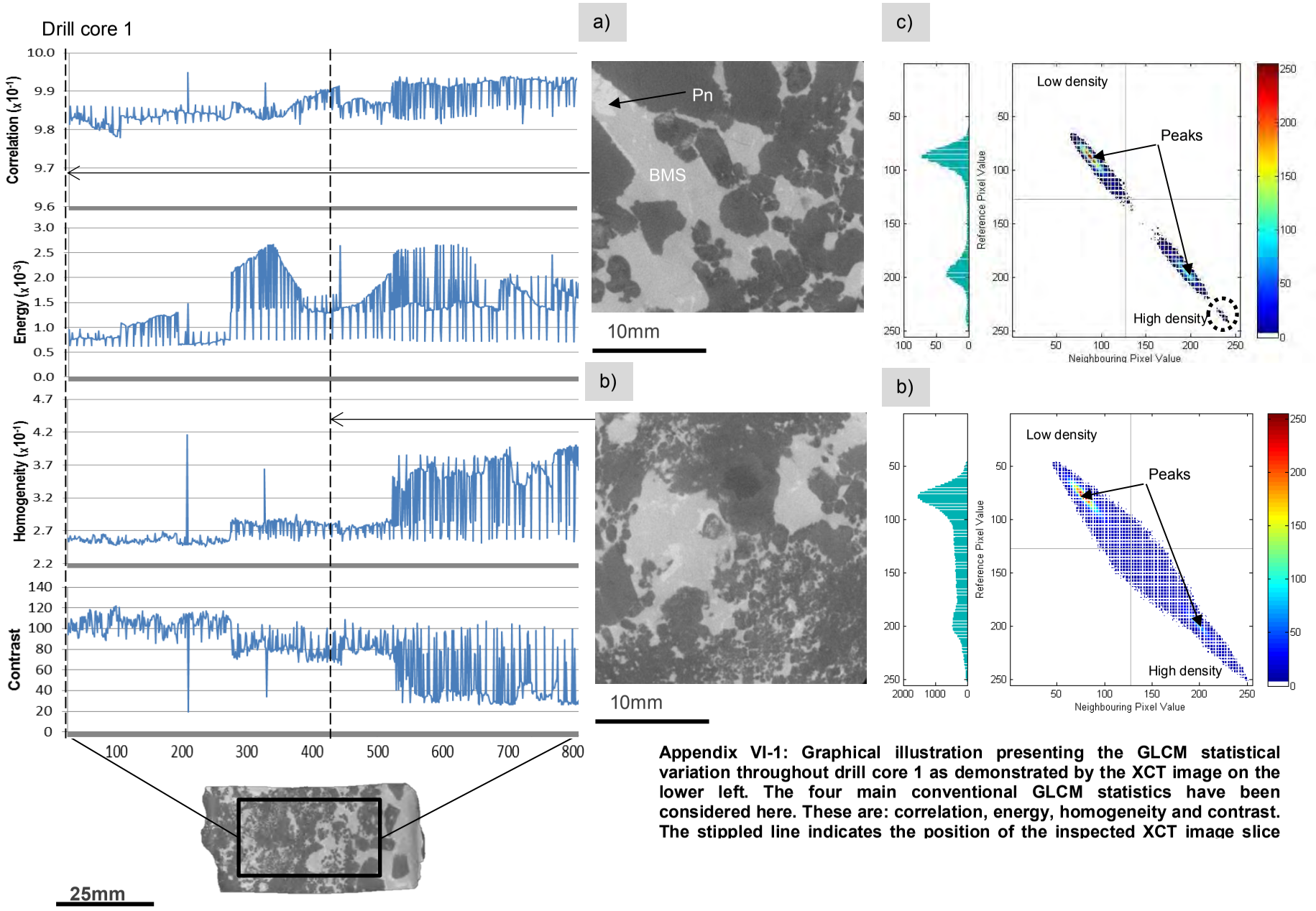

Appendix VI-1: Graphical illustration presenting the GLCM statistical variation throughout drill core 1 as demonstrated by the XCT image on the lower left. The four main conventional GLCM statistics have been considered here. These are: correlation, energy, homogeneity and contrast. The stippled line indicates the position of the inspected XCT image slice

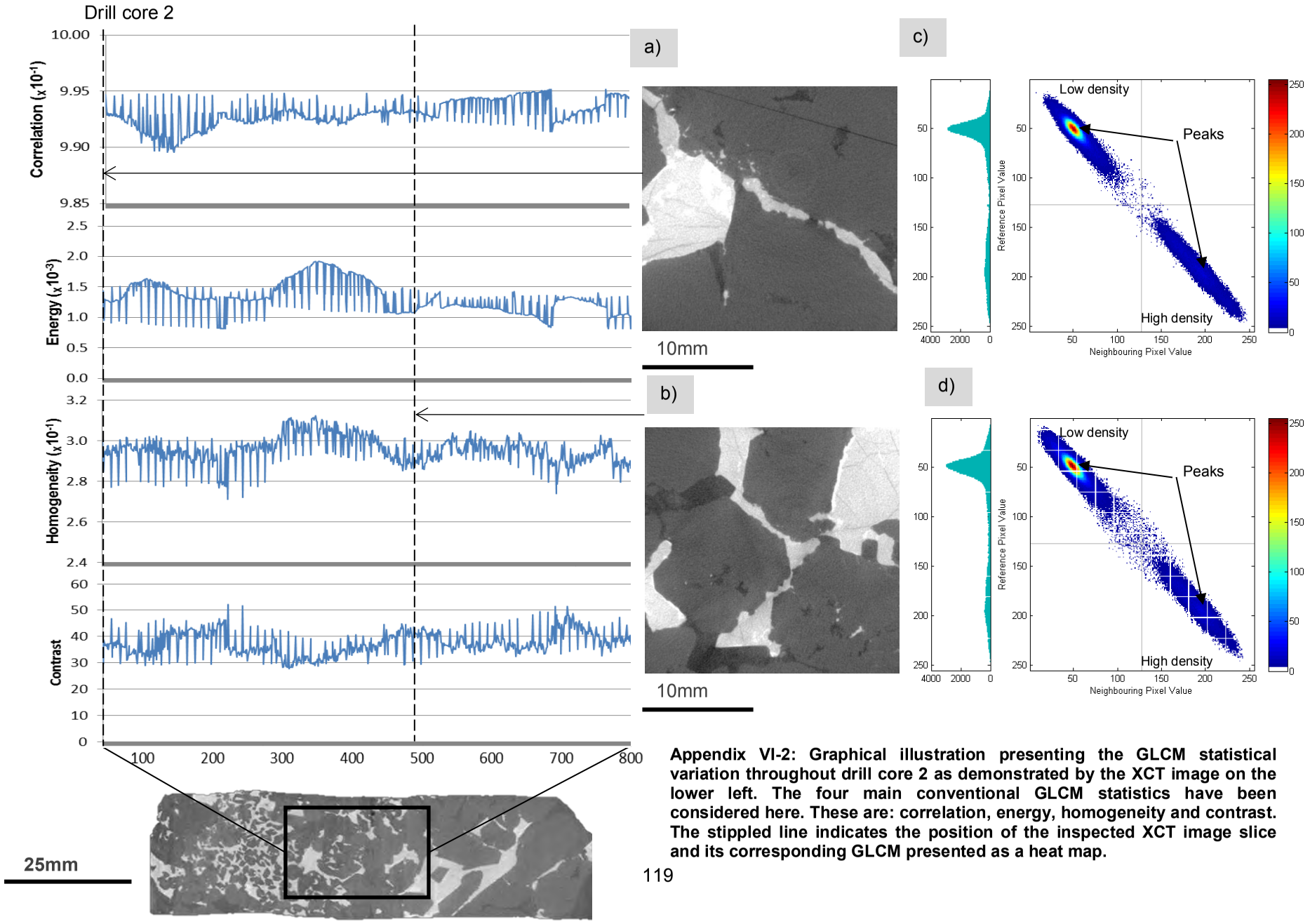

Appendix VI-2: Graphical illustration presenting the GLCM statistical variation throughout drill core 2 as demonstrated by the XCT image on the lower left. The four main conventional GLCM statistics have been considered here. These are: correlation, energy, homogeneity and contrast. The stippled line indicates the position of the inspected XCT image slice and its corresponding GLCM presented as a heat map.

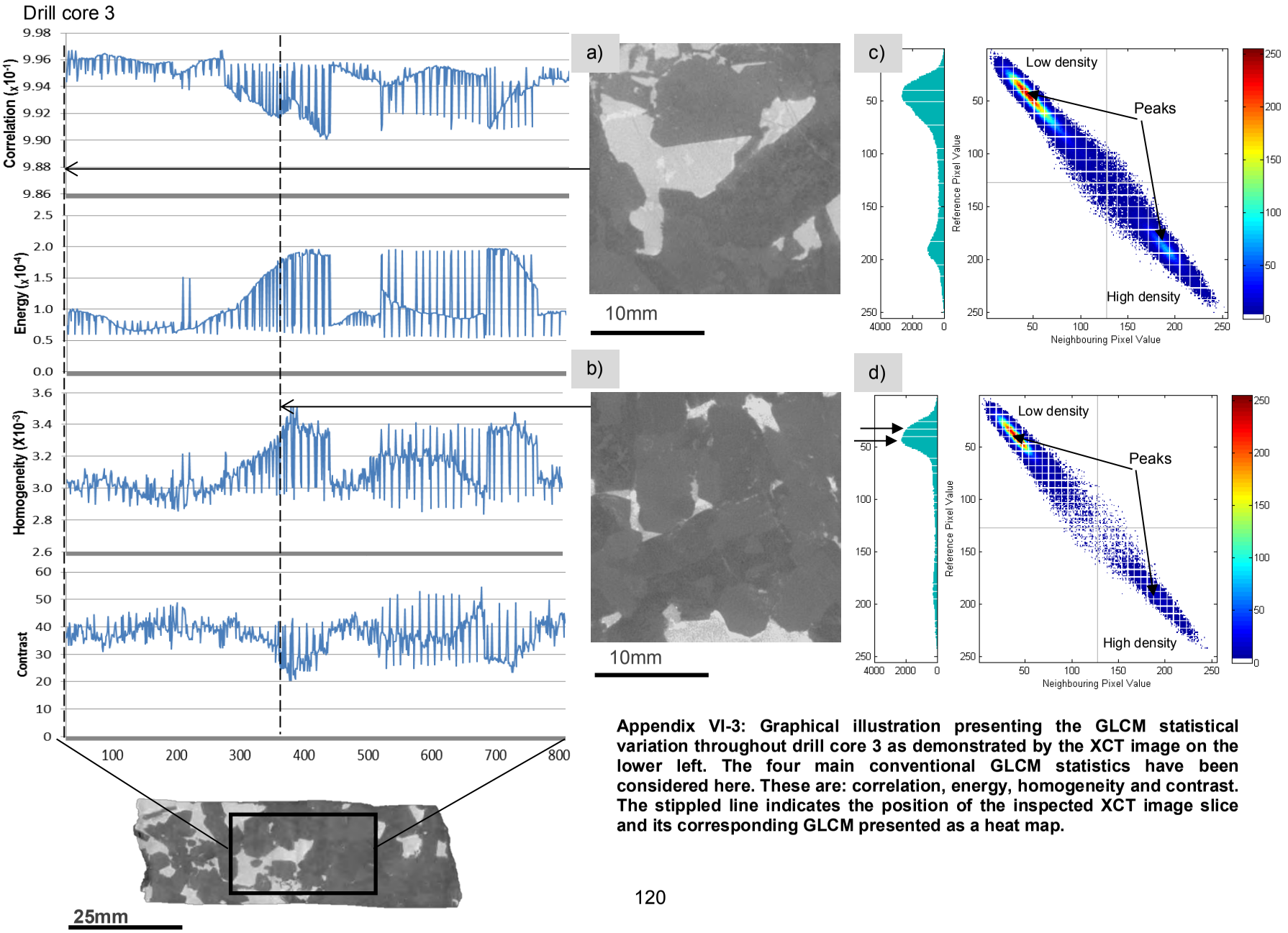

Appendix VI-3: Graphical illustration presenting the GLCM statistical variation throughout drill core 3 as demonstrated by the XCT image on the lower left. The four main conventional GLCM statistics have been considered here. These are: correlation, energy, homogeneity and contrast. The stippled line indicates the position of the inspected XCT image slice and its corresponding GLCM presented as a heat map.

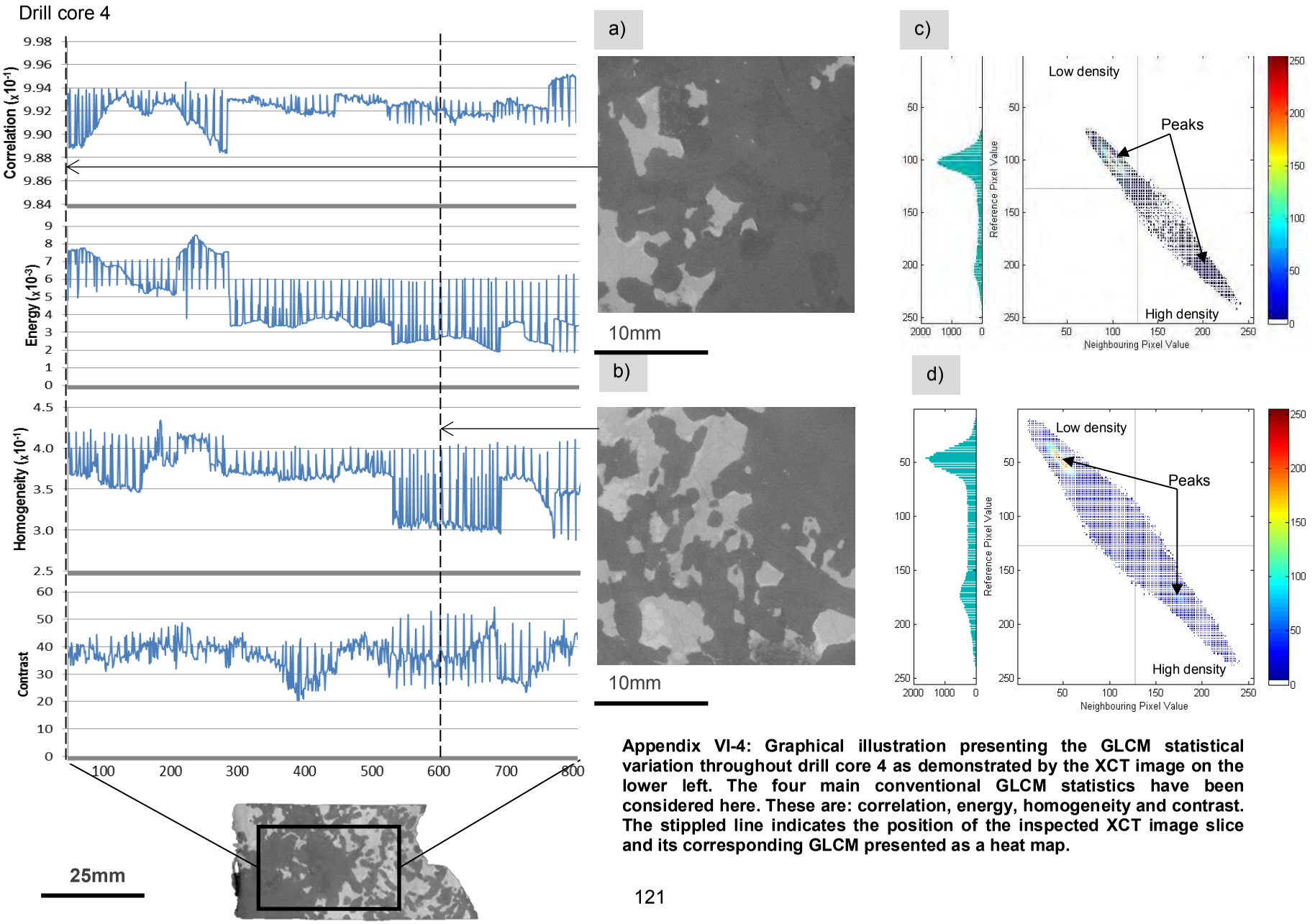

Appendix VI-4: Graphical illustration presenting the GLCM statistical variation throughout drill core 4 as demonstrated by the XCT image on the lower left. The four main conventional GLCM statistics have been considered here. These are: correlation, energy, homogeneity and contrast. The stippled line indicates the position of the inspected XCT image slice and its corresponding GLCM presented as a heat map.

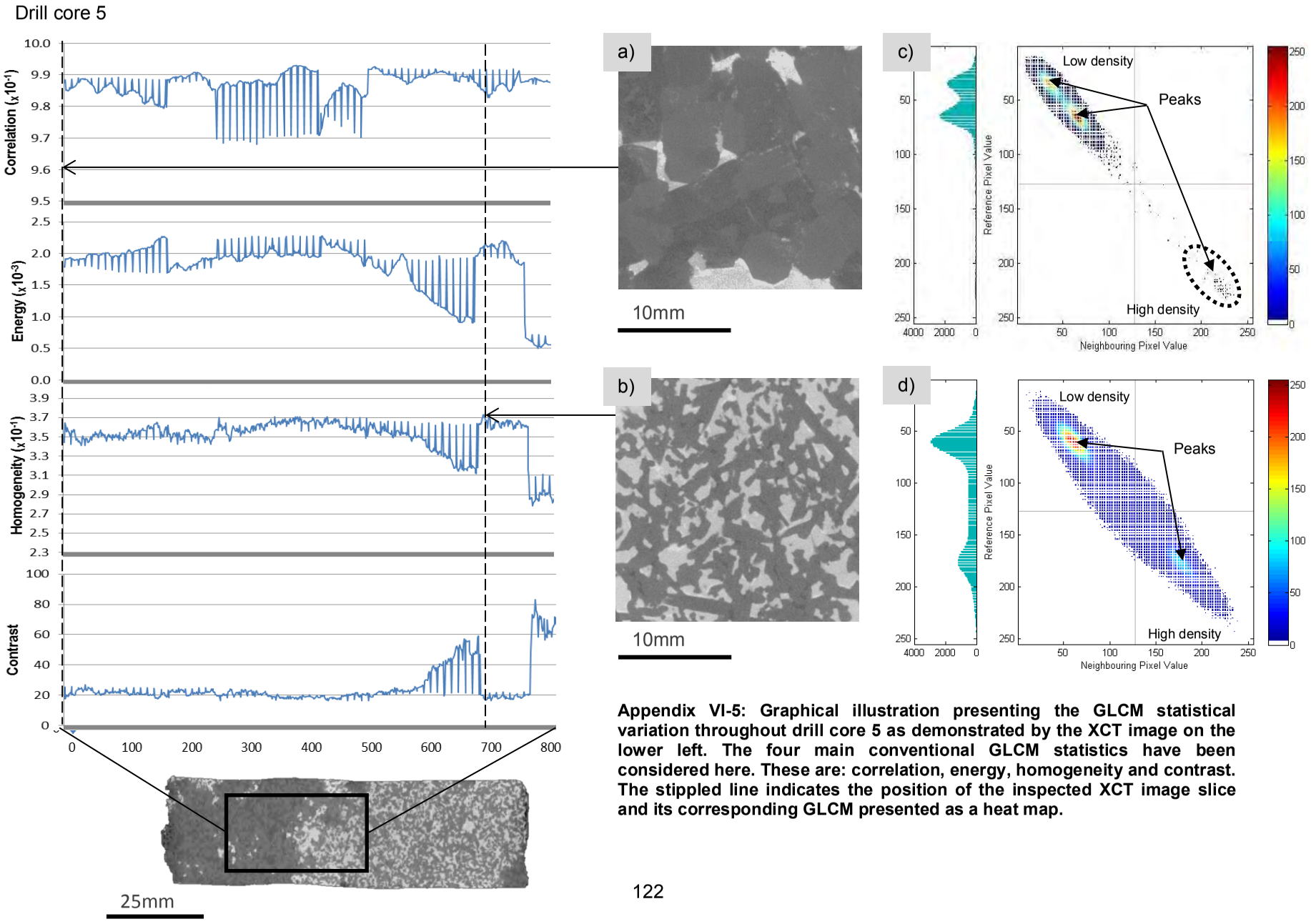

Appendix VI-5: Graphical illustration presenting the GLCM statistical variation throughout drill core 5 as demonstrated by the XCT image on the lower left. The four main conventional GLCM statistics have been considered here. These are: correlation, energy, homogeneity and contrast. The stippled line indicates the position of the inspected XCT image slice and its corresponding GLCM presented as a heat map.

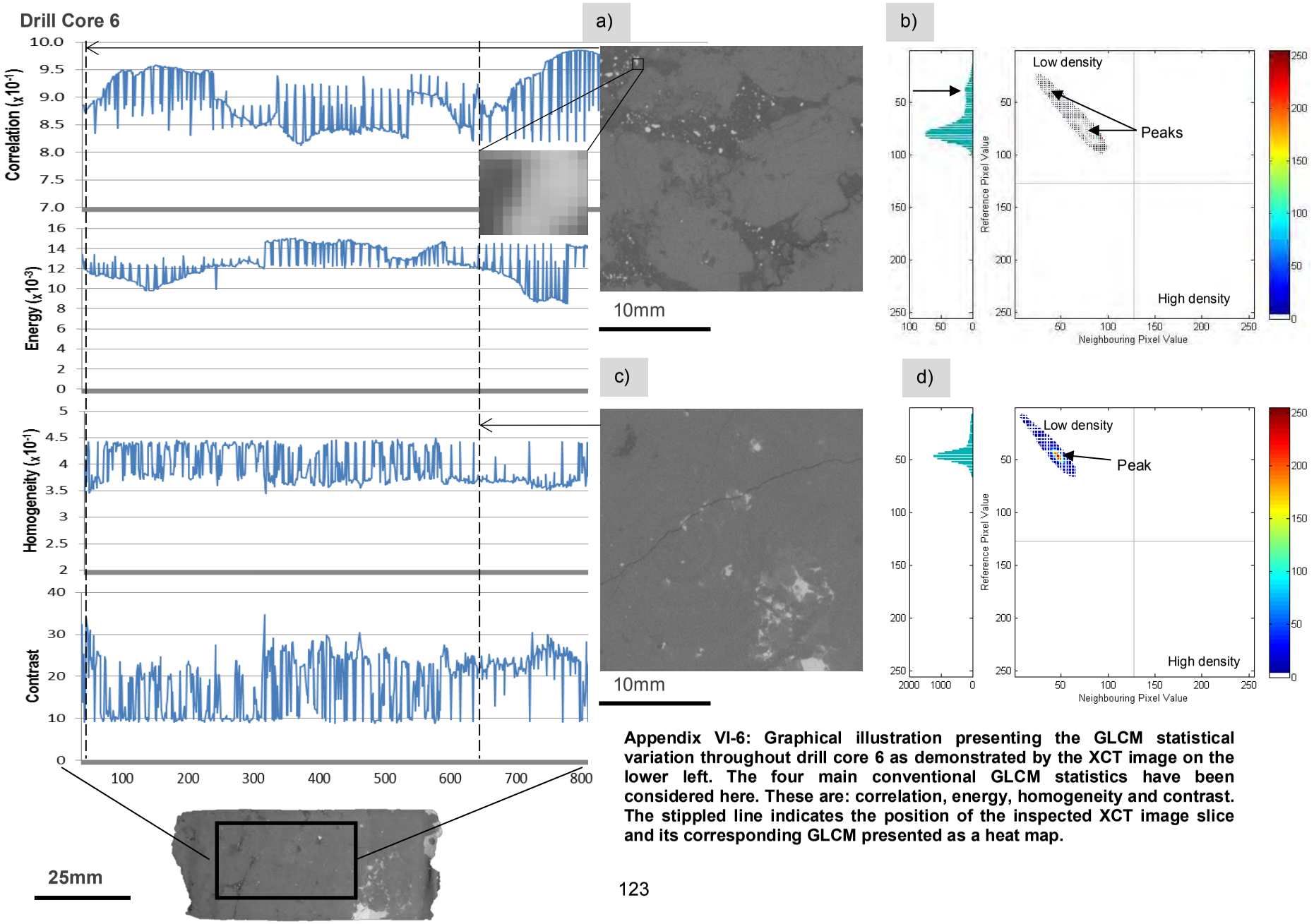

Appendix VI-6: Graphical illustration presenting the GLCM statistical variation throughout drill core 6 as demonstrated by the XCT image on the lower left. The four main conventional GLCM statistics have been considered here. These are: correlation, energy, homogeneity and contrast. The stippled line indicates the position of the inspected XCT image slice and its corresponding GLCM presented as a heat map.

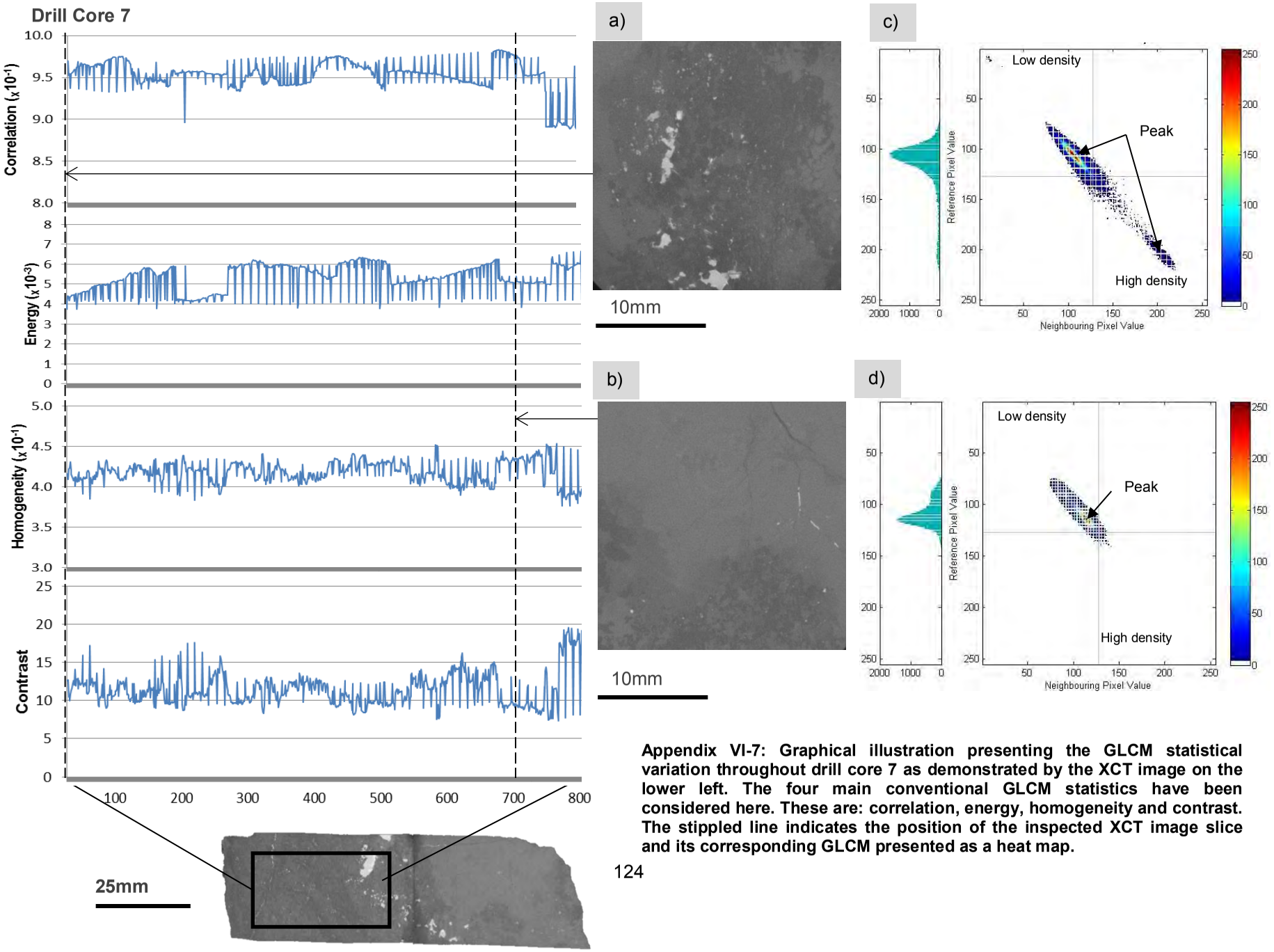

Appendix VI-7: Graphical illustration presenting the GLCM statistical variation throughout drill core 7 as demonstrated by the XCT image on the lower left. The four main conventional GLCM statistics have been considered here. These are: correlation, energy, homogeneity and contrast. The stippled line indicates the position of the inspected XCT image slice and its corresponding GLCM presented as a heat map.

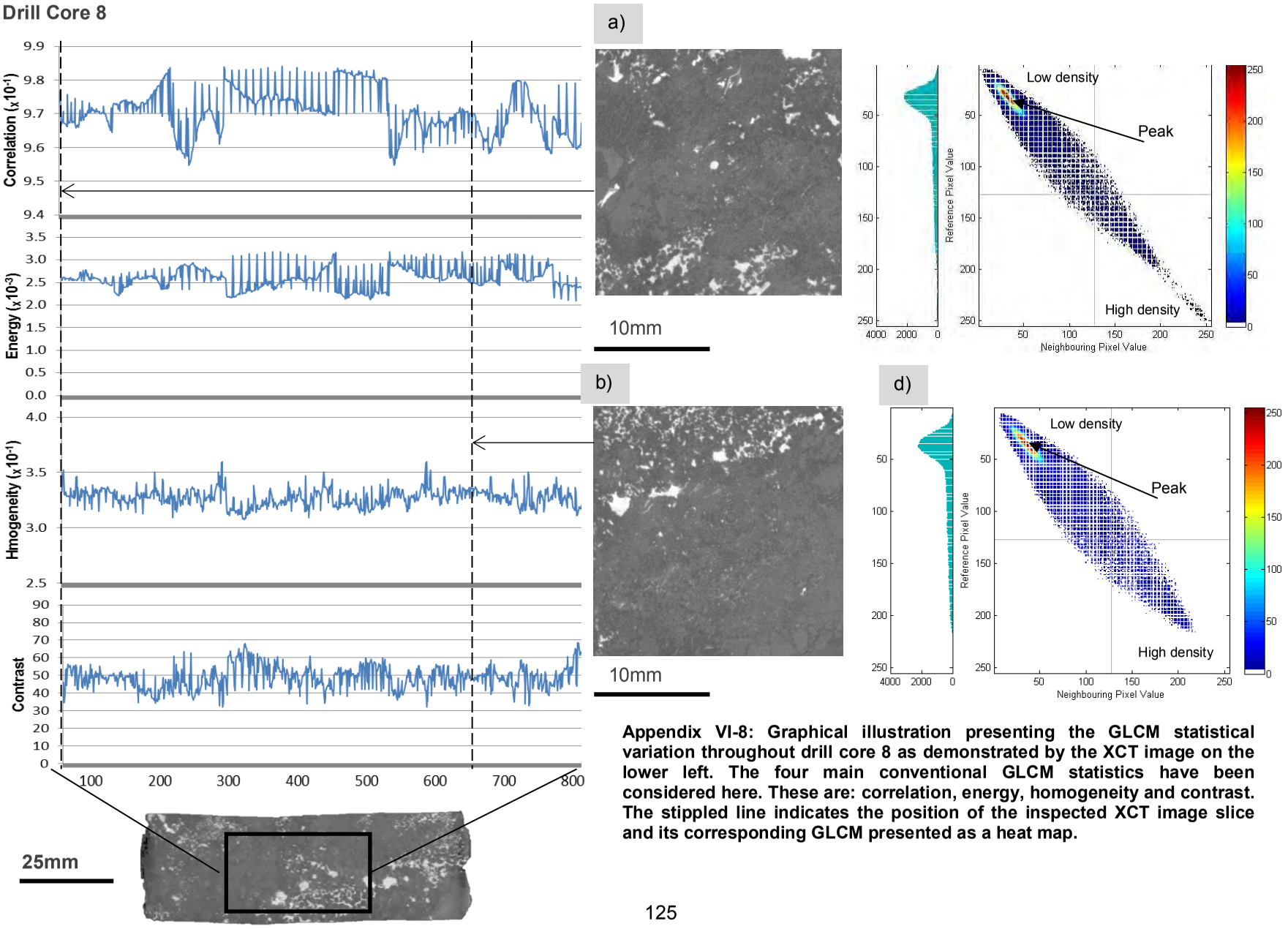

Appendix VI-8: Graphical illustration presenting the GLCM statistical variation throughout drill core 8 as demonstrated by the XCT image on the lower left. The four main conventional GLCM statistics have been considered here. These are: correlation, energy, homogeneity and contrast. The stippled line indicates the position of the inspected XCT image slice and its corresponding GLCM presented as a heat map.

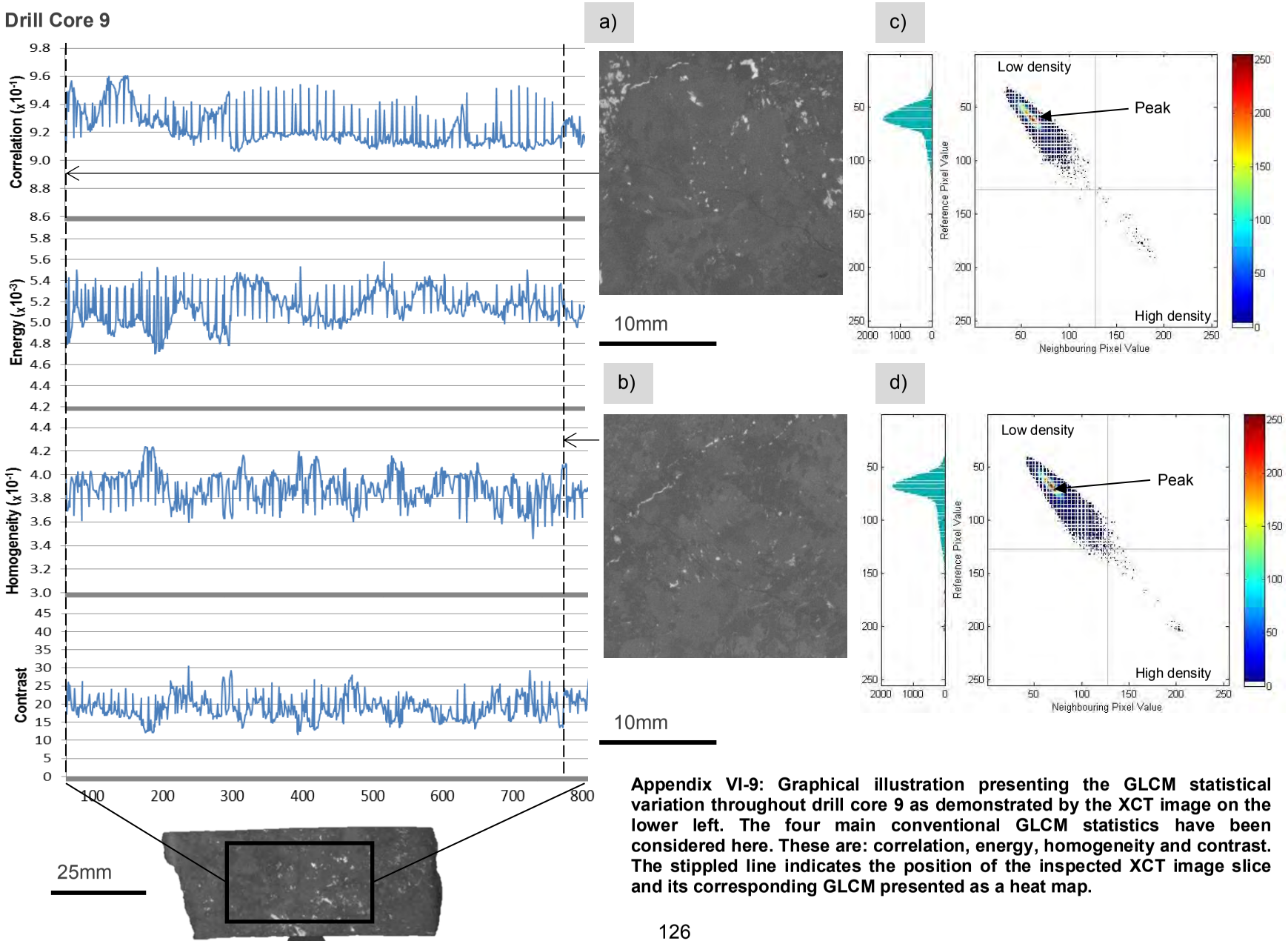

Appendix VI-9: Graphical illustration presenting the GLCM statistical variation throughout drill core 9 as demonstrated by the XCT image on the lower left. The four main conventional GLCM statistics have been considered here. These are: correlation, energy, homogeneity and contrast. The stippled line indicates the position of the inspected XCT image slice and its corresponding GLCM presented as a heat map.

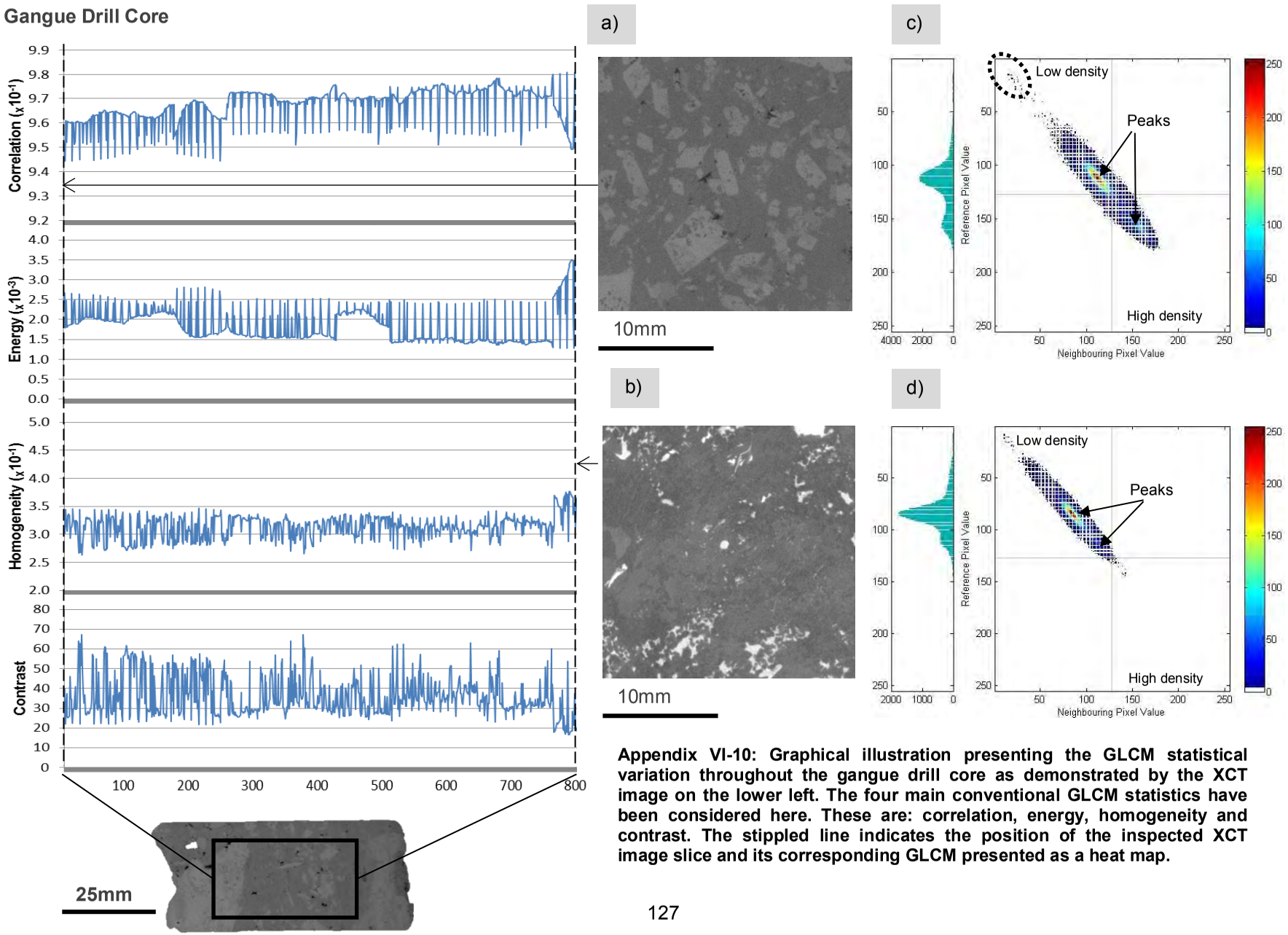

Appendix VI-10: Graphical illustration presenting the GLCM statistical variation throughout the gangue drill core as demonstrated by the XCT image on the lower left. The four main conventional GLCM statistics have been considered here. These are: correlation, energy, homogeneity and contrast. The stippled line indicates the position of the inspected XCT image slice and its corresponding GLCM presented as a heat map.

Appendix VI: listing the minimum, maximum and average of the correlation GLCM statistical value calculated from the region of interest analysed for each drill core.

Correlation ($_{x}10^{1}$)	Minimum	Maximum	Average
Ore 1	9.78	9.95	9.88
Ore 2	9.90	9.95	9.93
Ore 3	9.90	9.97	9.95
Ore 4	9.88	9.96	9.93
Ore 5	9.68	9.93	9.87
Ore 6	8.13	9.85	9.02
Ore 7	8.85	9.83	9.43
Ore 8	9.55	0.98	0.97
Ore 9	8.96	9.60	9.21
Gangue	9.44	9.84	9.66

Appendix VII: listing the minimum, maximum and average of the correlation GLCM statistical value calculated from the region of interest analysed for each drill core.

Energy ($_{x}10^{3}$)	Minimum	Maximum	Average
Ore 1	0.62	2.66	1.41
Ore 2	0.79	1.92	1.26
Ore 3	0.54	1.98	1.06
Ore 4	1.79	8.50	4.34
Ore 5	0.46	2.28	1.55
Ore 6	5.69	15.02	11.49

Ore 7	3.73	6.79	5.39
Ore 8	1.95	3.18	2.53
Ore 9	4.71	5.63	5.17
Gangue	1.19	3.58	1.96

Appendix VIII: listing the minimum, maximum and average of the energy GLCM statistical value calculated from the region of interest analysed for each drill core.

Homogeneity ($_{x}10^{1}$)	Minimum	Maximum	Average
Ore 1	2.46	4.16	3.07
Ore 2	2.71	3.12	2.93
Ore 3	2.84	3.51	3.11
Ore 4	2.82	4.34	3.63
Ore 5	2.59	3.68	3.32
Ore 6	3.45	4.49	3.89
Ore 7	3.76	4.53	4.13
Ore 8	3.05	3.60	3.27
Ore 9	3.36	4.24	3.84
Gangue	2.64	3.77	3.18

Appendix IX: listing the minimum, maximum and average of the homogeneity GLCM statistical value calculated from the region of interest analysed for each drill core.

Contrast	Minimum	Maximum	Average
Ore 1	19.24	121.81	70.07
Ore 2	27.63	53.33	38.21
Ore 3	20.41	54.45	37.66
Ore 4	10.02	77.29	28.82
Ore 5	16.22	94.41	35.24
Ore 6	8.73	34.74	19.03
Ore 7	7.36	20.87	12.58
Ore 8	31.94	80.96	50.31
Ore 9	11.60	40.94	20.53
Gangue	16.56	67.38	34.88

Appendix X: Digital appendix of all the calculated GLCM of each drill core in all 13 directions, available upon request.

Appendix XI: Assessment of Ethics in Research Projects

EBE Faculty: Assessment of Ethics in Research Projects

Any person planning to undertake research in the Faculty of Engineering and the Built Environment at the University of Cape Town is required to complete this form before collecting or analysing data. When completed it should be submitted to the supervisor (where applicable) and from there to the Head of Department. If any of the questions below have been answered YES, and the applicant is NOT a fourth year student, the Head should forward this form for approval by the Faculty EIR committee: submit to Ms Zakiya Chikte (Zakiya.chikte@uct.ac.za); New EBE Building, Ph 021 650 5739).
Please note – It is important to keep a signed copy of this form as students must include a copy of the completed form with the dissertation/thesis when it is submitted for examination.

Name of Principal Researcher/Student: Mitchel Jardine **Department:** Chemical Engineering

If a Student: Yes **Degree:** Master of Science **Supervisor:** Dr. Megan Becker

If a Research Contract indicate source of funding/sponsorship: NRF and SAMMRI

Research Project Title: 3D Quantitative Textural Analysis of Nickel Sulphide Ore using XCT and GLCM on Drill Core

Overview of ethics issues in your research project:

Question 1: Is there a possibility that your research could cause harm to a third party (i.e. a person not involved in your project)?	NO
Question 2: Is your research making use of human subjects as sources of data? If your answer is YES, please complete Addendum 2.	NO
Question 3: Does your research involve the participation of or provision of services to communities? If your answer is YES, please complete Addendum 3.	NO
Question 4: If your research is sponsored, is there any potential for conflicts of interest? If your answer is YES, please complete Addendum 4.	NO

If you have answered YES to any of the above questions, please append a copy of your research proposal, as well as any interview schedules or questionnaires (Addendum 1) and please complete further addenda as appropriate.

I hereby undertake to carry out my research in such a way that

- there is no apparent legal objection to the nature or the method of research; and
- the research will not compromise staff or students or the other responsibilities of the University;
- the stated objective will be achieved, and the findings will have a high degree of validity;
- limitations and alternative interpretations will be considered;
- the findings could be subject to peer review and publicly available; and
- I will comply with the conventions of copyright and avoid any practice that would constitute plagiarism.

- I will comply with the conventions of copyright and avoid any practice that would constitute plagiarism.

Signed by:

	Full name and signature	Date
Principal Researcher/Student:	Mitchel Anthony Jardine	15-02-2016

This application is approved by:

Supervisor (if applicable):	Dr Megan Becker	15-02-2016
HOD (or delegated nominee): Final authority for all assessments with NO to all questions and for all undergraduate research.	pp. J. Peters	15-02-2016
Chair : Faculty EIR Committee For applicants other than undergraduate students who have answered YES to any of the above questions.		

ADDENDUM 1: Please append a copy of the research proposal here, as well as any interview schedules or questionnaires:

ADDENDUM 2: To be completed if you answered YES to Question 2:

It is assumed that you have read the UCT Code for Research involving Human Subjects (available at http://web.uct.ac.za/depts/educate/download/uctcodeforresearchinvolvinghumansubjects.pdf) in order to be able to answer the questions in this addendum.

2.1 Does the research discriminate against participation by individuals, or differentiate between participants, on the grounds of gender, race or ethnic group, age range, religion, income, handicap, illness or any similar classification?	YES	NO
2.2 Does the research require the participation of socially or physically vulnerable people (children, aged, disabled, etc) or legally restricted groups?	YES	NO
2.3 Will you not be able to secure the informed consent of all participants in the research? (In the case of children, will you not be able to obtain the consent of their guardians or parents?)	YES	NO
2.4 Will any confidential data be collected or will identifiable records of individuals be kept?	YES	NO
2.5 In reporting on this research is there any possibility that you will not be able to keep the identities of the individuals involved anonymous?	YES	NO
2.6 Are there any foreseeable risks of physical, psychological or social harm to participants that might occur in the course of the research?	YES	NO
2.7 Does the research include making payments or giving gifts to any participants?	YES	NO

If you have answered YES to any of these questions, please describe how you plan to address these issues (append to form):

ADDENDUM 3: To be completed if you answered YES to Question 3:

3.1 Is the community expected to make decisions for, during or based on the research?	YES	NO
3.2 At the end of the research will any economic or social process be terminated or left unsupported, or equipment or facilities used in the research be recovered from the participants or community?	YES	NO
3.3 Will any service be provided at a level below the generally accepted standards?	YES	NO

If you have answered YES to any of these questions, please describe how you plan to address these issues (append to form)

ADDENDUM 4: To be completed if you answered YES to Question 4

4.1 Is there any existing or potential conflict of interest between a research sponsor, academic supervisor, other researchers or participants?	YES	NO
4.2 Will information that reveals the identity of participants be supplied to a research sponsor, other than with the permission of the individuals?	YES	NO
4.3 Does the proposed research potentially conflict with the research of any other individual or group within the University?	YES	NO

If you have answered YES to any of these questions, please describe how you plan to address these issues(append to form)